Profiling the Effects of L9' Mutations on the Function of the Human Adult Muscle Nicotinic Acetylcholine Receptor

Jacob Monast

A thesis submitted to the University of Ottawa in partial fulfillment of the requirements for the M.Sc. in Biochemistry

Department of Biochemistry, Microbiology, and Immunology

Faculty of Medicine

University of Ottawa

Abstract

The nicotinic acetylcholine receptor (nAChR) is a pentameric ligand-gated ion channel (pLGIC) and is a core component of the neuromuscular junction, facilitating fast synaptic transmission leading to muscle contraction. Mutations to the human adult muscle nAChR lead to various forms of congenital myasthenic syndrome (CMS), a disease characterized by progressive fatigable muscle weakness. A central channel pore constriction formed by a ring of five leucine residues (L9') forms part of the nAChR channel gate. CMS-causing mutations in the L9' residues lead to a form of CMS that results in longer channel opening times and a delayed signal decay. To understand better how L9' mutations in the human adult muscle nAChR influence channel function, I used two-electrode voltage clamp electrophysiology to perform a comprehensive mutant screen of all L9' residues in each subunit of the human adult muscle nAChR. This resulted in a total of 76 unique mutations: 19 L9' mutations consisting of every possible natural amino acid substitution in each subunit (α, β, ε, δ). The results of this screen show that while the polarity and size of a substituted residue contribute to its effect on channel function, increasing the polarity of the side chain typically has a more potentiating effect on channel function than does a change in size. The subunit in which the mutation is expressed also tailors the effect of a given mutation on channel function, with several δL9' mutations producing qualitatively different effects than equivalent mutations in other subunits. Because the majority of L9' mutations resulted in a gain-of-function, I originally postulated that interactions between L9' and surrounding residues stabilize the resting state with the elimination of such interaction through mutations destabilizing the resting state to promote channel gating. Using a double mutant cycle, I explored interactions between the L9' and adjacent non-L9' residues but found that there are only weak or no interactions that contribute to channel function. Instead, my data support the hypothesis that the nAChR operates via a hydrophobic gating mechanism, and that adjacent L9' residues are driven together by the hydrophobic effect to form a closed pore. L9' mutations that either increase the polarity or decrease residue size likely reduce the hydrophobic driving forces that stabilizes the resting state, thus leading to an enhancement in channel function.

Acknowledgements

Firstly, I would like to thank my supervisor Dr. John Baenziger for guiding me on this difficult journey. I learned much these past few years about how to properly present one's findings but I think I learned the most from getting grilled on my understanding of scientific articles at our Ion Channel Journal Club meetings. To get to where I wanted to be, I needed to know where I was, and you helped me learn from my mistakes. For this, I thank you.

I would also like to thank my TAC members Dr. Corrie daCosta and Dr. Eric Lee for their insightful comments and helpful discussions during our TAC meetings. Your comments greatly improved the trajectory of my project.

To my lab colleagues Mack and Jaimee, I would like to thank you for helping me around the lab and for stimulating conversations that greatly helped me focus my project. I also want to thank you for making the lab more fun, I had a lot of great laughs.

To my friends Sylvain, Mick, and Marc-André, you're some of the best friends I could ever hope for, and you've all made this bumpy ride a lot more fun. Here's to you guys!

I want to give a special thanks to Dr. Barry Kirschenbaum who taught me biology at UNIS in New York for my final two years of high school. I credit you with motivating me to pursue this Master's degree and impressing upon me the importance of the scientific method. Your inspiring words still resonate with me to this day and will continue to do so. Thank you.

To my brother Luc, you've always managed to encourage me to stay strong and laugh a little, even when the world weighed most heavily on us. To my sister Nadia, you've had to go through all the same trials as Luc or I have, but you went through them first, and in doing so, paved the way in part for our success. To both of you, I say the most colourful and beautiful times of our lives are still yet to come and I look forward to sharing those moments with you.

To my biggest supporters in life, Mom and Dad, you know that I couldn't have done it without you. You have taken care of me since the beginning and have been unwavering sources of support in the most trying of times. You've always been there for me, and so I will always be there for you no matter what. Love you two with all my heart.

Table of Contents

List of Abbreviations

3,4-DAP	3,4-diaminopyridine
$5HT_3$	Serotonin receptor
α-BTX	α-Bungarotoxin
$\Delta G_{C \rightarrow W}$	Free energy of transfer from cyclohexane to water
ε_r	Dielectric constant
Ω	Coupling constant
Å	Angstrom
ACh	Acetylcholine
AChBP	Acetylcholine-binding protein
AChE	Acetylcholinesterase
ANOVA	Analysis of variance
CD	Cytoplasmic domain
ChAT	Choline acetyltransferase
CMS	Congenital myasthenic syndrome
CNS	Central Nervous System
ColQ	Collagenic Tail Q
cRNA	Clonal ribonucleic acid
Cryo-EM	Cryogenic electron microscopy
DNA	Deoxyribonucleic acid
EC_{50}	Half-maximal effective concentration
ECD	Extracellular domain
GlyR	Glycine receptor
HEPES	4-(2-hydroxyethyl)-1-piperazineethanesulfonic acid
K_D	Distribution coefficient
LRP4	Lipoprotein-related protein 4
M1	Transmembrane α-helix 1
M2	Transmembrane α-helix 2

M3	Transmembrane α-helix 3
M4	Transmembrane α-helix 4
MA	Intracellular cytoplasmic α-helix
MD	Molecular Dynamics
MX	Amphipathic α-helix
MuSK	Muscle-specific kinase
nAChR	Nicotinic acetylcholine receptor
NMR	Nuclear magnetic resonance
PcDNA	Plasmid cloning DNA
PDB	Protein Data Bank
pLGIC	Pentameric ligand-gated ion channel
Rapsyn	Receptor-associated protein of the synapse
REFER	Rate-equilibrium free energy relationships
R→O	Resting to open
SNAP	Soluble NSF attachment proteins
SNAP25B	Synaptosomal-associated protein 25 isoform B
SNARE	SNAP-receptor
SNase	Staphylococcal nuclease
TEVC	Two-electrode voltage clamp
TMD	Transmembrane domain
UV	Ultraviolet radiation
WCA	Weeks-Chandler-Andersen
WT-nAChR	Wild-type human muscle nicotinic acetylcholine receptor

List of Figures

List of Tables

Chapter 1

General Introduction

1.0 Introduction

Genetic mutations are an inherent and essential component in the process of evolution. Some mutations confer advantages to certain individuals, other mutations have little to no effect on phenotype, while others result in deleterious consequences. Human genetic disorders can be attributed to one or multiple mutations in genes that code for proteins that perform physiological functions. Genetic diseases are difficult to treat because although the symptoms can sometimes be managed pharmaceutically, the underlying cause of the disease persists.

The subject of my thesis deals with the functional consequences of mutations to the human adult muscle nicotinic acetylcholine receptor (nAChR), a pentameric ligand-gated ion channel (pLGIC) that facilitates neuromuscular communication by regulating the flow of cations down their electrochemical gradients into muscle cells upon binding the neurotransmitter acetylcholine (ACh). Healthy neuromuscular transmission involves the coordinated actions of multiple proteins within and surrounding the synapse at the motor endplate. A mutation in any of the proteins present at the neuromuscular junction can potentially result in impaired neuromuscular transmission, leading to what is referred to as a Congenital Myasthenic Syndrome (CMS) (as reviewed by Engel *et al* 2015). While mutations to many proteins at the neuromuscular junction can lead to CMS, over half of all diagnosed CMS cases are due to mutations in the nAChR (as reviewed by Engel e*t al* 2015), emphasizing the centrality of the role played by the nAChR in neuromuscular transmission. Presently, there is no cure for CMS and treatments available are often limited, especially in severe cases. The lack of effective treatment partially stems from our lack of knowledge regarding the mechanism of channel gating, as it is not entirely known how ligand-binding is communicated to the channel gate during the gating transition.

Although many cases of CMS are caused by mutations of residues that line the ion permeation pathway of the nAChR, little is known regarding the mechanisms by which these mutations lead to altered nAChR function. My thesis focuses on pore-lining CMS-causing mutations with the ultimate goal of assessing how these mutations influence channel function. In this chapter, I will cover the different potential causes of CMS and will describe the structure and function of the human adult muscle nAChR. I will highlight the most up-to-date information regarding what is known about its gating mechanism, and will provide a clear explanation of my thesis objectives and how the findings from my work have shed light onto both the mechanisms

underlying CMS and, more generally, channel function. A greater understanding of how mutations in this region lead to CMS could eventually contribute to the design of beneficial therapeutic agents.

1.1 The nAChR

Nicotinic acetylcholine receptors are found throughout the body but are mainly expressed in the Central Nervous System (CNS) and muscle tissues. As members of the pLGIC superfamily, each nAChR is composed of five homologous subunits assembled together pseudo-symmetrically into a pentamer around a central axis perpendicular to the membrane. There are 17 different genes coding for different nAChR subunits which assemble to make different receptor subtypes, and these genes code to make α1-α10 (excluding α8, which is found in avian species), β1-β4, δ, γ, and ε subunits (as reviewed by Bertrand & Terry Jr. 2018). The nAChRs expressed in brain tissues are composed of various combinations of α2-α10 and β2-β4 subunits, arranged either as homo- or heteropentamers depending on the specific subunit composition. For instance, the α7 nAChR in the brain is a homopentamer made up of five identical α7 subunits and is involved in important cognitive processes such as learning and long-term memory (as reviewed by Levin *et al* 2006). Another neural subtype, the α4β2 nAChR in the brain mediates nicotine's addictive qualities and is composed of α4 and β2 subunits arranged in a stoichiometry of either $(\alpha4)_2(\beta2)_3$ or $(\alpha4)_3(\beta2)_2$ which confers the receptor either a high sensitivity or low sensitivity to nicotine respectively (Nelson *et al* 2003; Zwart & Vijverberg 1998). The muscle-type nAChR is restricted to two subtypes, adult and fetal, and are the only subtypes that incorporate the δ and either γ or ε subunits. The muscle-type nAChR possesses a stoichiometry of $(\alpha1)_2\beta1\delta\gamma$ or $(\alpha1)_2\beta1\delta\varepsilon$ corresponding to fetal form found in developing muscle and the adult form found in adult muscle respectively. The many different combinations of subunits result in receptors that differ in their conductance, agonist sensitivity, rates of desensitization, ion selectivity, and response to allosteric modulators (as reviewed by Albuquerque *et al* 2009). Note that this thesis focuses on muscle type nAChRs and uses the simplified nomenclature of $\alpha_2\beta\delta\gamma$ and $\alpha_2\beta\delta\varepsilon$ for the fetal and adult muscle forms respectively.

1.2 Medical Relevance - Congenital Myasthenic Syndrome

CMS refers to a collection of inherited disorders that result from impaired neuromuscular transmission at the motor endplate. CMS is characterized by progressive fatigable muscle weakness with symptoms varying in severity across afflicted individuals. The disease can be caused by mutations to a number of different proteins in the neuromuscular junction. Since the 1970s, CMS has been recognized as a disease clinically different from those that produce similar symptoms such as Myasthenia Gravis and Lambert-Eaton Syndrome, both of which are autoimmune disorders. Presently, novel CMS-causing mutations of genes that code for proteins at the neuromuscular junction are diagnosed through whole-exome sequencing with confirmation by Sanger sequencing (as reviewed by Engel *et al* 2015). Additional genetic and electrophysiological studies help in confirming diagnoses. Since diagnosing the condition can be difficult, physicians may mistakenly attribute an afflicted individuals' symptoms to another disorder, so it is believed that the actual prevalence of CMS is underreported. Despite advances in diagnostics, the available treatments for CMS are still inadequate, especially in more severe cases, and the treatment options available primarily depend on the cause of the specific CMS.

To fully understand how mutations lead to CMS, it is essential to describe the process of neuromuscular transmission. When an action potential reaches the terminus of a pre-synaptic neuron, a rise in intracellular calcium levels causes acetylcholine (ACh)-packed vesicles to fuse with the pre-synaptic membrane thus releasing ACh into the synaptic cleft (Figure 1.1). The released ACh diffuses across the synaptic cleft to bind to the nAChR on the post-synaptic membrane. The nAChR is a ligand-gated ion channel that opens upon ACh binding. In its resting state, the nAChR adopt a closed, non-conducting conformation, but upon ACh binding the nAChR, transitions to an open conformation that facilitates the flow of cations down their electrochemical gradients into post-synaptic cells. The flow of cations across the post-synaptic membrane causes depolarization of the membrane, eventually leading to muscle contraction. The ACh eventually disassociates from the ligand-binding site, is hydrolyzed by acetylcholinesterase (AChE) in the synapse, and the choline then taken up by the presynaptic nerve and recycled to re-form ACh (Figure 1.1). Mutations to several proteins encompassing the synaptic space can lead to CMS.

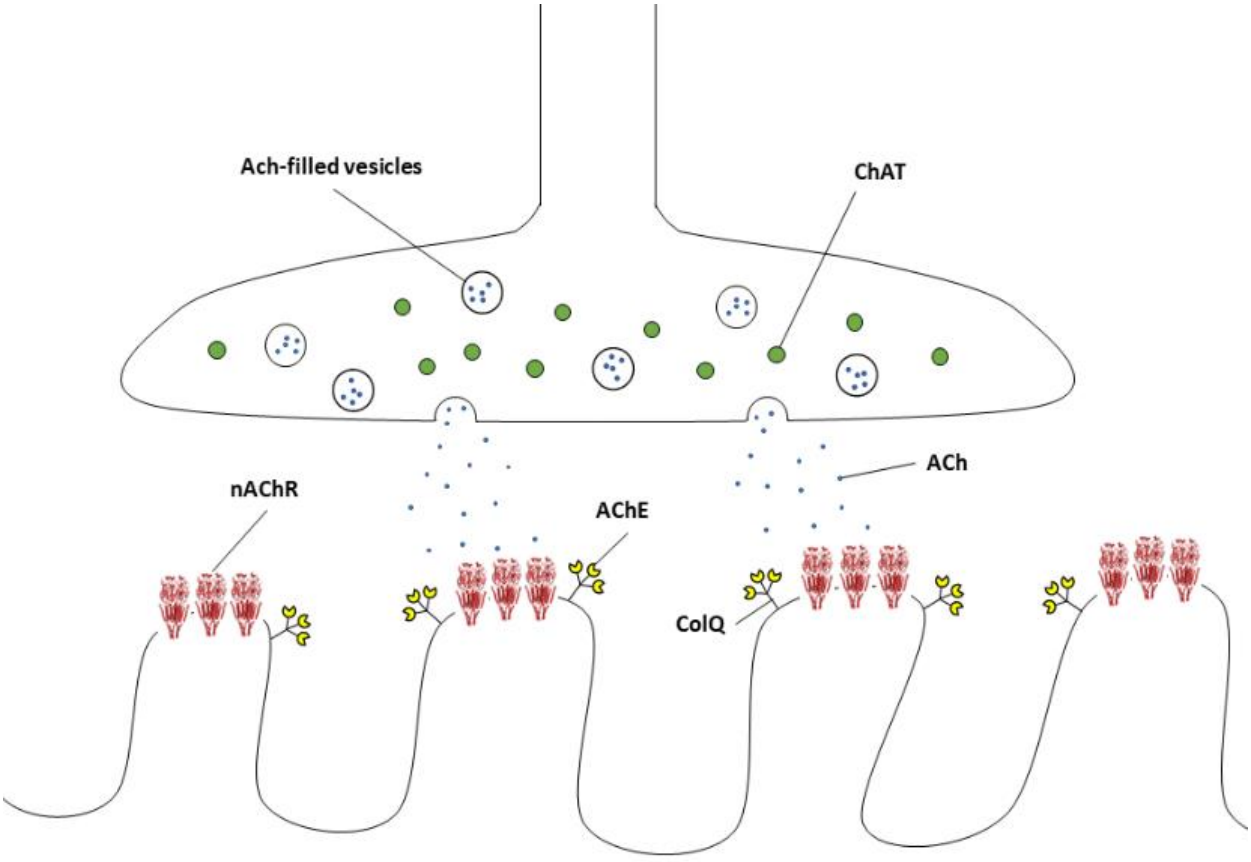

Figure 1.1: The Neuromuscular Junction. The neuromuscular junction is formed by the presynaptic nerve terminal, the synaptic cleft, and the post-synaptic membrane. The ACh is released from vesicles contained within the presynaptic terminal into the synaptic cleft and binds to the nAChRs on the post-synaptic membrane to elicit muscle contraction. The nAChRs are shown to be concentrated on the crests of the junctional folds of the motor endplate in a rapsyn-mediated process. AChE neutralizes ACh by cleaving it and the products are taken back up into the presynaptic terminal to be recycled into more ACh by ChAT.

1.2.1 CMS Classifications

A neuromuscular junction consists of the pre-synaptic motor neuron, the synaptic cleft, and the post-synaptic muscle fiber. The types of mutations leading to CMSs are subdivided by the location of the affected protein within the neuromuscular junction.

1.2.2 Pre-synaptic CMS

In the pre-synaptic terminal, the proper formation and release of ACh-containing vesicles into the synaptic cleft is required for normal neuromuscular transmission. Mutations in at least three different proteins associated with the pre-synaptic terminal have clinically been shown to disrupt neuromuscular function: choline acetyltransferase (ChAT), SNAP25B, and Synaptotagmin 2 (as reviewed by Engel *et al* 2015). ChAT is an enzyme located in the pre-synaptic terminal that catalyzes the transfer of the acetyl group from Acetyl-coA to a choline molecule, resulting in the synthesis of acetylcholine, the primary agonist for muscle-type nAChR (Figure 1.1). Mutations to ChAT that result in impaired function of the enzyme in turn impair production of ACh, and thus ultimately its release into the synaptic cleft. The severity of CMS due to ChAT deficiency appears to depend on the location and nature of the mutation, with mutations near the ChAT active site associated with the most severe forms (Shen *et al* 2011). People affected by ChAT deficiency typically suffer from apnea, with some patients presenting apneic symptoms from birth and others suffering apneic attacks later in life (Schara *et al* 2010).

Mutations in synaptotagmin 2 and SNAP25B, two proteins involved in ACh vesicle exocytosis, have also been shown to lead to CMS in humans. Synaptotagmin 2 is a presynaptic calcium sensor that triggers the process of ACh vesicle fusion with the presynaptic membrane. Synaptotagmin 2 has two functional C-terminal domains, namely C2A and C2B, both of which have crucial roles in synaptic transmission. Mutations to the C2B domain of the protein have been shown to impair neurotransmitter release leading to presynaptic CMS (Herrmann *et al* 2014). SNAP25B is one of three SNARE proteins that plats a mechanistic role in the fusion of ACh-filled vesicles with the presynaptic membrane to allow their release into the synapse. A diagnosed mutation of SNAP25B in a human patient was shown to result in significant reduction in the number of ACh-filled vesicles released into the synapse (Shen *et al* 2014)

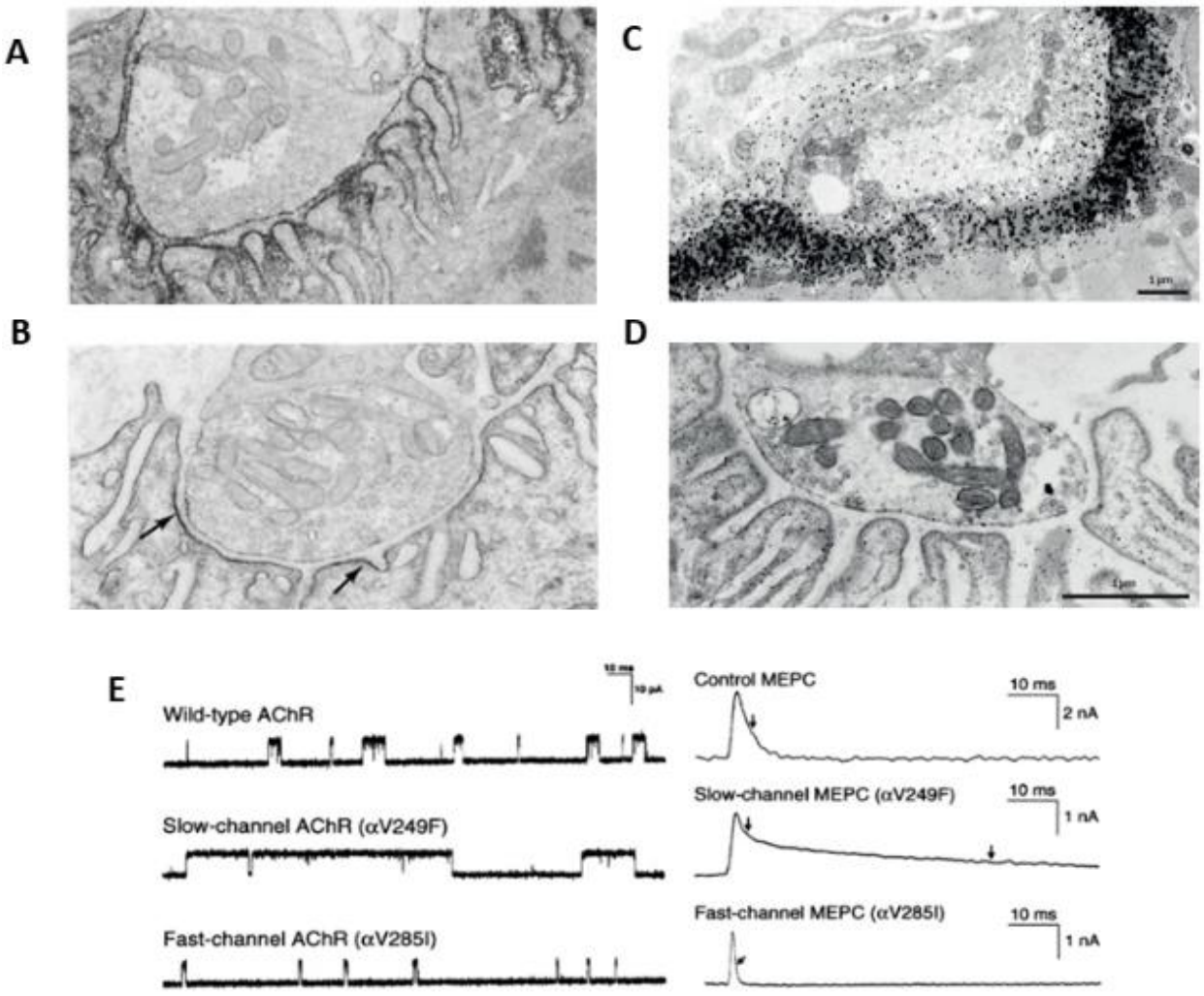

Figure 1.2: Effects of various Congenital Myasthenic Syndromes. (A) Ultrastructural localization of AChR at a motor endplate for a healthy individual and **(B)** a CMS patient suffering from AChR deficiency (EM images A+B reproduced from Ohno *et al* 1997 with permission from Andrew Engel). The black arrows draw attention to the degeneration of junctional folds and the reduced staining of AChR. **(C)** Electron cytochemical localization of AChE in a healthy individual and **(D)** in an AChE-deficient patient due to ColQ mutations (EM images C+D reproduced from Engel *et al* 2015 with permission from Dr. Andrew Engel). The lack of AChE expression is visualized by the lack of black dots within the synaptic space. **(E)** A single channel recording and a miniature endplate current (MEPC) of nAChRs from a control patient (top panel), a slow-channel syndrome patient (middle panel), and a fast-channel syndrome patient (lower panel) (image reproduced from Sine & Engel 2006 with permission from Dr. Steven Sine). Refer to 'Permissions' section for journal licenses and acknowledgments.

1.2.3 Synaptic CMS

Acetylcholinesterase (AChE) is the enzyme responsible for breaking down ACh in the synaptic cleft, thus terminating its action on the nAChR, and subsequently allowing choline to be uptaken into the pre-synaptic terminal where it will be used again to produce more ACh. AChE maintains its position by anchoring itself to the post-synaptic membrane through a domain known as ColQ, a triple-stranded collagen tail (Figure 1.1). Mutations to the ColQ domain have been shown to truncate the collagen anchor, causing defects in AChE function, leading to a CMS (Figure 1.2C+D) (Ohno *et al* 1998). Additionally, mutations to the catalytic triad of residues contained in the AChE active site result in a loss of enzymatic activity (Shafferman *et al* 1992).

1.2.4 Post-synaptic CMS

Post-synaptic CMSs account for the majority of all CMS cases (as reviewed by Engel *et al* 2015). While the nAChR facilitates neuromuscular transmission by opening a pathway for cations across the muscle cell membrane in response to ACh binding, other proteins implicated in CMS are localized to the post-synaptic membrane and are involved in the proper formation and maintenance of synaptic endplate structures.

The agrin-MuSK-LRP4 signaling pathway is responsible for the proper development of the neuromuscular junction, an especially important role being the clustering of nAChRs on the crests of junctional folds of the post-synaptic membrane (as reviewed by Zong & Jin 2013). Agrin is a proteoglycan secreted by growing motor neurons. Agrin forms a complex with the integral membrane protein LRP4 to activate MuSK receptors on skeletal muscle. Following MuSK activation, rapsyn proteins are then recruited to the site to initiate the process of nAChR clustering on the post-synaptic membrane (as reviewed by Zong, & Jin 2013). Some mutations in the proteins involved in this cascade alter their ability to interact with partners and thus hinder the formation of the multi-protein complex that is required to elicit the noted downstream effects (Maselli *et* al 2012; Maselli *et al* 2010; Ohkawara *et al* 2014). Other mutations reduce their expression, limiting the function of both the affected protein and its binding partners to limit development of the motor endplate (Xi *et al* 2017; Chevessier *et al* 2004). Several mutations result in degeneration or destruction of the motor endplate, impairing synaptic transmission.

There have also been diagnosed CMS cases involving mutations to other synapse-related proteins, including glycosylation-related enzymes, but many of these mutations are rare and have only been diagnosed in singular cases. It is likely that CMS-causing mutations to other synaptic proteins will be discovered in the future.

1.2.5 CMS subtypes caused by defects in the nAChR

Mutations to the nAChR account for most cases of post-synaptic CMS, with these mutations leading to loss of nAChR expression on the cell surface (primary nAChR deficiency) and/or impaired nAChR function. Mutations leading to impaired function are typically referred to as kinetic mutations and are further classified as either slow-channel or fast-channel mutations.

1.2.6 Primary nAChR deficiency

A number of CMS patients have been identified with "Primary nAChR deficiency", which arises from missense, nonsense, splice site, or promoter region mutations in any of the five genes that code for the different nAChR subunits (*CHRNA1*, *CHRNB1*, *CHRND*, *CHRNG*, and *CHRNE*) (Figure 1.2A+B). Mutations in the ε subunit of the human adult nAChR have the highest observed clinical frequency (as reviewed by Engel *et al* 2015). The higher frequency of these mutations is likely due to two factors. First, the fetal $\alpha_2\beta\delta\gamma$ nAChR is expressed during muscle development, so mutations in the adult ε subunit do not impact on the development of the neuromuscular junction but instead influence neuromuscular communication later in life. In contrast, mutations that prevent expression of the α, β, δ, or γ subunits are usually fatal prior to birth (Engel *et al* 1996). Second, the mutated ε subunit can be phenotypically rescued by the fetal γ subunit. Note that in adult muscle only approximately 10% of normal nAChR expression levels are achieved with the γ subunit substitution, meaning only about 10% of the normal amount of nAChRs are present on the surface on the cells of an affected patient. The fetal γ subunit also confers lower conductance and longer open times to the rescued nAChRs compared to the adult-type ε nAChRs, making it a suboptimal replacement for a mutated ε subunit (Mishina *et al* 1986).

1.2.7 Slow-Channel Syndrome

Mutations to the nAChR that lead to prolonged channel opening times and a slower signal decay compared to wild-type are referred to as slow-channel mutations (Figure 1.2E). A mutation

at or near the ligand-binding site could cause slow-channel syndrome by enhancing the binding affinity for ACh, thus decreasing the probability of release, prolonging the open duration of the channel (Sine *et al* 1995). A mutation does not necessarily need to be close to the ligand-binding site for it to substantially affect its properties, as is the case for the αN217K mutation in the M1 helix of the transmembrane domain, which causes a decrease in the rate of ligand dissociation with only minor gating effects (Wang *et al* 1997). Similarly, a mutation in the transmembrane domain could cause slow channel syndrome by increasing the stability of the open state relative to the closed state. Slow-channel syndrome mutations lead to excess signal transmission, and enhanced desensitization.

1.2.8 Fast-Channel Syndrome

Fast-channel syndrome results from shorter open channel durations and an accelerated decay of the endplate potential, leading to premature termination of neuromuscular transmission (Figure 1.2E). The fast channel syndrome is typically caused by a recessive fast-channel mutation in one allele along with a low-expresser mutation or null-mutation in the other allele, and rarely can be caused by two recessive fast-channel mutations. A mutation near the ligand-binding site in the ECD can cause fast-channel syndrome by decreasing the affinity of the receptor for ACh (Ohno *et al* 1996; Sine *et al* 2002; Shen *et al.* 2012). Mutations near the transmembrane domain can alter gating kinetics, destabilizing the open state of the channel, and also leading to a slowing of the opening rate and an acceleration of the closing rate (Wang *et al.* 1999). Both of these effects result in a lower probability of channel opening at physiological concentrations of ACh.

1.2.9 Treatment Options

A variety of treatments exist for the various forms of CMS, but the kind of treatment available depends on the specific cause of CMS of the afflicted individual (as reviewed by Engel *et al* 2015). For presynaptic CMSs such as ChAT-deficiency where there is insufficient production and release of ACh, pyridostigmine can be used as an AChE inhibitor, allowing ACh to reside in the synapse for longer to stimulate a greater number of nAChRs despite lower quantal release. Amifampridine (3,4-DAP) is a potassium channel-blocker, reducing potassium efflux from the pre-synaptic terminal, prolonging action potential duration. The use of amifampridine along with pyridostigmine is useful because it causes an increase of ACh released by the presynaptic terminal

(Engel 2007). The aforementioned drugs can be used to treat patients with primary nAChR deficiency, since elevated synaptic ACh levels can somewhat compensate for a decreased response to ACh caused by low nAChR numbers on the cell surface. Patients suffering from fast-channel syndrome would also benefit from the combination of these drugs, since both act to increase the concentration of ACh in the synapse, which would counter the effects of premature signal termination. For slow-channel syndrome, channel blockers are the main line of treatment, as the channels are open for too long and cause overstimulation and desensitization of the muscle cell. Fluoxetine, an antidepressant, and quinidine, a cardiovascular medication, are both able to block the nAChR ion channel and can be used to treat slow-channel syndrome, preventing excess stimulation of the nAChR (Fukudome *et al* 1998; Harper *et al* 2003). There is also more recent evidence that long-term treatment with fluoxetine can have neuroprotective effects through reduced subsynaptic DNA damage at endplates (Zhu *et al.* 2015).

1.3 nAChR Structure

The first visual structural determinations of the muscle-type nAChR were obtained from cryo-electron microscopy (cryo-EM) studies of the nAChR from *Torpedo marmorata*, an electric fish with a high concentration of fetal muscle-like nAChRs in its specialized electric organ (Unwin 1993). In 1993, Nigel Unwin produced a 9Å resolution cryo-EM structure of the *Torpedo* nAChR, which suggested that the five subunits of the muscle nAChR are assembled pseudo-symmetrically into a pentamer around a central axis pore. This structure revealed the rough positions of various secondary structural elements, but with much of the structural detail still unresolved. At the same time, residues involved in ligand-binding and gating were being identified rapidly through other biochemical and biophysical methods, as discussed below.

A major advance came in 2001, when a protein known as acetylcholine-binding protein (AChBP) derived from *Lymnaea stagnalis* was successfully crystallized and an x-ray structure at 2.7Å resolution was determined (Brejc *et al.* 2001). The AChBP, a non-channel homopentamer, is homologous to the extracellular domain of the nAChR, contains five ligand-binding sites, and shares approximately 24% sequence identity with the extracellular domain of the α7 nAChRs. This structure suggested that the extracellular domain from each subunit of the nAChR is composed primarily of ten β-strands and various connecting loops twisted into a β-sandwich conformation (Brejc *et al.* 2001). Using the AChBP structure, in 2003 Unwin's laboratory produced an atomic

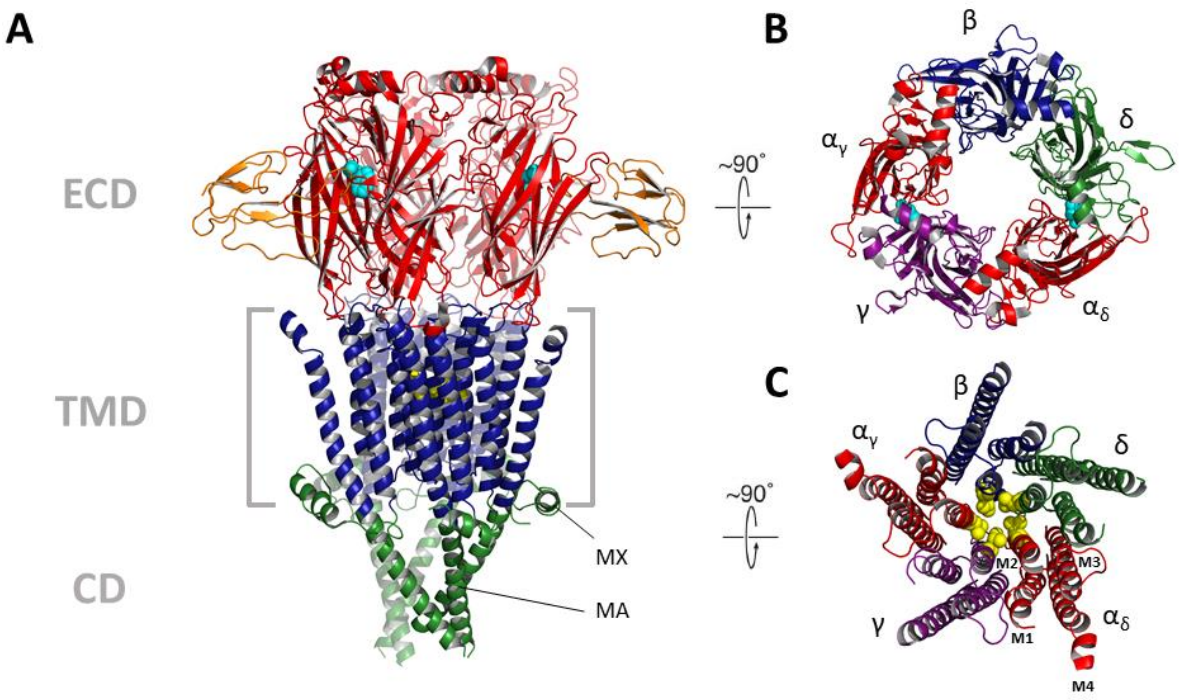

Figure 1.3: The Muscle-type nAChR. (A) Full-length structure of the closed-state muscle-type nAChR based on the cryo-EM structure of *Tetronarce califarnica* nAChR at 2.7Å resolution with bound α-BTX (PDB: 6UWZ). The nAChR is divided into the ECD (red), the TMD (blue) and the CD (green). The two α-BTX molecules are bound near the C-loops of the α subunits and are shown in orange. The brackets show the approximate dimensions of the plasma membrane and serve as a set of demarcation lines separating the domains. The cytoplasmic domain's amphipathic post-M3 helix is denoted as MX. The CD's MA helices are continuous with the TMD's M4 helices and form an inverted cone. **(B)** Top-down view of the ECD, showing the color-coded constitutive subunits. ACh makes an important cation-pi interaction with W149 (cyan spheres) when binding to the ECD, which is near the binding site at the α/γ-ε and α/δ interfaces. The α-BTX molecules were removed for clarity. **(C)** Top-down view of the TMD. Innermost are the M2 helices which form the channel pore and contribute five leucines (L9') that form the gate of the channel (yellow spheres). The M1 and M3 helices are adjacent to one another and are located behind M2 to shield it from the lipid environment. Outermost are the M4 helices which make extensive contacts with lipids of the plasma membrane.

model of the nAChR showing that the transmembrane domain has four membrane-spanning α-helices per subunit, labelled M1-M4, with M2 lining the channel pore, the M1 and M3 helices shielding the pore from lipids, and M4 being the most outwardly facing and extensively interacting with lipids in the membrane (Miyazawa *et al* 2003). In 2005 this model was refined to a resolution of 4Å (PBD: 2GB9). This higher resolution model clarified that the nAChR exhibits three domains: the extracellular domain (ECD) which contains the agonist binding sites, the transmembrane domain (TMD) which contains the permeation pathway and channel gate, and the cytoplasmic domain (CD) which consists of a disordered loop connecting to a long intracellular MA α-helix with the five MA helices forming an inverted cone (Unwin 2005) (Figure 1.3). The inverted cone contains fenestrations that link the channel pore to the cytoplasm to facilitate ion flow (Figure 1.3).

Recently, a new cryo-EM structure of the closed-state of the *Torpedo californica* (renamed *Tetronarce californica*) muscle nAChR bound to α-bungarotoxin (α-BTX) (PDB: 6UWZ) was published with an improved resolution of 2.7Å (Rahman *et al* 2020). The newer 2.7Å *Torpedo* structure revealed that M4 and MA form a single continuous helix (Rahman *et al* 2020). It also showed that there is a short amphipathic MX helix located just prior to M4 where it straddles the TMD-CD interface (Rahman *et al* 2020). With the emergence of the new 2.7Å structure of the full-length *Torpedo* nAChR, better modeling of the human muscle-type nAChR became possible.

1.3.1 The Agonist-binding Site

In both the fetal and adult muscle nAChR, there are two agonist binding sites per pentamer, with the binding sites located in the ECD, at the interfaces between α and both γ/ε and δ subunits. The α subunit, termed the principal face, and a non-α subunit, either the δ and γ/ε subunits termed the complementary face form the αδ and αε/αγ agonist sites respectively, while the β subunit is not involved in ligand-binding. The principal face of each binding site contributes residues critical for ligand binding from three distinct loops termed loops A, B and C, and the complementary face also provides such residues in loops D, E, and F (Figure 1.4). These loops line the binding site with several highly conserved hydrophobic and aromatic residues that contribute to agonist binding. Aromatic ligand-binding residues from loops A, B, C, and D form an 'aromatic box' that chelates the ammonium group of ACh (Brejc *et al* 2001; Celie *et al* 2004). One of these residues, αW149, located on loop B is especially important to function as it forms a direct cation-π

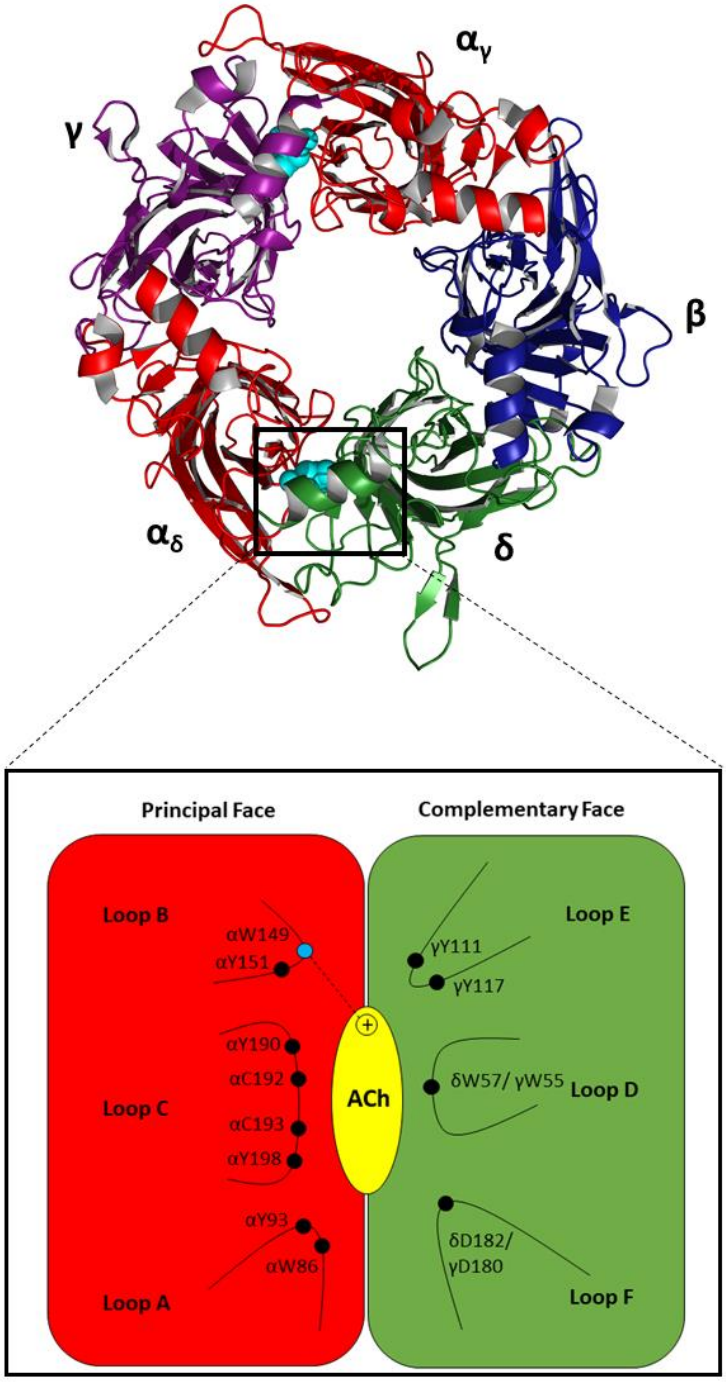

Figure 1.4: The Agonist-Binding Site. The ECD contains two agonist-binding sites that are located at the interface of a principal subunit (α) and a complementary subunit (δ or γ/ε). Ligand-binding residues are located on Loops A, B and C of the principal subunit and loops D, E, and F of the complementary subunit. The αW149 residue which makes an important cation-π interaction (dotted line) with the quaternary ammonium group of ACh is labelled as cyan spheres in the top panel and as a cyan circle in the bottom panel. Ligand-binding residues provided by the complementary face of the binding site depend on subunit identity.

interaction with the quaternary amine of ACh (Zhong *et al* 1998). Other principal and complementary face residues shown in Figure 1.4 are crucial in shaping the ACh-binding pocket and coordinating ACh into a stable orientation within the pocket.

1.3.2 The ECD-TMD Coupling Interface

The ECD and TMD are separated by a network of loops connecting the two domains which allows for the action of agonist-binding in the ECD to be transmitted to the channel gate in the TMD. The ECD and TMD are covalently connected in each nAChR subunit by the extracellular β10 strand and the pre-M1 α-helix loop in the TMD. Residues that make up the ECD-TMD interface are provided by three loops from the ECD (β1-β2 loop, the β6-β7 (Cys)loop, β8-β9 loop) and one linker from the TMD (M2-M3 linker). A study using nAChR chimeras showed that not only are specific residues in the ECD-TMD interface necessary for coupling of binding to gating, but also that the compatibility between the ECD and TMD is dependent on the specific identity of those residues (Bouzat *et al* 2004). The study showed that chimeras formed from the ECD and TMD of different pLGICs are functional, suggesting similar gating mechanisms in different pLGICs, and the identity of the specific coupling residues at the interface likely impart each pLGIC with different gating kinetics.

1.3.3 The Channel Pore

The channel pore provides a pathway across the membrane for cation permeation and contains the channel gate, which controls the movement of cations across the membrane. The pore is located along the central axis of the TMD and lined primarily by the five M2 helices (Miyazawa *et al*. 2003; Unwin 2005; Rahman *et al* 2020). Residues along the M2 helices are identified by a 'prime' numbering system in which the number 0 denotes a conserved lysine residue in each subunit near the bottom of the M2 helix, with increasingly positive prime numbers denoting residues towards the extracellular surface (Miller 1989).

The channel pore is lined by three rings of polar and negatively-charged residues which determine the charge selectivity of the nAChR, with two of these rings located near the extracellular surface (20' and 24' positions), and one ring located near the intracellular surface of the pore (-1') (Figure 1.5). The 20' and -1' charge selectivity residues are located directly on M2, while the 24' residues are located on the M2-M3 linker (Rahman *et al* 2020). The polar and

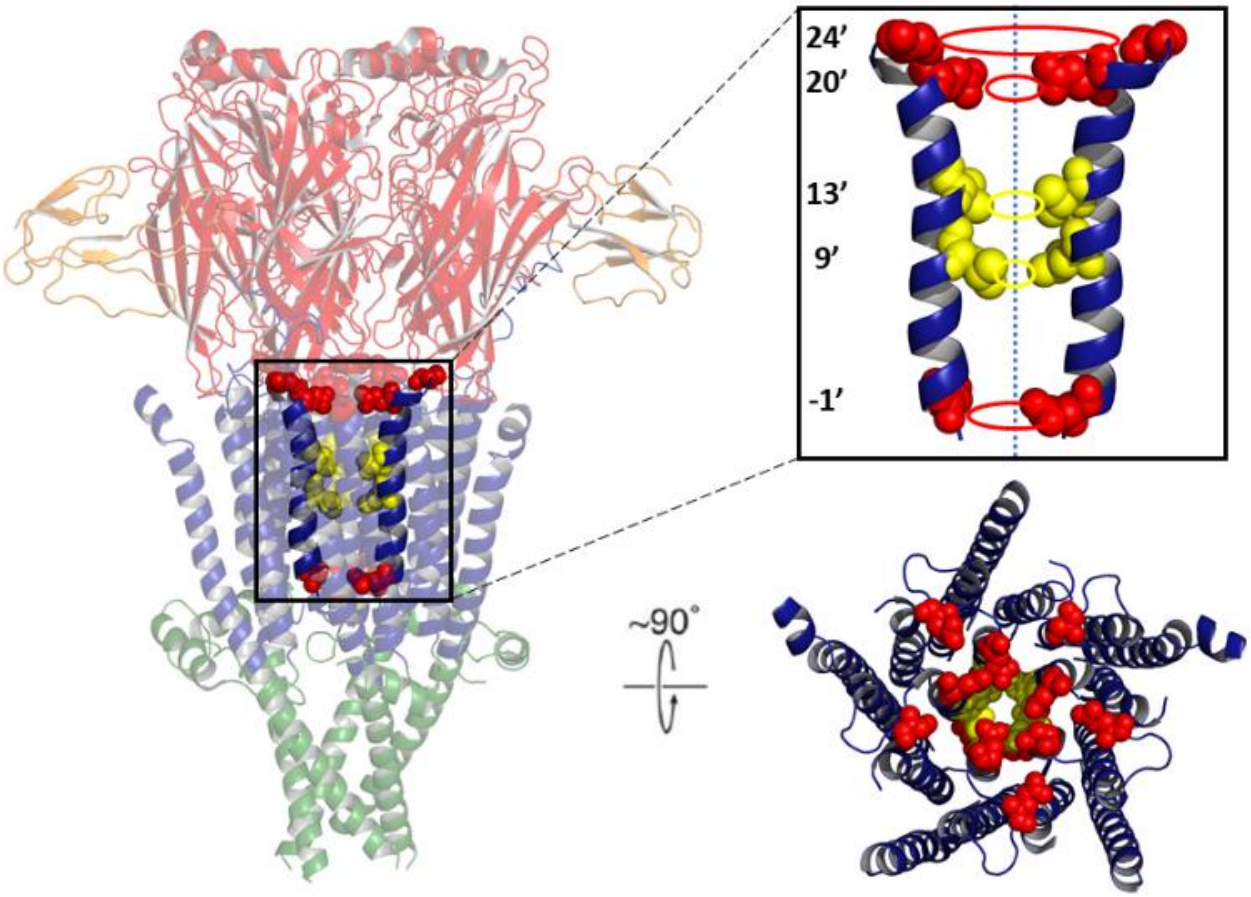

Figure 1.5: The Channel Pore. Within the TMD, five M2 helices are arranged in a circular pattern to form the ion channel pore. The two highlighted α-helices are the innermost M2 helices of the α subunits to show the distribution of rings of residues that contribute to gating, ion selectivity, and the physical pore profile. In the right panel, the β, δ, and γM2 helices have been removed for clarity. Both ends of the pore are flanked by rings of charged residues (red spheres) that make up the selectivity filter with the 20' and 24' rings near the extracellular end and the -1' ring located near the intracellular end. The central part of the pore contains two rings of hydrophobic residues, L9' and V13' (yellow spheres) which control the flow of ions through a hydrophobic gating mechanism.

negatively charged residues in the rings serve to concentrate cations near the extracellular and intracellular ends of the channel pore and to promote selective passage of cations (Imoto *et al* 1988). Results from initial experiments aimed at deciphering the location of the gate initially suggested that it is located near the 9' and 13' residues (Unwin 1993; White & Cohen 1992; Blanton *et al* 1998) or possibly more intracellularly (Akabas *et al* 1994; Wilson & Karlin, 1998). Later studies, however, identified the five highly conserved leucine residues at the 9' position (L9') as the most likely candidate for the gate as these residues form the most constricted part of the pore in the closed state (Miyazawa *et al* 2003; Unwin 2005; Rahman *et al* 2020). The L9' residues also appear to widen the most upon ACh-binding (Unwin & Fujiyoshi, 2012). Above the 9' position is another ring of conserved valine residues located at the 13' position. Together, these two rings of leucine (L9') and valine (V13') residues create a tapering hydrophobic environment that renders ion passage energetically unfavorable in the closed state (Beckstein & Sansom 2006; Shen *et al* 2016) (Figure 1.5).

1.4 Agonist-induced Gating

A key feature of the gating mechanism is that the binding of ACh in the ECD initiates a conformational change in protein structure that causes the TMD channel gate to open, allowing cation permeation across the membrane. An understanding of the gating mechanism and the chemical properties of the channel gate is crucial to understanding how pore-lining mutations distort channel function and lead to CMS.

The action of ACh-binding in the ECD is communicated over a distance of about 60Å to the channel gate in the TMD, presumably involving the precise movements of hundreds of residues. It was initially debated whether gating occurred through concerted movements of all these residues at once, or whether a different mechanism was at play. A 2000 study using a rate-equilibrium free energy relationships (REFER) analysis was performed on the muscle-type nAChR. The REFER analysis provides a snapshot of where along the reaction path from the resting (R) to the open (O) state a residue at a specific site exists at the R-to-O transition state. The REFER analysis yields phi (Φ) values, with Φ values of =1 indicating that the studied residue is already in an open conformation at the transition state, and Φ = value of 0 indicates that the residue remains in R at the transition state (Grosman *et al* 2000). The analysis showed that residues near the agonist-binding site have Φ values near 1 indicating that they are already in an open-like conformation at

the R-to-O transition state, while residues located near the channel gate have Φ values near 0.2, suggesting that they remain in a closed-like confirmation at the R-to-O transition state. A gradient of Φ values between 1 and 0.2 was observed for residues along the physical pathway between the agonist site and channel gate. These results suggest that the gating transition occurs via a 'conformational wave', starting with residue movements near the agonist-binding site and progressively radiating to the lower portions of the receptor in a 'wave-like' manner.

To understand how the conformational change is transmitted from the ECD to the channel gate, researchers generated a chimera consisting of the AChBP fused to the transmembrane region of the $5HT_{3A}$ receptor in order to elucidate if (1) the chimera would still be able to function in coupling binding to gating, and if so (2) which residues strongly contribute to coupling binding to gating (Bouzat *et al* 2004). Initially, the chimera did not elicit any detectable ACh-induced currents, suggesting that the interface between the two domains was incompatible. However, upon switching out the AChBP residues in 3 of its loops (β1-β2 loop, Cys-loop, β8-β9 loop) with their $5HT_{3A}$ counterparts, the resulting new chimera was able to elicit ACh-induced current, demonstrating a successful coupling of agonist binding to channel gating. The compatibility of the two domains from different receptor types also suggests similarities in pore-opening mechanisms among pLGICs. Additionally, a 2005 study was published revealing a 'principal pathway' linking agonist binding to channel gating through interactions between residues of the loops near the ECD-TMD interface (Lee & Sine 2005). The researchers identified several residues at the ECD-TMD interface that were strongly coupled and had a strong influence on gating function, suggesting that these residues were involved in transmitting the action of ligand-binding into channel gating. The emergence of the new 2.7Å *Torpedo* structure, however, provides a new template for interpreting the 2005 study. Specifically, residues originally thought to participated in the ECD/TMD interface were displaced from the interface in the new structure.

1.4.1 Hydrophobic Gating

While many ion channels contain a physical gate acting to sterically hinder the permeation of ions across the channel in the closed state, the nAChR contains a different kind of gate. Specifically, residues originally thought to participated in the ECD/TMD interface were displaced from the interface in Rahman *et al*'s newer 2.7Å resolution *Tetronarce* structure (2020) compared to Unwin's 4Å resolution *Torpedo* structure (2005). It was later revealed that the pore in the closed

state has a radius of approximately 3.5Å, which is larger than the dehydrated radius of a cation such as K^+ or Na^+ (Miyazawa *et al* 2003). However, the radius of the closed pore is too small to allow a cation with its first hydration shell through, and in the absence of hydrophilic groups that can compensate for the loss of water, crossing the hydrophobic L9'/V13' region is energetically unfavorable. Therefore, rather than occluding ion flow as a physical barrier in the closed state, the channel gate instead presents an energetic barrier to permeation (Figure 1.6).

The properties of such a gate were explored extensively in a 2001 molecular dynamics (MD) simulation by Beckstein *et al*. A strong line of evidence providing information related to hydrophobic gating comes from ever-improving molecular dynamics (MD) simulations. At the current time, MD simulations are often restricted to the nanosecond timescale mainly due to current computing power. But these simulations represent the best way to visualize what is happening in the channel pore on a molecular level and have been shown to provide useful information in assigning functional states to structures. The 2001 MD simulation run by Beckstein *et al* established that fixed-width nanopores could be hydrophobically gated by tuning the hydrophobicity of the pore walls such that beyond a certain hydrophobicity threshold, water molecules could no longer cross the pore. The width, length, and hydrophobicity of the nanopore were key factors in the gating process. However, the researchers weren't sure whether the mechanism was applicable to biological ion channels.

Prior to performing an MD simulation on a model based on the nAChR M2 bundle, another nanopore MD study was conducted to highlight the role of pore geometry and surface chemistry in influencing the gate's permeation characteristics (Beckstein & Sansom 2004). This study showed that when the pore wall was tuned to be highly hydrophobic, water molecules remained stuck in the upper portion of the pore in a vapor state, unable to pass through, and that by increasing the polarity of the pore wall through a high density of local charges, this increases the probability of the pore becoming water filled. Subsequently, to test whether a hydrophobic gating mechanism was plausible for the nAChR channel pore, the researchers generated another MD simulation that consisted of the bundle of 5 M2 helices to simulate the nAChR pore. When they tested whether an artificially induced constriction of radius 3.5Å at the L9', V13', and V17' (L17' in non-α) positions was sufficient to prevent the permeation of sodium ions across the membrane, they found that at this radius, the nAChR was functionally closed and did not allow cation permeation (Beckstein &

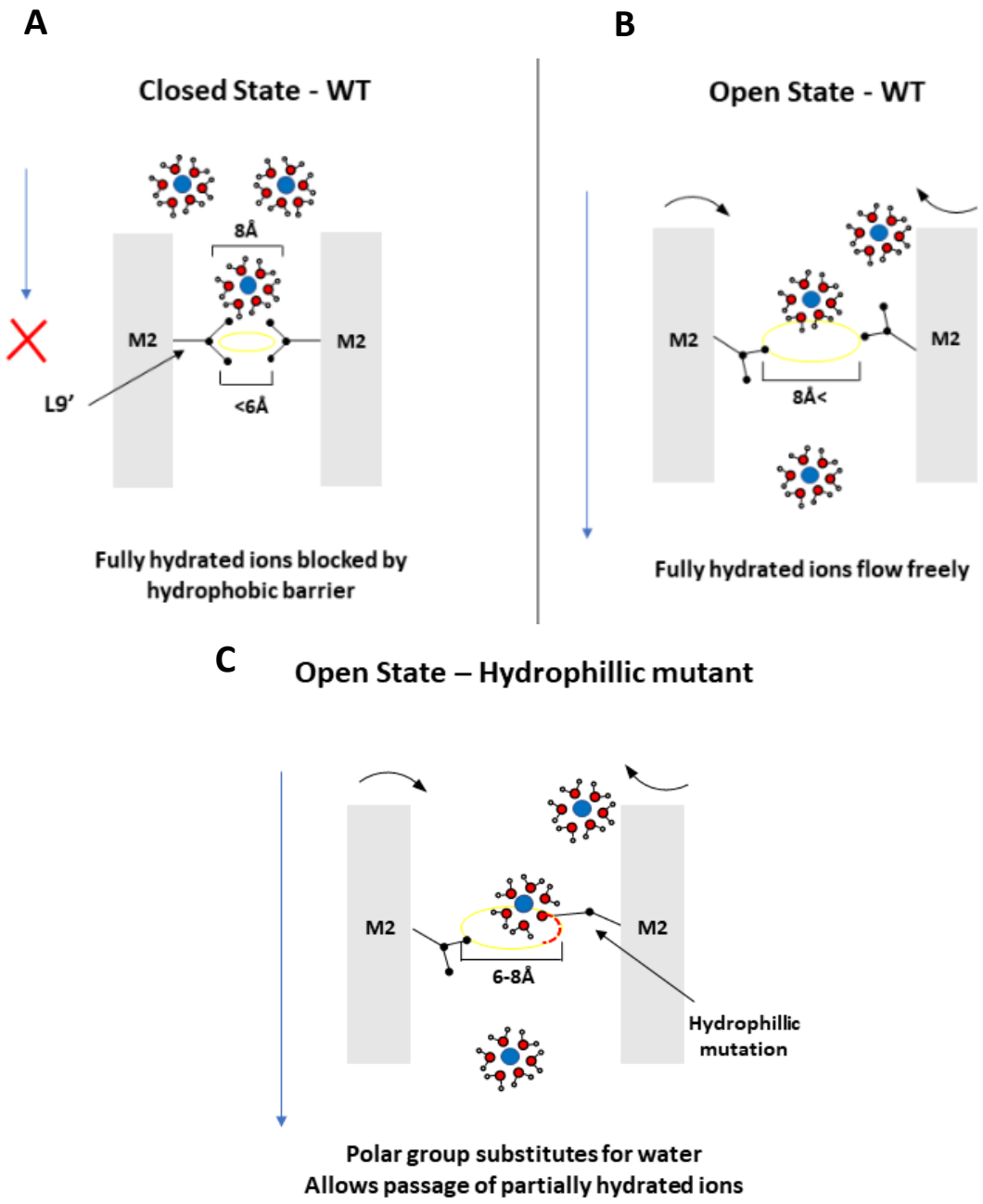

Figure 1.6: Hydrophobic Gating Mechanism. (A) In the closed state of WT nAChR, the L9' residues form a constriction in the pore of about 6Å wide, which is larger than the diameter of a dehydrated Na^+ or K^+ ion, but the ion's effective diameter is in fact 8Å due to the highly ordered shell of water molecules surrounding it. This presents an energetic barrier to ion permeation. **(B)** With movement of the M2 helices, the pore widens and the cations are now able to pass through the pore with their hydrations shells intact. **(C)** For a nAChR with a pore-facing hydrophilic mutation introduced near the gate, it is plausible that the hydrophilic functional groups of the mutant residue can compensate for the loss of water molecules around the cation. This proposed effect may allow for the passage of partially hydrated ions and alter the shape and chemistry of the mutated gate.

Sansom 2006). This simulation showed that a 3.5Å-radius constriction at any of these hydrophobic positions along the pore could theoretically prevent ion permeation by making it energetically unfavorable for ions to cross the barrier while retaining their first hydration shells. Thus, such a channel could be functionally annotated as closed. Extrapolating from this study, a channel gate rendered more hydrophilic by a mutation could possibly allow partially-hydrated ions to pass through due to the hydrophilic side chain interacting with a passing cation, substituting an interaction with a water molecule. An illustration describing this possible mechanism is shown in Figure 1.6.

1.5 CMS-causing mutations in the channel pore

CMS-causing mutations have been discovered in all subunits of muscle-type nAChR and in all three of its domains (as reviewed by Engel *et al* 2003). Mutations that lead to primary nAChR deficiency are distributed throughout the three domains and have been found in all subunits, although as noted above, the vast majority are found in the ε subunit. Mutations that lead to fast-channel CMS have been found in all subunits except β, and are mostly located in the ECD near the agonist-binding site or near the ECD-TMD interface (Figure 1.7). In contrast, many mutations that lead to slow-channel CMS are located in the TMD (Figure 1.8). Furthermore, a large proportion of these are found on the pore-lining M2 helices with those on the α, δ, and γ/ε subunits interacting with residues on the adjacent M1 and M3 helices or the neighboring M2 helices of other subunits (Rahman *et al* 2020), and those on the β subunit facing the channel lumen. Specifically, slow-channel CMS-causing mutations in the β subunit have been found at L9' and V13' positions (Engel *et al* 1996; Gomez *et al* 1996; Shen *et al* 2016) which as noted, are highly conserved residues though to form the channel gate. The specific CMS-causing mutations at these two critical sites in the nAChR are discussed in more detail below.

1.5.1 Pore-lining mutations as a probe of channel function

To gain more insight into the mechanisms by which mutations in the channel gate influence nAChR function and lead to CMS, researchers have explored in different studies how different physico-chemical properties at the 9' and 13' positions influence channel function. Several such studies used an electrophysiology method called TEVC (Two-Electrode Voltage Clamp), an instrument that allows the measuring of the whole-cell currents of *Xenopus* oocytes in response to

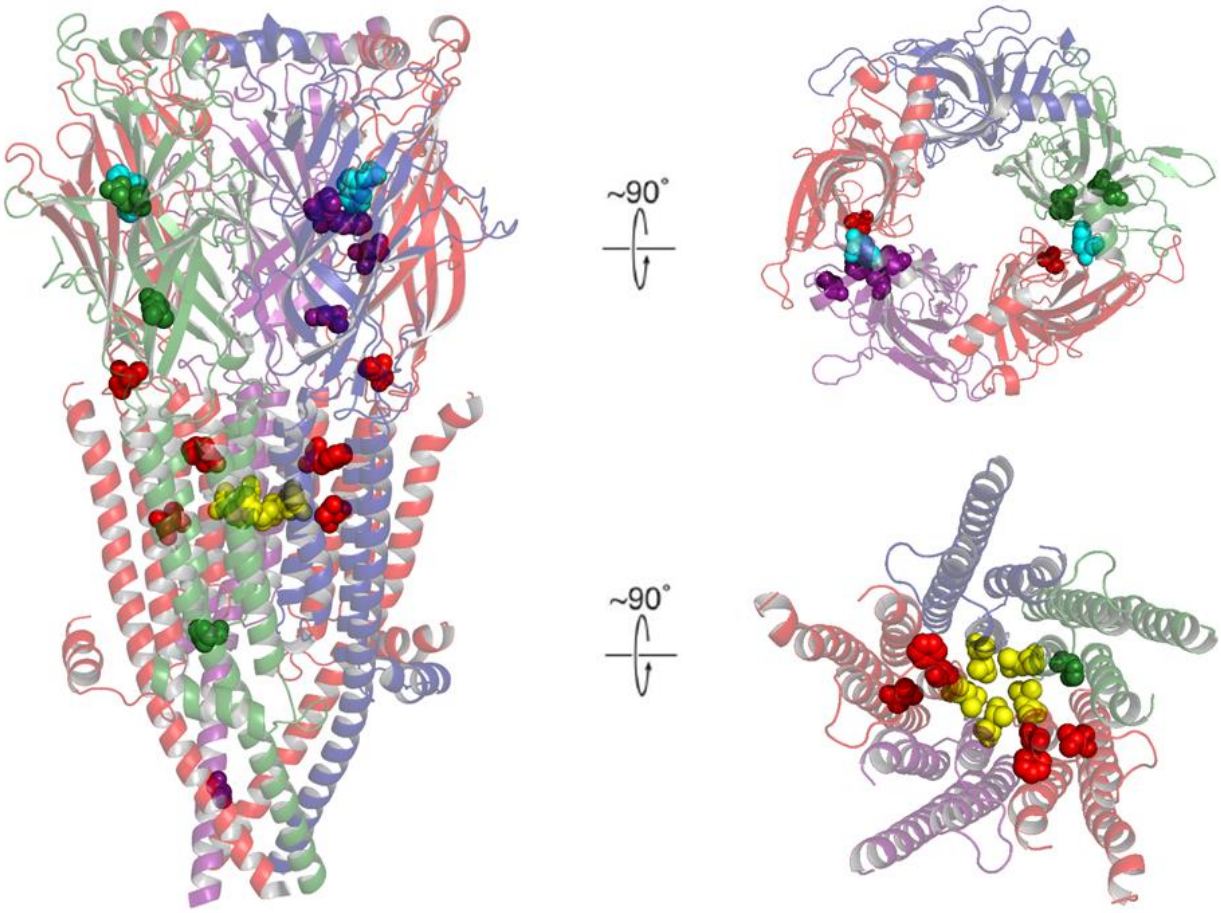

Figure 1.7: Known Fast-Channel mutations. This human homology model was made using SWISS-MODEL, based on the 2.7Å resolution 6UWZ structure shows mutations that have been found to cause a fast-channel CMS, leading to a decrease in channel open time and accelerated signal decay. These mutations are mostly found in the ECD of subunits near the agonist-binding sites and near the ECD-TMD interface. The residue mutation sites implicated in fast-channel CMS are shown as color-coded spheres according to the identities of the subunits carrying them: the α subunits and associated mutations are shown in red, β in blue, ε in purple, and δ in green. The cyan spheres highlight the αW149 residues which make an important cation-pi interaction with ACh, approximating the location of the agonist-binding site, and the yellow spheres highlight the five L9' residues, representing the channel gate.

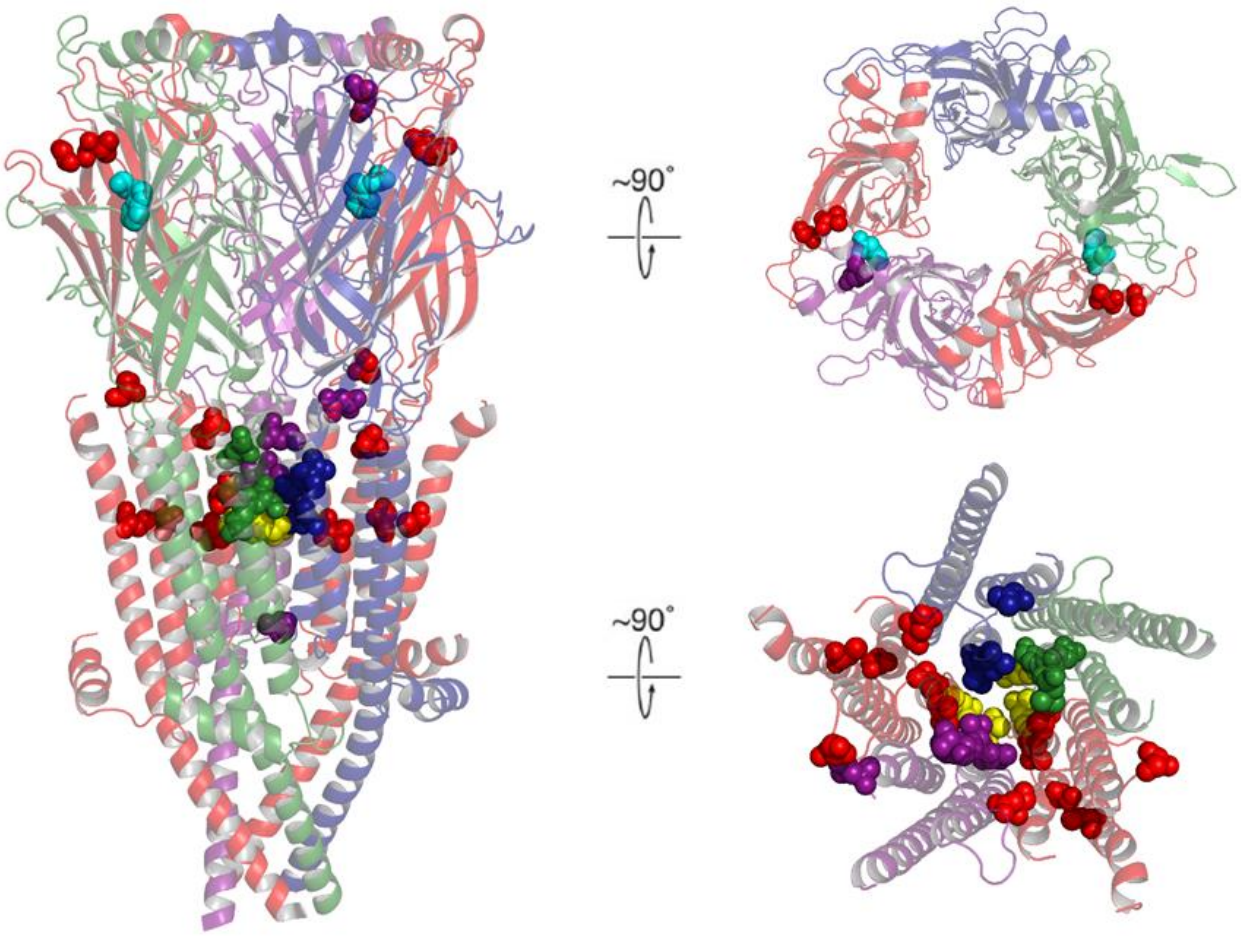

Figure 1.8: Known Slow-Channel mutations. This human homology model was made using SWISS-MODEL based on the 2.7Å resolution 6UWZ structure shows mutations that cause a slow-channel CMS, leading to an increase in channel open time and prolonged signal decay. Most of these mutations are found in the TMD, and of those found in the TMD, most are located on the M2 helix. These slow-channel pore-lining mutations are thought to face adjacent helices in the α, δ, and ε subunits while the β subunit mutations mostly face the channel lumen. The residue mutation sites implicated in slow-channel CMS are shown as color-coded spheres according to the identities of the subunits carrying them: the α subunits and associated mutations are shown in red, β in blue, ε in purple, and δ in green. The cyan spheres highlight the αW149 residues which make an important cation-pi interaction with ACh, approximating the location of the agonist-binding site, and the yellow spheres highlight the five L9' residues, representing the channel gate.

increasing concentrations of agonist by holding the membrane potential at a pre-determined constant voltage. From the agonist-concentration response, the concentration of agonist required to elicit a half-maximal response, EC_{50} is determined. This value depends on both agonist affinity and the gating equilibrium constants that govern the coupling of agonist-binding to channel-gating. A mutation-induced increase in EC_{50} relative to wild-type means that the mutation requires a higher concentration of agonist to elicit an equivalent half-maximal concentration-response. This change could reflect a decrease in the affinity of the nAChR for agonist, or a reduced ability to couple binding to gating as a result of an energetic stabilization of the resting over the open state. In contrast, a mutant-induced decrease in EC_{50} means that a lower concentration of ACh is needed to elicit a half-maximal response relative to wild-type, which could be due to an enhanced affinity of ACh for its binding site or an augmented ability to couple agonist-binding to channel gating as a result of an energetic stabilization of the open state over the resting state. Thus, when EC_{50} is increased by a mutation, a channel's function is said to be impaired, but when EC_{50} is lowered by a mutation, channel function is said to be enhanced. Given that the mutations discussed here are located in the channel pore and are thus physically distant from the agonist sites, changes in EC_{50} *likely* reflect altered coupling of agonist binding to channel gating.

In 1991, a study was conducted on homomeric chick brain α7 nAChRs in which the L9' residue was mutated to a series of hydrophobic and polar residues and channel function was assessed by measuring whole-cell and single channel responses to ACh (Revah *et al* 1991) (Figure 1.9). This study showed that while mutations to the pore altered channel function, the polar mutations (especially L9'T) had the most pronounced effect by altering the rates of desensitization and by reducing the concentration of ACh needed to elicit channel opening, thus decreasing EC_{50}. The authors noted that the effects of hydrophobic substitutions on channel function were less severe compared to polar mutations, suggesting that the hydrophobic character of the native L9' residue contributes to the restriction of ion permeation and desensitization functions.

Following this development, a series of important mutations at the L9' positions were studied in other nAChRs to further explore how the physico-chemical properties of these channel gate residues influence function, and how different types of mutations at these conserved sites disrupt normal channel gating. Two similar studies performed in 1995 tested the effects of substituting polar residues for L9' in the mouse muscle fetal nAChR on channel function (Filatov & White

1995; Labarca *et al* 1995). One study showed that the δL9'T and γL9'T mutations individually shifted the dose-response relationship towards lower concentrations, thus reducing the concentration of ACh necessary to elicit channel opening, and that the simultaneous mutations shifted the relationship in an additive manner, suggesting that each mutation affected channel function independently (Filatov & White 1995). A second study using mouse fetal nAChR tested the effects of L9'S mutations in each of the nAChR subunits, first individually and then in combination, eventually testing the effects of all five L9'S substitutions simultaneously (Labarca *et al* 1995). The results showed that a single L9'S mutation shifted the dose-response relationship to the left by about 10-fold, regardless of which subunit was mutated (Figure 1.9). Compared to the dose-response curve of the WT-nAChR, a left-shift of the dose response curve signifies that a smaller concentration of agonist is required to elicit the same response (gain-of-function), while a right shift signifies that larger concentrations of agonist are required to elicit the same response (loss-of-function). Furthermore, the study showed that each subsequent L9'S mutation introduced into the nAChR shifted the dose-response further to the left by another 10-fold, with two mutations causing a 100-fold gain-of-function, three mutations causing a 1000-fold gain of function and so on until the maximum of five mutations. The implications of these findings are that the L9' residues were important for normal gating function and that each L9' residue contributes to channel gating independently and symmetrically.

A year later in 1996, a more extensive study was conducted on mouse fetal nAChR in which the L9' residues of each subunit were individually mutated to a series of natural and unnatural amino acids (Kearney *et al* 1996). The researchers wanted to study how altering residues that supposedly moved during gating affected channel function. They tested the effects of changing L9' side chain volume and polarity on channel function through the introduction of additional methyl group to enhance side chain volume and the introduction of hydroxyl groups to increase the polarity of the region. The results showed that the effect of increasing side chain volume at L9' led to receptors with higher EC_{50}s requiring more ACh relative to WT to achieve half-maximal activation, while the addition of polar functional groups to the L9' position produced a decrease in EC_{50}, requiring less ACh for activation and thus leading to the stabilization of the open state relative to the resting state (Figure 1.9). It was also noted that the introduction of stereoisomers (isoleucine vs. *allo*-isoleucine) also caused a change in channel function relative to wild-type, which shows the importance of precise orientation for optimal channel function. These results

A

Mutant	EC50 (μM)	Fold-change
α7 WT	115	N/A
α7 L9'F	30	3.83
α7 L9'V	6.2	18.6
α7 L9'S	0.8	144
α7 L9'T	0.7	164

B

# L9'S Mutations	Mutant	EC50 (μM)	Fold-change
0	WT	24.0	N/A
1	α	1.29	18.6
	β	0.531	45.2
	δ	1.91	12.6
	γ	0.486	49.4
2	α+α	0.202	119
	β+γ	0.050	480
	β+δ	0.208	115
	γ+δ	0.043	558
3	α+α+β	0.010	2400
	α+α+γ	0.015	1600
	α+α+δ	0.008	3000
	β+δ+γ	0.010	2400
4	α+α+β+δ	0.002	12000
	α+α+γ+δ	0.002	12000
5	α+α+β+γ+δ	<0.001	<24000

C

Mutant	EC50 (μM)	Fold-change
WT	50	N/A
βL9'I	28	1.79
δL9'I	15	3.33
γL9'I	77	0.65
βL9'V	18	2.78
δL9'V	35	1.43
γL9'V	35	1.43
βL9'S	1.5	33.3
δL9'S	1.2	41.7
γL9'S	4.5	11.1

Figure 1.9: EC_{50} data from past L9' mutagenesis studies. (A) Data from the Revah *et al* 1991 study on homomeric α_7 receptors. The study showed that polar mutants were more 'sensitive' to ACh than nonpolar mutants. **(B)** Data from the Labarca *et al* 1995 study on mouse muscle-type fetal receptors. The data suggested that L9'S mutations potentiate channel function equally and through independent mechanisms. **(C)** Data from the Kearney *et al* 1996 study on mouse muscle-type fetal receptors. The study highlighted the differences in EC_{50} change caused by polar substitutions as compared to nonpolar substitutions.

aligned with those of the previous studies, showing that the distinct chemical environment surrounding the L9' position has a strong influence on channel gating, with hydrophobic substitutions affecting channel function less and polar substitutions enhancing channel function more by comparison.

Furthermore, a number of mutations at the L9' and V13' positions lead to CMS. In the same year as the Kearney *et al* study (Kearney *et al* 1996), a human patient was diagnosed with a severe CMS caused by a leucine-to-methionine substitution at the βL9' position (Gomez *et al* 1996). The βL9'M mutation resulted in an 8-fold increase in channel open time compared to wild-type and caused extensive remodeling of the post-synaptic membrane. While methionine is a hydrophobic substitute, which may be better tolerated than a polar mutation at the gate, the macroscopic effects of even subtle changes to nAChR function in a human can still be severe.

In a 2016 study by Shen *et al*, multiple diagnosed pore-lining mutations to the 13' position were shown to cause CMS. The βV13'A and εV13'A mutations were shown to increase channel open times fourfold and increase 'gating efficiency' by 30-fold. When the researchers applied V13'A mutations to the α and δ subunits, channel open times increased four- and eight-fold respectively, keeping in mind there are two α subunits per receptor. This suggests that each valine in the V13' ring contributes to channel gating equally, a finding that shows similarities to findings from Labarca *et al*'s 1995 study focusing on the L9' ring which suggested that each L9' residue contributed to channel gating equally and symmetrically (Figure 1.9).

Recently, an αL9'R mutation was diagnosed in a human patient that allows the conduction of chloride at positive potentials, thus transforming the nAChR from a cation- to an anion-selective ion channel (Cetin *et al* 2019). This was the first recorded instance of a charged residue replacing the native leucine at the L9' position. Intuitively, the mutation would be expected to have very grave consequences on both the channel at the molecular level and the human patient compared to a mutation in a similar location that is closer in its chemical properties to the native leucine residue, such as the βL9'M mutation. However, while the patient harbouring the αL9'R mutation presented with motor difficulties since birth, the patient was still able to walk at age 14 while the patient harbouring the βL9'M mutation in the 1996 Gomez *et al* study was wheelchair-bound by age 13. Despite the mutation causing reduction in current amplitude of over 96%, the patient harbouring the αL9'R mutation still had approximately 25% of functional wild-type receptors, blunting the

deleterious impact of the mutation. These differences in pathologies highlight an important gap in our knowledge regarding how specific mutations exert their effects on channel function and potentially lead to CMS. This thesis seeks to address this gap in knowledge.

1.6 Thesis Objectives

My interest in L9' mutations stems from three observations. First, the functional effects of mutations at the L9' location show that the side chain chemistry at this position in all subunits of the fetal muscle nAChR has a huge impact on channel function, with L9'S mutations additively leading to an incredible 10^5-fold gain of function. The L9' position is far from the agonist-binding site, so the functional effects of these mutations are not likely a result of altered agonist-affinity. Instead, they likely reflect a change in coupling of binding to gating. Understanding how these mutations influence function should thus provide valuable insight into the mechanisms underlying channel gating. Second, as a number of mutations at the L9' position lead to CMS, understanding how changes in side chain chemistry influence nAChR function will provide insight into the molecular basis of this potentially devastating disease. Finally, preliminary data (unpublished) from the Baenziger lab had shown that βL9'S and δL9'S mutations in the adult muscle nAChR lead to gains in function of 116-fold and 37-fold, respectively, not the 10-fold gains-of-function expected based on the Labarca *et al* study with fetal muscle nAChRs. Furthermore, the αL9'S mutation did not express, while the βL9'S/δL9'S double mutant led to only a 246-fold gain-of-function, much less than the 4315-fold gain-of-function expected if the mutations are independent and thus additive, again as was suggested for the fetal nAChR. Our preliminary data thus suggested that the human adult nAChR may have a different network of inter-residue interactions involving L9' than the mouse fetal nAChRs.

To understand better how L9' mutations in the adult muscle nAChR influences channel function and thus cause CMS, I have performed a comprehensive mutant screen of all L9' residues in each subunits of the human adult muscle-type nAChR (methods in Chapter 2). I generated 19 different L9' mutations consisting of every possible natural amino acid substitution in each subunit, for a total of 76 unique mutations. Using electrophysiology, I have assessed how side chains volume, polarity, and hydrophobicity influences channel function (Chapter 2). I also probed in more detail the mechanisms by which the L9' residues from each subunit contribute to the energetics of channel function (Chapter 3). Specifically, I used a mutant cycle analysis to estimate

how interaction between L9' and adjacent residues contributed to the relative stabilities of the resting and open states to influence channel gating. My findings are discussed in the context of our current understanding of the mechanisms of channel gating (Chapter 4). I also speculate how this new insight could possibly assist in future pharmacological therapy.

Chapter 2

Functional effects of side chain size and polarity at the pore-lining 9’ position

2.0 Introduction

The overarching goal of my thesis is to understand how mutations at the L9' position alter channel function and thus lead to CMS. While many CMS-causing mutations have been identified in the TMD, few of them directly face the channel pore. The pore-facing mutations that have been characterized, βL9'M (Gomez *et al* 1996) and αL9'R (Cetin *et al* 2019), show clear differences in both their effects on channel function and their pathologies in humans. In fact, the highly polar αL9'R mutation has less severe effects on human health than the relatively conservative hydrophobic βL9'M mutation. On the other hand, preliminary studies suggest that polar L9' substitutions enhance channel function more than hydrophobic substitutions (Revah *et al* 1991), although the effects of a given mutation on channel function depend on the specific subunit carrying the mutation (Kearney *et al* 1996). These preliminary findings suggest that a comprehensive characterization of the effects of L9' substitutions on channel gating is clearly required to fully understand the role of these key residues in channel function.

Based on these previous observations, I hypothesized that both the nature of the substituted residue and the affected subunit likely play a role in tailoring the effect of each mutation on channel function. In order to better understand the functional role of each L9' residue in the human adult nAChR, I changed the L9' residue of each subunit to every naturally-occurring amino acid substitution (i.e. other than the wild-type leucine), resulting in a total of 76 different engineered mutations. My functional characterization of these mutants showed that in the α, β, and ε subunits, substitutions at the L9' position that are relatively similar in terms of size and hydrophobicity to the native leucine typically led to mild gain-of-function phenotypes. Polar and charged substitutions typically led to moderate-to-large gains-of-function. In contrast, I found that many polar L9' substitutions in the δ subunit had relatively little effect on channel function. The data suggest that while the microenvironments surrounding each 9' position influence the impact of a particular mutation on channel function, the size and hydrophobicity of the wild-type L9' side chains are optimized to produce ideal gating characteristics for the muscle-type nAChR to fulfill adult human physiological motor functions.

2.1 Materials and Methods

2.1.1 Mutant cRNA Design

Wild-type human α1, β1, δ, and ε nAChR-pRBG4 clones were kindly provided by Steven Sine. The nAChR subunit DNA was transferred from pRBG4 into the pcDNA3 vector as an EcoRI fragment. The α1, β1, δ, and ε nAChR-pcDNA3 was linearized with XhoI and capped cRNA was produced by *in vitro* transcription using the mMESSAGE mMACHINE® T7 kit (Ambion). The concentration of cRNA was determined at Abs260 and the integrity of the RNA was determined by agarose gel electrophoresis. All mutants were created using QuikChange™ Site-Directed Mutagenesis kits (Agilent) and verified by sequencing using the forward T7 and reverse Sp6 promoters.

2.1.2 Oocyte Preparation

Xenopus laevis frogs were obtained and their oocyte lobes were surgically removed and harvested. *Xenopus* oocyte lobes containing stage V-VI oocytes were cut into smaller pieces, placed into a petri dish and treated with a mixture of collagenase B and trypsin inhibitor (Sigma-Aldrich) dissolved in ND96 buffer (5 mM HEPES, 96 mM NaCl, 2 mM KCl, 1 mM $MgCl_2$, 2 mM pyruvate), and supplemented with antibiotics (10ml/L penicillin/streptomycin, and 50mg/mL Kanamycin). The process, known as defolliculation, degrades the collagen-rich extracellular connective tissue in which the oocytes are embedded and releases individual oocytes from the lobes. The oocyte mixture was then placed on a Belly Dancer® shaker for 2 hours to allow the collagenase reaction to proceed, occasionally pipetting the mixture to encourage dislodgement of loosened oocytes. After 2 hours, the cellular debris were dumped and the oocytes were washed 3-4 times using ND96+Ca^{2+} (the Ca^{2+} halts the collagenase reaction). Once the oocytes were washed, individual oocytes were selected and sorted under a microscope into a separate petri dish based on overall quality, taking oocyte color, shape, and consistency into consideration.

2.1.3 Electrophysiology

Oocytes designated for wild-type nAChR expression were injected in a stoichiometric ratio of 5 ng of α1 subunit cRNA along with 2.5 ng of each wild-type β1, δ, and ε subunit cRNA. Oocytes designated for mutant nAChR expression were injected in a 2:1:1:1 stoichiometric ratio

for α1, β1, δ, and ε respectively but because mutants vary in their expression, actual ng values injected varied from 5ng/2.5ng to 20ng/10ng for α vs. non-α subunits respectively. Oocytes were allowed to incubate from 1-7 days at 16˚C in ND96+Ca^{2+} buffer depending on the specific expression time of a given mutant. Injected oocytes were then placed in the RC-1Z oocyte chamber (Harvard Apparatus; Hamden, CT) containing prepared HEPES buffer (96 mM NaCl, 2mM KCl, 1.8 mM BaCl2, 1 mM MgCl2, 10 mM HEPES, pH 7.3). Whole cell currents were recorded using a TEVC apparatus (OC-725C oocyte clamp; Holliston, MA). The whole cell currents were recorded while flowing the HEPES buffer through the oocyte chamber.

Whole cell currents were recorded from injected oocytes immersed in HEPES buffer with 1 μM of added atropine to prevent activation of endogenous calcium-activated chloride channels via muscarinic acetylcholine receptors. Currents through the membrane in response to increasing acetylcholine concentrations were generally measured with the transmembrane voltage clamped at -60mV for oocytes expressing wild-type nAChRs. The holding potential varied among mutants, depending on their expression, with some robustly expressing mutants clamped at -20mV and low-expressing mutants clamped as high as -120mV. The concentrations of acetylcholine used for wild-type nAChR-expressing oocytes ranged from 1 μM to 100 μM. This concentration range was altered as required for specific mutants.

Dose responses for each mutant were acquired from at least two different batches of oocytes and were repeated at least 8 times wherever possible. Each individual dose-response experiment was normalized (I/Imax) and fitted with a variable slope sigmoidal dose-response using GraphPad Prism**.** The individual half maximal effective concentrations (EC_{50}) for ACh and the Hill coefficients from each experiment were averaged to give the values standard deviation.

2.2 Results

In order to understand how side chain size and polarity at the pore-lining 9’ position influence channel function, I generated 19 different mutations at this position in each subunit of the human adult muscle nAChR (76 mutants) and characterized the effects of each mutation using TEVC electrophysiology on wild-type and transfected oocytes. The WT human adult muscle nAChR ($\alpha_2\beta\varepsilon\delta$) expressed robustly in *Xenopus* oocytes and responded to ACh in a concentration-dependent manner, yielding an EC_{50} = 8.22 ± 1.87μM (n = 126) (Figure 2.1), in agreement with

other published EC_{50} values for the WT human muscle nAChR (Thompson & Baenziger 2020; Domville & Baenziger 2018). As noted in the Introduction to this thesis, each EC_{50} value is a weighted composition of the rate constants for both agonist-binding/dissociation and channel opening/closing. As the mutations studied here (i.e. the L9' in the channel pore) are physically distant from the agonist-binding site, mutation-induced changes *likely* reflect changes to channel function (opening and/or closing) with an increase in EC_{50} indicating a loss of channel function (weaker coupling of agonist binding to channel gating) and a decrease in EC_{50} corresponding to an increase in channel function (enhanced coupling of agonist binding to channel gating).

2.2.1 Choice of hydrophobicity scales

To assess the effects of residue size and polarity on channel function, I plotted the measured EC_{50} value for each mutant in each subunit as a function of both properties. The generation of a plot of EC_{50} versus side-chain polarity, however, depends on the selection of an appropriate scale that defines the relative polarities or hydrophobicities of the 20 different side chains. Although several published scales rank the hydrophobicities of amino acids, these scales all differ in the methods used for their measurement. Some scales mainly take into account the physico-chemical properties of the entire amino acid, some are only focused on residue side chains, and others are based on the tendencies of a given residue to be found on the water-exposed surface of a protein versus the protein interior. As such, there is currently no single unified hydrophobicity scale that takes into account all these characteristics.

I therefore first assessed the suitability of several scales to measure the effect of side chain polarity at the 9' position. Some scales were rejected because they focused mainly on the distribution of residues between the interior and exterior of a protein, without focusing on physico-chemical aspects of residues (Janin 1979; Rose *et al* 1985). The Kyte-Doolittle hydrophobicity scale was rejected because while it is useful in predicting and identifying the regions of a protein sequence with high propensity to form transmembrane helices, the scale is based on a computer program that continuously measures the average hydropathy along the length of a pre-determined amino acid sequence (Kyte & Doolittle 1982). The relative 'hydropathy' values assigned to the different side-chains represent average tendencies to be found in a transmembrane helix among a large group of tested proteins.

In a more recent scale created using MD simulations, researchers measured relative hydrophobicities by simulating the contact angle of a water nanodroplet to planar surfaces made from both parallel and anti-parallel β-strands consisting only the single residue of interest (Zhu *et al* 2016). Hydrophobic surfaces make water bead up with a contact angle >90º because the hydrogen bonds water makes with itself are more favourable compared with those making contact with the surface, and the converse is true for hydrophilic surfaces. The contact angle method (Zhu *et al* 2015) worked well to distinguish hydrophilic from hydrophobic residues and even relative hydrophobicities among the hydrophobic residues, but could not discern different degrees of polarity among the polar residues, showing a water contact angle of 0º for all hydrophilic and charged residues except threonine and serine, indicating complete wetting behavior. As a result, the relative polarities of the polar residues had to be extrapolated using the excess chemical potential of a purely repulsive methane-sized Weeks-Chandler-Andersen (WCA) hard-sphere solute at the 2D peptide network surface-bulk interface. Since the WCA theory of uniform liquids implies that while the structure of liquid of water can be understood by separating the attractive and repulsive components of their intermolecular interactions, attractive intermolecular forces largely 'cancel out' in dense uniform liquids. This means that the structure of such a liquid is mostly determined by repulsive forces and can be approximated by simulating a simpler reference fluid with purely repulsive intermolecular forces (Widom 1967; Weeks *et al* 1971, Weeks *et al* 1997). However, while the intermolecular repulsive forces in a homogenous liquid mostly determine structure at higher densities, as the density of a liquid decreases, the intermolecular attractive forces begin to play a larger role in shaping the structure of the liquid. Therefore, while a simulated WCA purely-repulsive solute can be used to approximate the structure of dense liquids, the WCA solute becomes less accurate at simulating the structure of a liquid at lower densities. At the muscle-type nAChR channel gate, the density of water is expected to fluctuate during opening and closing, and is expected to sharply drop upon closing, suggesting that the simulated WCA pure-repulsive solute from the study may not be able to accurately represent the structure and behavior of water molecules at the channel gate. Additionally, it is worth mentioning that the WCA theory employed in this particular study applies to uniform liquids, which may not be directly applicable to ion channels since the water is expected to also contains additional solutes like cations. Given these characteristics, and the fact that the 9' position is not located on a flat planar surface, but rather a heterogeneous dynamic surface made the use of this scale less attractive for

this thesis.

The scale I eventually chose for assessing the relative hydrophobicities of side chains is the scale devised by Wolfenden *et al* in a 1988 study, which assessed residue side chain hydrophobicity by measuring the distribution-, measured by the distribution coefficient K_D of chosen solutes between two phases formed from a binary mixture of cyclohexane and water. The specific solutes were chosen to represent the side-chains of amino acids: for example, methanol (CH_3OH) was chosen to represent the side-chain of serine ($R = CH_2OH$). The use of solutes that mimic the amino acid side chains is advantageous because 1) the amine and carboxyl functional groups of the amino acids do not change upon mutation (except for proline), and 2) this choice eliminates the complication that the zwitterionic quaternary amine and free carboxyl groups can interact favourably with aqueous solvent to influence the measured K_D values.

Note that I also chose this scale because, while the use of distribution coefficients of side chains to assess their relative hydrophobicities has been a common tool used to construct many hydrophobicity scales, the choice of nonpolar solvent is important. It is important because while water is the actual polar solvent present in cells, the protein interior in a heterogeneous environment and thus cannot be precisely replicated using a non-polar solvent. Therefore, the best choice of non-polar solvent must be made based on a comparison of its properties compared to those of the protein interior. Some scales, such as the Wimley-White (1996) hydrophobicity scale, use the partitioning between water and 1-octanol, with 1-octanol representing the hydrophobic phase. While there are several reasons why 1-octanol can be a good nonpolar phase that more closely resembles the interior of a protein or a lipid bilayer, there are specific reasons, in the context of this thesis, that makes the use of cyclohexane as a nonpolar phase more suitable. Organic hydroxylic solvents like 1-octanol are able to 'drag' a considerable amount of water (equivalent to a concentration of 2.3M) into the phase as polar solutes cross the interface between the phases (Tsai *et al* 1993). As water molecules enter the nonpolar phase, they increase the polarity of the phase, reducing its nonpolar character. When using cyclohexane as a nonpolar phase, only a small concentration of dissolved water (0.002M) is dragged in by polar solutes present due to cyclohexane's lack of hydrogen-bonding capability. Additionally, previous studies have suggested that the relative hydrophobicities of certain residue side chains can change depending on which nonpolar phase is used, and that some nonpolar solvents can exert specific interactions on side

chain functional groups (Wolfenden *et al* 1981). For example, tryptophan is classified as less hydrophobic than leucine, valine, isoleucine, methionine and phenylalanine when using cyclohexane or chloroform as a nonpolar phase, but is classified as the most hydrophobic residue when using an alcohol such as 1-octanol as the nonpolar phase, suggesting that alcohols can exert a specific effect on the indole group of tryptophan (Leo *et al* 1971). The use of cyclohexane as a nonpolar phase circumvents these problems because it cannot participate in hydrogen-bonding and represents a truly nonpolar phase, as reflected by the low dielectric constant ($\varepsilon_r = 2$) of cyclohexane versus 1-octanol ($\varepsilon_r = 10$), which are both much lower compared to water ($\varepsilon_r = 80$). Instead of having a hydrophobic reference phase which could somewhat mimic the interior of a protein, the main purpose behind choosing cyclohexane as the reference phase was to have the largest difference in polarity between the phases, with water acting as a strongly polar phase and cyclohexane representing a truly nonpolar phase. Additionally, the hydrophobic channel gate is a region where there is thought to be no water penetration in the resting state, an environment that is better modeled by a solvent such as cyclohexane. Furthermore, the cyclohexane-to-water side chain distribution coefficients obtained from this study have been shown to be well-correlated with the tendencies of different residues to be found in the middle of a transmembrane helix (Wolfenden 2007). This tendency is dictated by the endoplasmic reticulum translocon's ability to recognize transmembrane helices based on the amino acid sequence presented (Hessa *et al* 2005).

Finally, to construct a hydrophobicity scale, Wolfenden et al. calculated the free energy of transfer from cyclohexane to water ($\Delta G_{C\rightarrow W} = -RTlnK_D$) for each side chain in kcal/mol. The $\Delta G_{C\rightarrow W}$ value of a side chain is also known as its 'hydration potential', and it describes how readily it will cross from the nonpolar cyclohexane to water. A side chain with a positive $\Delta G_{C\rightarrow W}$ value will not readily cross from cyclohexane into water and thus is hydrophobic, while a side chain with a negative $\Delta G_{C\rightarrow W}$ value will readily cross from cyclohexane into water and thus is hydrophilic.

2.2.2 αL9' screen

I first generated L9' mutations in the α subunit, as it is found in two copies per nAChR pentamer. Out of 19 αL9' mutants, 11 mutants expressed in oocytes to a level where ACh-induced currents could be detected. Representative whole-cell current responses to varying concentrations of ACh for 5 gain-of-function αL9' mutants (αL9'I, αL9'V, αL9'Q, αL9'F, αL9'E) are presented

in Fig. 2.1 (see also Fig. S1), along with representative concentration-response curves. The EC_{50} values for each L9' mutant obtained from the measured concentration-response curves are summarized in Table 2.1. Most of the aliphatic substitutions at the αL9' position gave functional expression, except for αL9'A and αL9'P. In each case where expression was detected, the aliphatic side chains led to either no effect (αL9'V and αL9'I) or to gain-of-function phenotypes (αL9'M, αL9'G) with the αL9'G mutation leading to a relatively large ~500-fold gain-of-function. The aromatic αL9'F substitution also led to a substantial gain-of-function (~90-fold), while neither αL9'Y nor αL9'W expressed. The neutral hydrogen-bonding substitutions, αL9'C, αL9'T, αL9'N, αL9'Q, αL9'H expressed and led to modest ~10-fold to relatively large ~600-fold gains-of-function for αL9'C and αL9'H, respectively. The αL9'S mutation, which in the fetal muscle nAChR gives a 119-fold gain of function, did not express (Labarca *et al* 1995). Although most of the charged substitutions at the α9' position, including αL9'D, αL9'K and αL9'R, did not express, αL9'E gave robust functional expression with a relatively large ~500-fold gain-of function.

2.2.2.1 Effect of side chain volume at the αL9' position

The effect of residue size at the 9' position on channel function was assessed by plotting the $\log EC_{50}$ value for each substitution as a function of the mean residue volume in $Å^3$ (Harpaz *et al* 1994) (Figure 2.2A). Although there is a weak trend suggesting that increasing side chain size leads to a decrease in channel function (i.e. an increase in EC_{50} value), this trend may be skewed by the large gain-of-function observed with αL9'G, and is likely influenced by the polarity of the side chain substitution. In fact, when the EC_{50} values of the non-polar and polar substitutions are separated, the reverse trend is observed – although again the αL9'G mutation remains an outlier. Specifically, for the non-polar aliphatic substitutions, αL9'I, αL9'V, αL9'M and αL9'F, there is a decrease in the $\log EC_{50}$ values (i.e. gains-of-function) with increasing side chain volume. Similarly, a decrease in the $\log EC_{50}$ values is observed with the polar substitutions αL9'C, αL9'T, αL9'N, αL9'Q, αL9'E and αL9'H. The general gain-of-function observed with increasing side chain volume may reflect a destabilization of the closed state, albeit one exerted through different mechanisms for non-polar and polar substitutions. One possible explanation for the decrease in EC_{50} with increasing size of the hydrophobic side chains is that the larger side chains lead to steric conflicts with adjacent L9' residues, leading to a destabilization of the resting state relative to the open state which would lead to enhanced channel gating and thus a decrease in EC_{50} values.

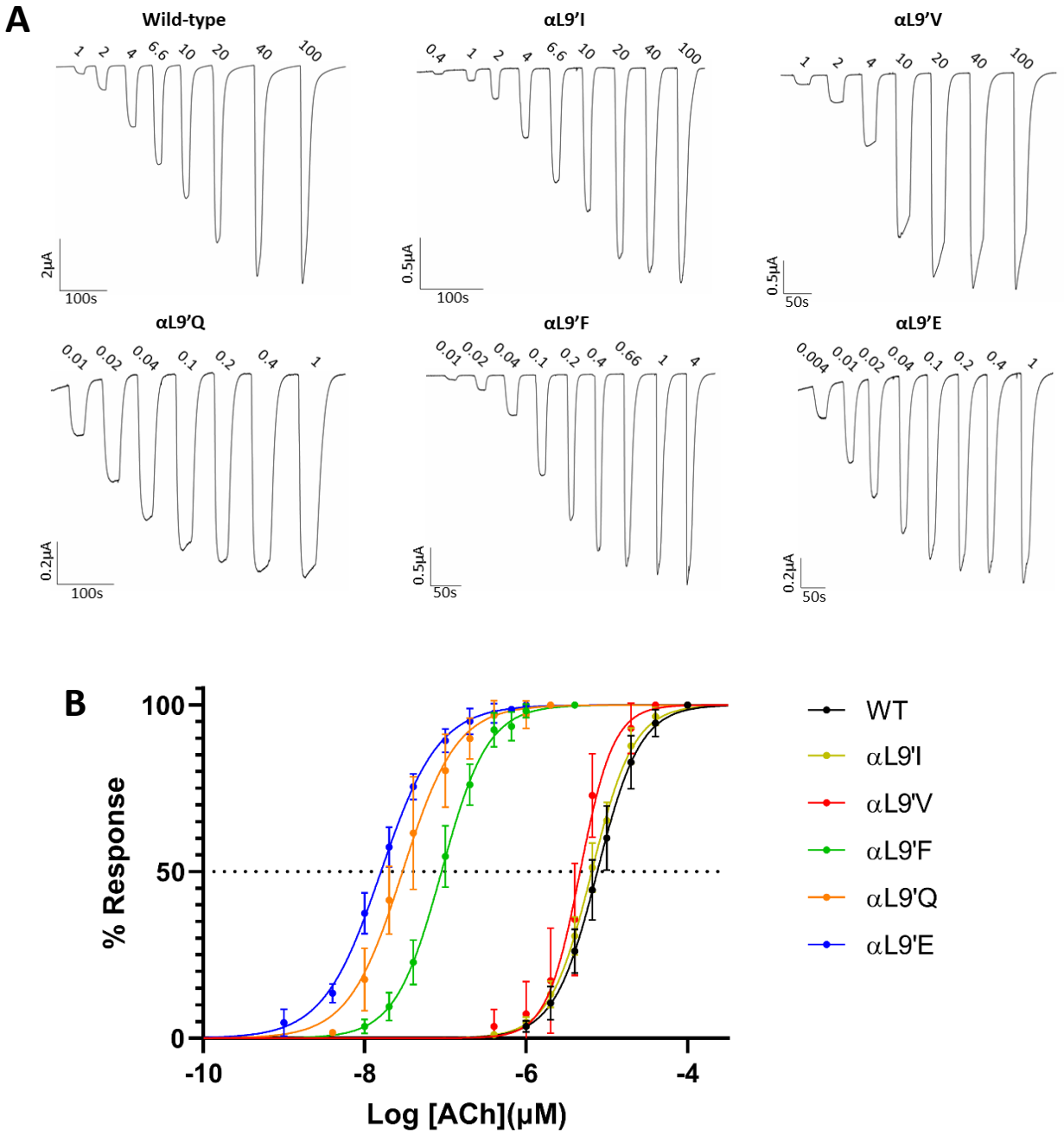

Figure 2.1: Functional Characterization of αL9' mutants. (A) Whole-cell currents were recorded using TEVC electrophysiology. Currents were recorded from *Xenopus laevis* oocytes expressing WT and mutant nAChRs in response to increasing concentrations of ACh. A variety of hydrophobic, polar and charged αL9' mutants are shown here. Each trace represents currents generated by a single WT or αL9' mutant, with the mutant identity displayed above the trace. Each peak corresponds to the current elicited by a single concentration, with the specific concentration displayed above the peak, measured in μM. A scale is present on the lower left corner of each trace to indicate the change in current flowing through the cell measured in μA on the y-axis and the time elapsed since the start of recording measured in seconds on the x-axis. **(B) Dose-Response Relationships** of the corresponding mutants in (A). The WT mutant is represented by the black curve. Curve shifts to the left of WT indicate gains-of-function.

Table 2.1 – Role of side-chain volume and chemistry at αL9' in nAChR function

	Dose Response[a]					
Mutant	**EC_{50} (μM)**	**Hill Slope**	***n***	**Residue Volume ($Å^3$)**	**$\Delta G_{C\rightarrow W}$[d]**	**Fold-Change[e]**
WT	8.22 ± 1.87	1.61 ± 0.18	126	164.6	4.92	N/A
αL9'I	6.25 ± 1.41[b]	1.68 ± 0.18	8	164.9	4.92	1.31
αL9'V	5.58 ± 2.58[b]	1.81 ± 0.39	10	139.1	4.04	1.47
αL9'M	0.80 ± 0.13[b]	1.88 ± 0.12	8	167.7	2.35	10.3
αL9'A	**No current[c]**	-	6	-	-	-
αL9'G	0.017 ± 0.005[b]	1.69 ± 0.66	8	63.8	0.94	498
αL9'P	**No current[c]**	-	6	-	-	-
αL9'F	0.094 ± 0.018[b]	1.50 ± 0.11	8	193.5	2.98	87.6
αL9'W	**No current[c]**	-	6	-	-	-
αL9'Y	**No current[c]**	-	6	-	-	-
αL9'C	0.65 ± 0.09[b]	2.03 ± 0.14	8	103.5	1.28	12.7
αL9'S	**No current[c]**	-	6	-	-	-
αL9'T	0.28 ± 0.04[b]	1.72 ± 0.20	8	120	-2.57	29.5
αL9'N	0.038 ± 0.006[b]	1.65 ± 0.38	9	127.5	-6.64	217
αL9'Q	0.029 ± 0.015[b]	1.41 ± 0.18	5	149.4	-5.54	286
αL9'H	0.013 ± 0.006[b]	1.56 ± 0.60	8	159.3	-4.66	648
αL9'E	0.016 ± 0.003[b]	1.24 ± 0.12	9	140.8	-6.81	511
αL9'D	**No current[c]**	-	6	-	-	-
αL9'K	**No current[c]**	-	6	-	-	-
αL9'R	**No current[c]**	-	6	-	-	-

[a] Measurements were performed 2-7 days after injection of cRNA. Error values represent standard deviations.
[b] $p<0.0001$ relative to wild-type control via one-way ANOVA followed by Dunnett's post-hoc test.
[c] Oocytes were tested 2-7 days after injection of 5-20ng of mutant cRNA and showed no dose response.
[d] Side-chain free energy of transfer from cyclohexane to water (kcal/mol)
[e] Calculated by dividing EC_{50} of mutant by EC_{50} of wild-type.

In addition, such steric conflicts may be exacerbated by substitutions in the α subunit as there are two of them per pentamer. This may explain why αL9'F results in such a large gain-of-function (88-fold) compared to the same mutation in non-α subunits whose effects range from a small 4-fold gain-of-function (βL9'F) to a small 2-fold loss-of-function (δL9'F).

In contrast, the large gain-of-function observed for the small αL9'G mutation reflect other factors. The L9' residues are in an ordered pseudosymmetrical arrangement in the resting state, with their proximity to one another leading to optimal hydrophobic contacts that contribute to the stability of the resting state (Miyazawa *et al* 2003). Although larger hydrophobic side chains may lead to steric conflicts as discussed above, a major reduction in size may reduce van der Waals contacts, in turn reducing the hydrophobic driving force keeping the L9' residues close in the resting state, possibly allowing the penetration of water into the hydrophobic girdle to the extent that there is a destabilization of the resting state. Placing a glycine in the middle of an α-helix is also expected to render it more flexible, which could feasibly affect multiple sets of interactions within the receptor during the gating transition since the displacement of the αM2 helices are thought to be the main drivers of channel opening (Unwin *et al* 2002). It is important to note, however, that the smaller αL9'A mutation did not express, making the αL9'G mutation the only example of a substantial decrease of side chain size at this position, and so the observed trend should be interpreted with caution.

Finally, for polar mutations, Fig 2.2A appears to show that generally, as residue volume increases, EC_{50} decreases, indicating an increase in channel function. Both neutral hydrogen-bonding residues and charged residues have their hydrogen-bonding functional groups at the ends of their side chains, therefore, increasing side chain volume may place these functional groups closer to the central axis of the channel pore. The much larger gain-of-function observed for the αL9'E mutation compared to the same mutation in other subunits may be primarily due to the presence of two negative charges in close proximity, which may strongly repel one another, driving the L9' residues apart, and thus destabilizing the closed state.

2.2.2.2 Effect of side chain polarity at the αL9' position

The effect of residue polarity on channel function was assessed further by plotting the resulting $\log EC_{50}$ values as a function of the side-chain free energy of transfer from cyclohexane to water ($\Delta G_{C\rightarrow W}$) (Radzicka & Wolfenden 1988) (Figure 2.2B). The plot shows that generally, as

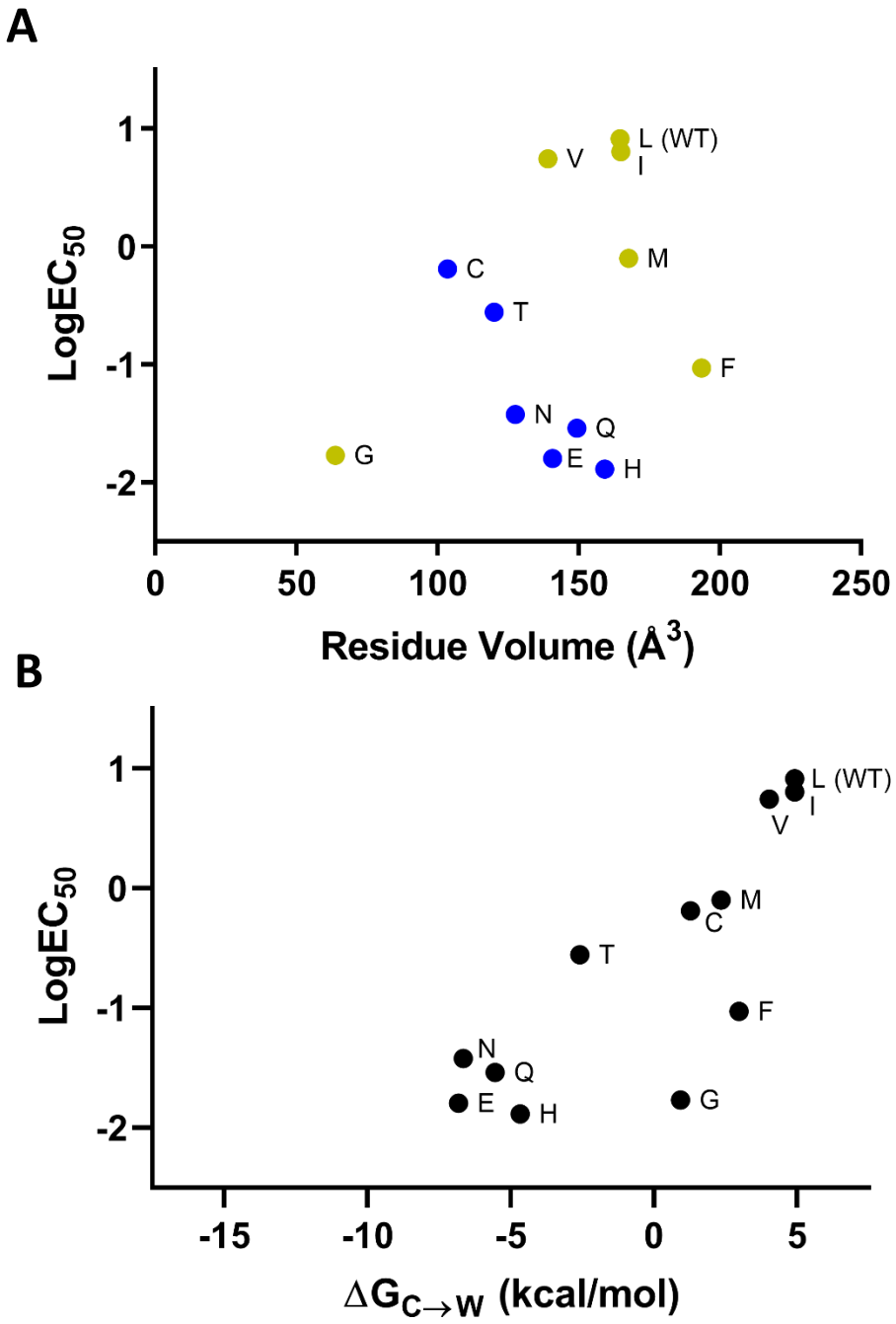

Figure 2.2: The effect of side-chain hydrophobicity and occupying volume at the αL9' position on channel function. (A) A plot of the side chain volumes against the $LogEC_{50}$ of all expressing αL9' mutants. Polar side-chains are colored in blue and hydrophobic side chains are colored in yellow. The x-axis represents the volume (measured in $Å^3$) that each residue occupies in space. **(B)** A plot of the residue side chain free energy of transfer from cyclohexane to water ($\Delta G_{C\rightarrow W}$) against the $LogEC_{50}$ of all expressing αL9' mutants. Each dot represents an αL9' mutant with the substituting residue denoted by the corresponding single letter code. A more positive $\Delta G_{C\rightarrow W}$ value corresponds to increasing solubility in cyclohexane relative to water and thus increasing hydrophobicity. The converse is true for side chains with more negative values.

the polarity of the substituted side-chain increases, the EC_{50} decreases resulting in gains-of-function. Some outliers such as αL9'F and αL9'G mutants appear to skew the correlation, but these side chains have special properties, as discussed above. In the absence of these outliers, the correlation between side-chain polarity and wild-type channel function is strong. Neutral hydrogen-bonding polar mutations such as αL9'N and αL9'Q may potentiate channel function by decreasing the hydrophobic character of the channel gate, whereby interactions between the polar substitute and solvent becomes more favourable than interactions with neighbouring L9' residues. While the close association of native L9' residues effectively excludes water molecules from the gate region in wild-type, an increase in favourable interactions with solvent molecules caused by the introduction of a more polar residue at a 9' position could feasibly bias the receptor towards the open state, easing the R→O gating transition (Beckstein & Sansom 2006). The αL9'H mutation resulted in the largest gain-of-function among all mutants tested in this thesis. In bulk water, the histidine side chain is expected to have a pKa of about 6.00, suggesting that the side chain is mostly deprotonated at physiological pH 7.4 and therefore uncharged. Additionally, while the pKa of side chains are known to change when placed in a medium with a different dielectric constant, the pKa of a side chain placed in a more hydrophobic environment tends to shift in the direction that promotes the neutral form of the side chain, since charged species are inherently unstable in hydrophobic environments. Therefore, the histidine side chains introduced by the αL9'H mutation are not expected to experience repulsion due to two identical charges in close proximity, as would be expected in the case of the αL9'E mutation, suggesting a different reason for the large observed potentiation as will be further explored in the discussion.

2.2.3 βL9' screen

Out of 19 βL9' mutants generated, 18 expressed in oocytes to a level where ACh-induced currents could be detected. Representative whole-cell current responses to varying concentrations of ACh for various βL9' mutants (βL9'V, βL9'M, βL9'A, βL9'K, βL9'S, βL9'D) are presented in Fig. 2.3 (see also Fig. S2), along with representative concentration-response curves The EC_{50} values obtained from the measured concentration-response curves for each βL9' mutant are summarized in Table 2.2. All aliphatic substitutions at the βL9' position gave functional expression. As with the α subunit, aliphatic substitutions led to small (βL9'I, βL9'V, and βL9'P)

to moderate gains-of-function (βL9'M, βL9'A) with the βL9'G mutant leading to a relatively large 54-fold gain-of-function.

Unlike mutations in the α subunit, all three bulky aromatic substitutions led to functional nAChR expression, with βL9'F leading to a small 4-fold gain-of-function while the more polar βL9'W and βL9'Y mutations led to moderate gains-of-function at 11- and 30-fold respectively. The mildly polar neutral hydrogen-bonding substitutions, βL9'C, and βL9'T led to moderate and large 21- and 32-fold gains-of-function respectively, exerting a similar but slightly more potent effect on channel function compared to the equivalent αL9'C and αL9'T mutations. The comparatively more polar neutral hydrogen-bonding substitutions βL9'S, βL9'N, βL9'Q and βL9'H all led to large gains-of-function ranging from 73- to 116-fold increases in channel function. Both negatively-charged mutants βL9'E and βL9'D expressed robustly and led to large 59- and 246-fold gains-of-function respectively, the latter of which resulted in the highest potentiation of channel function among all βL9' mutants tested. While βL9'R did not result in detectable expression, the positively-charged βL9'K mutant produced a 31-fold gain-of-function.

2.2.3.1 Effect of side chain volume at the βL9' position

Figure 2.4A shows the plot of βL9' mutant $\log EC_{50}$ values against their corresponding residue volumes. The plot shows that for aliphatic hydrophobic substitutions generally, a decrease in residue volume is correlated with a decrease in $\log EC_{50}$ (gain-of-function), although this trend is weak and slightly skewed by the CMS-causing βL9'M mutation, which potentiates channel function to a comparatively higher degree than expected given that its volume is similar to the WT leucine. The distribution of the volume in the βL9'M side chain however, differs from that of other residues that cause less potentiation of channel function, such as βL9'I and βL9'V, in that βL9'M presents a single methyl group at the end of its side chain, while βL9'I and βL9'V both present two methyl groups in a branched configuration, a feature shared in common with the WT leucine. The branched methyl groups of the other substitutions as well as that of the native leucine may contribute to the hydrophobic nature of the gate and thus may contribute to the stability of the resting state.

As for the hydrophobic aromatic substitutions βL9'F and βL9'W, an increase in side chain size also appears to be correlated with a decrease in $\log EC_{50}$. Noticeably, the potentiation of channel function caused by the βL9'F mutation (4-fold) is much less compared to the equivalent

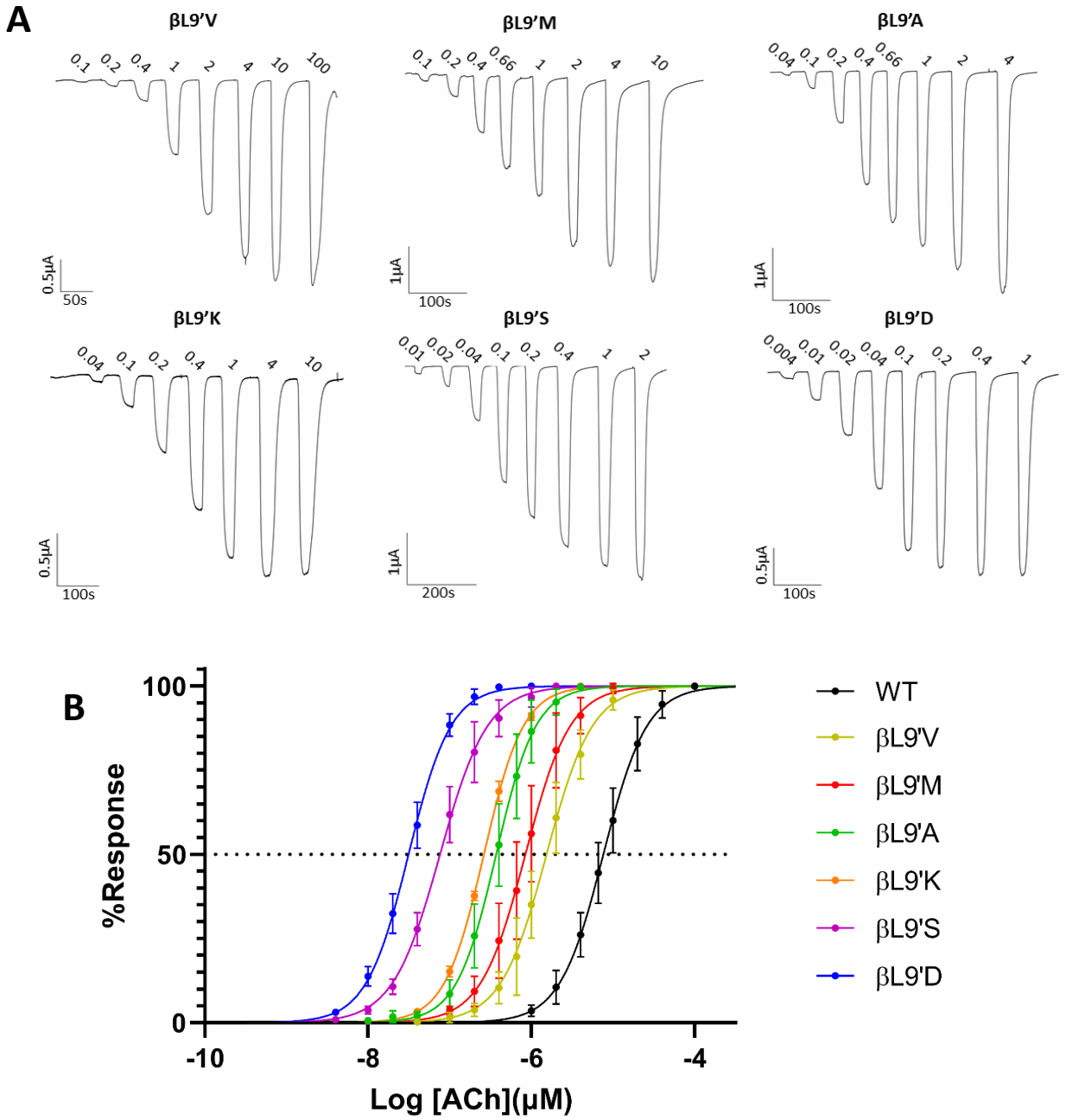

Figure 2.3: Functional Characterization of βL9' mutants. (A) Whole-cell currents were recorded using TEVC electrophysiology. Currents were recorded from *Xenopus laevis* oocytes expressing WT and mutant nAChRs in response to increasing concentrations of ACh. A variety of hydrophobic, polar and charged βL9' mutants are shown here. Each trace represents currents generated by a single WT or βL9' mutant, with the mutant identity displayed above the trace. Each peak corresponds to the current elicited by a single concentration, with the specific concentration displayed above the peak, measured in μM. A scale is present on the lower left corner of each trace to indicate the change in current flowing through the cell measured in μA on the y-axis and the time elapsed since the start of recording measured in seconds on the x-axis. **(B) Dose-Response Relationships** of the corresponding mutants in (A). The WT mutant is represented by the black curve. Curve shifts to the left of WT indicate gains-of-function.

Table 2.2 – Role of side-chain volume and chemistry at βL9' in nAChR function

	Dose Response[a]					
Mutant	**EC_{50} (μM)**	**Hill Slope**	***n***	**Residue Volume ($Å^3$)**	**$\Delta G_{C\rightarrow W}$[d]**	**Fold-Change[e]**
WT	8.22 ± 1.87	1.61 ± 0.18	126	164.6	4.92	N/A
βL9'I	3.52 ± 1.45[b]	1.77 ± 0.22	12	164.9	4.92	2.33
βL9'V	1.60 ± 0.47[b]	1.60 ± 0.14	21	139.1	4.04	5.15
βL9'M	0.91 ± 0.36[b]	1.68 ± 0.23	17	167.7	2.35	9.02
βL9'A	0.42 ± 0.11[b]	1.76 ± 0.23	28	90.1	1.81	19.6
βL9'G	0.15 ± 0.04[b]	1.91 ± 0.28	18	63.8	0.94	53.6
βL9'P	1.53 ± 0.30[b]	1.49 ± 0.24	8	123.1	N/A	5.37
βL9'F	1.86 ± 0.38[b]	1.74 ± 0.09	8	193.5	2.98	4.42
βL9'W	0.76 ± 0.14[b]	1.73 ± 0.16	8	231.7	2.33	10.9
βL9'Y	0.28 ± 0.05[b]	1.63 ± 0.07	8	197.1	-0.14	29.5
βL9'C	0.40 ± 0.11[b]	1.78 ± 0.19	8	103.5	1.28	20.5
βL9'S	0.071 ± 0.017[b]	1.57 ± 0.33	51	94.2	-3.40	116
βL9'T	0.26 ± 0.08[b]	1.73 ± 0.19	27	120	-2.57	31.7
βL9'N	0.11 ± 0.01[b]	1.75 ± 0.03	8	127.5	-6.64	72.8
βL9'Q	0.085 ± 0.017[b]	1.64 ± 0.37	8	149.4	-5.54	96.8
βL9'H	0.10 ± 0.02[b]	1.63 ± 0.16	8	159.3	-4.66	81.5
βL9'E	0.14 ± 0.02[b]	1.76 ± 0.13	8	140.8	-6.81	59.1
βL9'D	0.033 ± 0.006[b]	1.62 ± 0.09	8	117.1	-8.72	246
βL9'K	0.26 ± 0.02[b]	1.79 ± 0.07	8	170	-5.55	31.4
βL9'R	**No current[c]**	-	-	-	-	-

[a] Measurements were performed 2-7 days after injection of cRNA. Error values represent standard deviations.
[b] $p<0.0001$ relative to wild-type control via one-way ANOVA followed by Dunnett's post-hoc test.
[c] Oocytes were tested 2-7 days after injection of 5-20ng of mutant cRNA and showed no dose response.
[d] Side-chain free energy of transfer from cyclohexane to water (kcal/mol)
[e] Calculated by dividing EC_{50} of mutant by EC_{50} of wild-type

αL9'F mutation (88-fold), which introduces two phenylalanine residues into the pore. The polar aromatic βL9'Y mutation, which contains an additional -OH group in the *para* position, differs little in size but potentiates channel function to a larger extent (30-fold) than the βL9'F (4-fold) mutation. The increased polarity caused by the presence of the -OH group may be responsible for the observed increase in potentiation. Among neutral hydrogen-bonding mutants βL9'C, βL9'T, βL9'N, βL9'Q, and βL9'H, an increase in side-chain size appears to slightly correlate with an increase in channel function, but this correlation is skewed by the large potentiation of channel function observed from the βL9'S mutant. An inspection and comparison of the βL9'C and βL9'S side chains, however, could provide an explanation as to why the βL9'S mutation potentiates channel function to such a large extent. These two side chains are relatively small and differ only by the identity of the functional group on their ends; the βL9'C mutant carries a thiol (-SH) group while the βL9'S mutant contains a hydroxyl (-OH) group. While the reduction in side chain size compared to the wild-type leucine likely plays a role in potentiation of channel function for both of these mutants, the oxygen atom of the hydroxyl group is more electronegative than the sulfur atom of the thiol group, thereby rendering the serine side chain more polar by comparison, leading to a greater reduction in the hydrophobicity of the channel gate, thus in turn destabilizing the resting state to a greater extent. The other neutral hydrogen-bonding mutants contain different functional groups, and their identities are likely to play a role in altering channel function in addition to their size. Among negatively-charged residues, the smaller βL9'D mutation potentiates channel function to a higher degree compared to βL9'E (246- and 59-fold respectively), which follows the same trend observed among the same mutations in the ε and δ subunits. Since only βL9'K, and not βL9'R expressed to a detectable level in oocytes, no effect of size among positively-charged mutants could be established for the βL9' position.

2.2.3.2 Effect of side chain polarity at the βL9' position

Figure 2.4B shows βL9' mutant $\log EC_{50}$ values plot against their corresponding $\Delta G_{C\rightarrow W}$ values. The plot shows that, in general, mutants with polar side chains potentiate channel function more than mutants with hydrophobic side chains. The correlation between the $\Delta G_{C\rightarrow W}$ values of mutants and their $\log EC_{50}$ values, suggests that as polarity of a mutant side-chain increases, its EC_{50} decreases, resulting in increasingly large gains-of-function. The correlation appears to be much stronger among mutants with aliphatic hydrophobic and aromatic side chains, than among

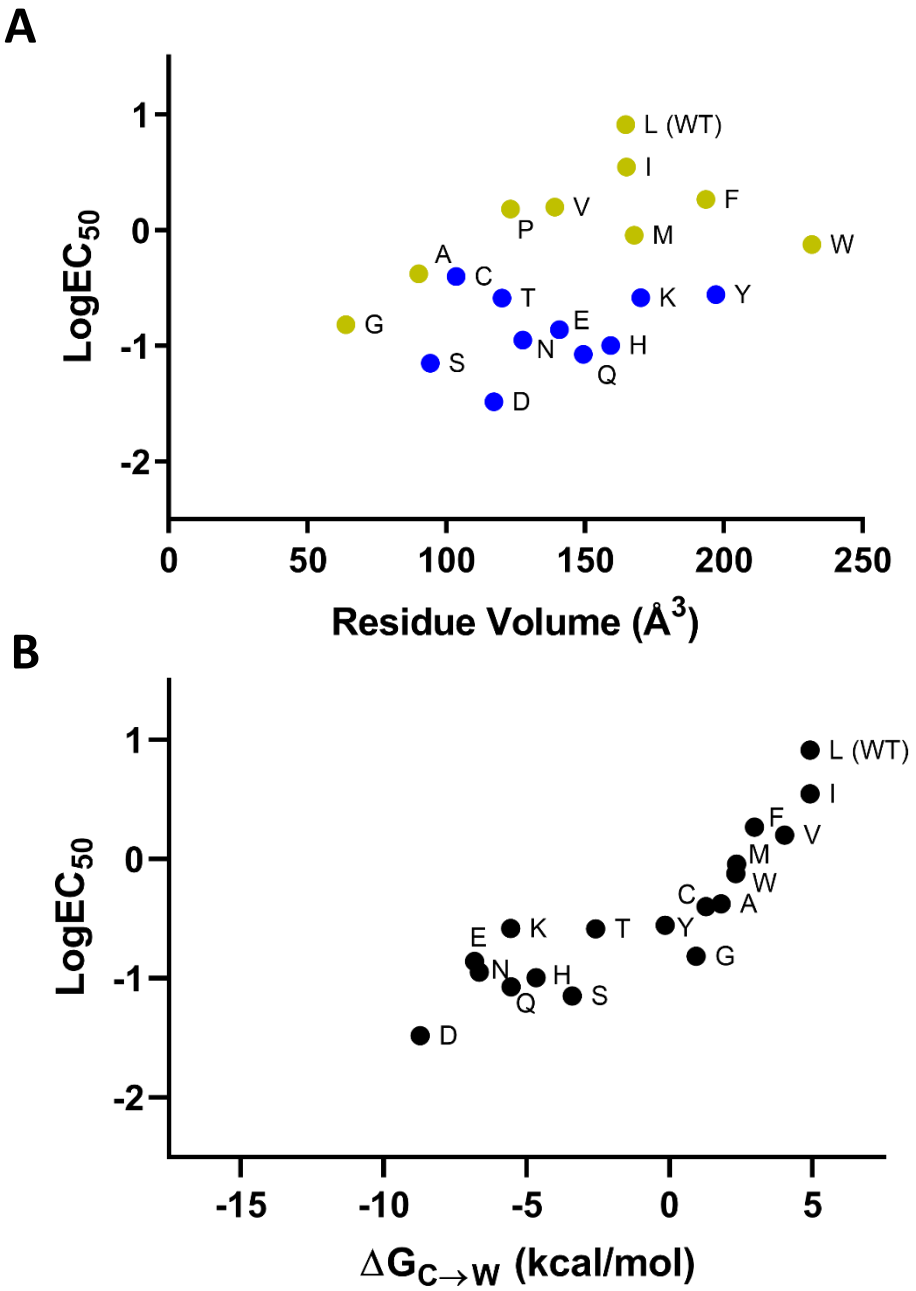

Figure 2.4: The effect of side-chain hydrophobicity and occupying volume at the βL9' position on channel function. (A) A plot of the side chain volumes against the $\log EC_{50}$ of all expressing βL9' mutants. Polar side-chains are colored in blue and hydrophobic side chains are colored in yellow. The x-axis represents the volume (measured in $Å^3$) that each residue occupies in space. **(B)** A plot of the residue side chain free energy of transfer from cyclohexane to water ($\Delta G_{C\rightarrow W}$) against the $\log EC_{50}$ of all expressing βL9' mutants. Each dot represents a represents an βL9' mutant with the substituting residue denoted by the corresponding single letter code. A more positive $\Delta G_{C\rightarrow W}$ value corresponds to increasing solubility in cyclohexane relative to water and thus increasing hydrophobicity. The converse is true for side chains with more negative values.

mutants with polar side chains. Interestingly, the βL9'Y, βL9'K and βL9'T mutants all potentiated channel function to a similar degree, resulting in 30-fold, 31-fold and 32-fold gains-of-function respectively. While there is a clear difference in the relative polarity of each side-chain, each of these side chains possesses both hydrophobic and polar components, with βL9'Y containing a benzene ring tipped with a hydroxyl group, βL9'K containing a long hydrocarbon tail tipped with a positively charged amino group, and βL9'T containing both a methyl and a hydroxyl group. While Fig. 2.4B shows a general trend of decreasing EC_{50} with decreasing side-chain hydrophobicity, it does also show a trend, albeit a weaker one, of increasing side-chain polarity and decreasing EC_{50}. The trend is skewed by the effects both of the βL9'K and βL9'S mutants on channel function, the former of which results in a higher EC_{50} than what would be predicted by the trend, and the latter of which results in a lower EC_{50} than what the trend would predict. The higher- and lower-than-expected $\log EC_{50}$ values of the βL9'K and βL9'S mutants respectively suggests that factors other than the polarity of their side chain may influence their effects on channel function.

2.2.4 εL9' screen

I next generated 19 L9' mutations in the ε subunit, 16 of which expressed in oocytes to a level where ACh-induced currents could be detected. Representative whole-cell current responses to varying concentrations of ACh for various εL9' mutants are presented in Fig. 2.5 (see also Fig S3), along with representative concentration-response curves. The EC_{50} values for each εL9' mutant obtained from the measured concentration-response curves are summarized in Table 2.3.

All aliphatic substitutions at the εL9' position expressed robustly and led to a range of effects on channel function. The εL9'P mutation led to no discernible changes in channel function compared to wild-type while εL9'I, εL9'V, and εL9'M mutations led to small gains-of-function (ranging from 2- to 5-fold) and εL9'A and εL9'G mutations led to moderate (14-fold) and large (40-fold) gains-of-function respectively. With the exception of εL9'P, this trend is broadly similar to that which is observed among the same mutants in the β subunit. Among aromatic substitutions, both εL9'F and εL9'W led to small gains-of-function, potentiating channel function 2-fold and 8-fold respectively, while the εL9'Y mutant did not result in detectable currents. All neutral hydrogen-bonding substitutions expressed robustly except for εL9'S, which in its fetal nAChR

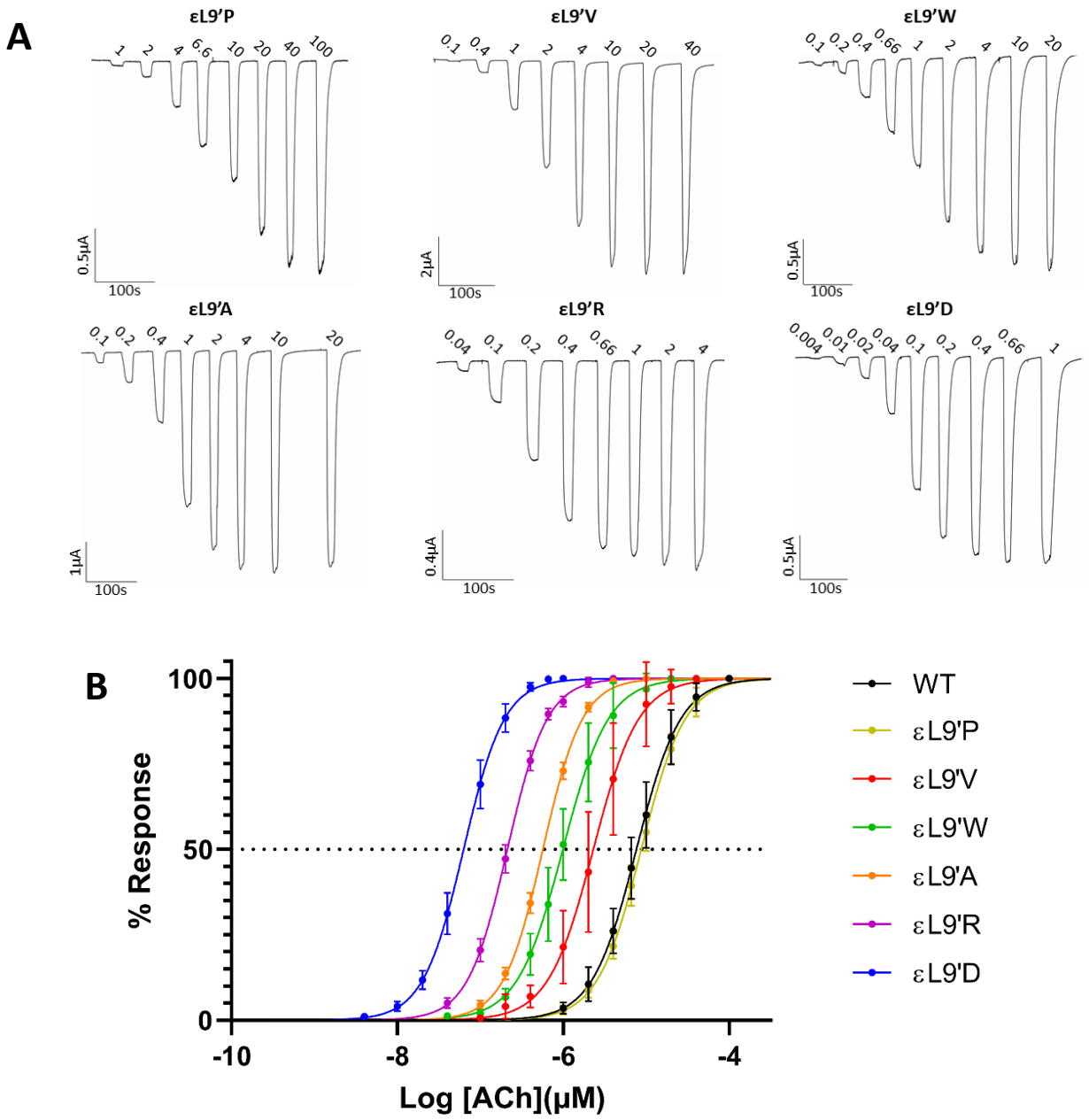

Figure 2.5: Functional Characterization of εL9' mutants. (A) Whole-cell currents were recorded using TEVC electrophysiology. Currents were recorded from *Xenopus laevis* oocytes expressing WT and mutant nAChRs in response to increasing concentrations of ACh. A variety of hydrophobic, polar and charged εL9' mutants are shown here. Each trace represents currents generated by a single WT or εL9' mutant, with the mutant identity displayed above the trace. Each peak corresponds to the current elicited by a single concentration, with the specific concentration displayed above the peak, measured in μM. A scale is present on the lower left corner of each trace to indicate the change in current flowing through the cell measured in μA on the y-axis and the time elapsed since the start of recording measured in seconds on the x-axis. **(B) Dose-Response Relationships** of the corresponding mutants in (A). The WT mutant is represented by the black curve. Curve shifts to the left of WT indicate gains-of-function.

counterpart, the γ subunit, leads to a 49-fold increase in channel function (Labarca *et al* 1995). The εL9'C and εL9'T mutants both led to a small 7-fold increase in channel function while the εL9'N, εL9'Q, and εL9'H mutations led to moderate-to-large gains-of-function ranging from 27- to 43-fold. Both negatively-charged substitutions expressed robustly but led to different gain-of-function phenotypes with the εL9'E mutant potentiating channel function 24-fold while the εL9'D mutant resulted in a large 125-fold increase in channel function, which follows the same trend as in the β and δ subunits. While the positively-charged εL9'K mutant did not result in any detectable expression, the εL9'R mutant did express and resulted in a large 39-fold gain-of-function.

2.2.4.1 Effect of side chain volume at the εL9' position

Figure 2.6A shows the plot of εL9' mutant $\log EC_{50}$ values against their corresponding residue volumes. Among aliphatic hydrophobic mutants, the plot shows a weak correlation between a decrease in residue size and a decrease in $\log EC_{50}$ values, but this correlation is skewed both by the εL9'M and εL9'P mutants. The εL9'M mutant potentiated channel function slightly more than expected given its similar size to the wild-type leucine, but as previously mentioned, the lack of a branched hydrophobic structure with two methyl groups, may contribute to its lower-than-expected EC_{50}, and it should be noted that across all subunits, L9'M mutations consistently potentiate channel function more than L9'I or L9'V mutations. The εL9'P mutation, which introduces a smaller hydrophobic side chain into the pore, leads to no discernible change in channel function, which is in contrast to the effect of the same mutation on the β subunit which leads to a 5-fold gain-of-function, but similar to the effect of the same mutation on the δ subunit (1.3-fold gain-of-function). Although the proline side chain is smaller than that of the wild-type, the unique cyclic side chain is expected to promote rigidity and/or bending of the M2 helix, which may be conducive for near WT-like gating at the εL9' and δL9' positions, but not the βL9' position.

Among aromatic substitutions, Fig. 2.6A shows that as εL9' side-chain size increases, there is a decrease in $\log EC_{50}$ (increase in channel function). Among uncharged hydrogen-bonding polar mutants, the plot shows that as residue size increases, channel function also increases, with the exception of εL9'T which has a larger residue volume but produces the same EC_{50} value as εL9'C. The εL9'T and εL9'C mutant side chains are interesting to compare, because while their introduction into the pore both potentiate channel function to the same degree (7.4-fold), they each possess different functional groups and differ in size. The εL9'C and εL9'T mutants both introduce

Table 2.3 – Role of side-chain volume and chemistry at εL9' in nAChR function

	Dose Response[a]					
Mutant	**EC_{50} (μM)**	**Hill Slope**	***n***	**Residue Volume ($Å^3$)**	**$\Delta G_{C\rightarrow W}$[d]**	**Fold-Change[e]**
WT	8.22 ± 1.87	1.61 ± 0.18	126	164.6	4.92	N/A
εL9'I	3.41 ± 0.58[b]	1.83 ± 0.17	12	164.9	4.92	2.41
εL9'V	2.38 ± 1.26[b]	1.74 ± 0.34	10	139.1	4.04	3.46
εL9'M	1.67 ± 0.50[b]	1.68 ± 0.11	8	167.7	2.35	4.93
εL9'A	0.59 ± 0.05[b]	1.76 ± 0.13	8	90.1	1.81	13.9
εL9'G	0.21 ± 0.03[b]	2.04 ± 0.17	8	63.8	0.94	39.7
εL9'P	9.16 ± 1.40	1.59 ± 0.11	8	123.1	N/A	0.90
εL9'F	5.12 ± 1.74[b]	1.75 ± 0.29	8	193.5	2.98	1.60
εL9'W	1.07 ± 0.41[b]	1.60 ± 0.20	5	231.7	2.33	7.70
εL9'Y	**No current[c]**	-	6	-	-	-
εL9'C	1.11 ± 0.18[b]	1.75 ± 0.12	8	103.5	1.28	7.41
εL9'S	**No current[c]**	-	6	-	-	-
εL9'T	1.11 ± 0.45[b]	0.91 ± 0.21	8	120	-2.57	7.42
εL9'N	0.31 ± 0.08[b]	1.70 ± 0.13	9	127.5	-6.64	26.6
εL9'Q	0.24 ± 0.11[b]	1.87 ± 0.16	8	149.4	-5.54	35.0
εL9'H	0.19 ± 0.06[b]	1.69 ± 0.08	8	159.3	-4.66	43.1
εL9'E	0.35 ± 0.06[b]	1.75 ± 0.15	9	140.8	-6.81	23.8
εL9'D	0.066 ± 0.011[b]	1.74 ± 0.17	8	117.1	-8.72	125
εL9'K	**No current[c]**	-	6	-	-	-
εL9'R	0.21 ± 0.02[b]	1.80 ± 0.06	10	192.8	-14.92	38.9

[a] Measurements were performed 2-7 days after injection of cRNA. Error values represent standard deviations.
[b] $p<0.0001$ relative to wild-type control via one-way ANOVA followed by Dunnett's post-hoc test.
[c] Oocytes were tested 2-7 days after injection of 5-20ng of mutant cRNA and showed no dose response.
[d] Side-chain free energy of transfer from cyclohexane to water (kcal/mol).
[e] Calculated by dividing EC_{50} of mutant by EC_{50} of wild-type.

a smaller side chain into the pore compared to the native leucine, but the εL9'C mutant presents a mildly polar thiol group into the pore, while the εL9'T mutant introduces both a more polar hydroxyl group and a hydrophobic methyl group simultaneously. While the more polar hydroxyl group of the εL9'T mutant might be expected to contribute to a greater destabilization of the resting state than the thiol group of the εL9'C mutant, and thus lead to a comparatively greater increase in channel function, the additional hydrophobic methyl group of the εL9'T side chain may compensate for the destabilizing effect of its hydroxyl group by decreasing the pore radius and/or engaging in favourable interactions with the other L9' residue side chains compared to the εL9'C side chain. There are only two negatively-charged mutants in the screen but the effect of their size on channel function appears to be opposite to the neutral hydrogen-bonding mutants, in that the smaller εL9'D mutant potentiates channel function more than the εL9'E mutant, a trend which is also observed in the β and δ subunits.

2.2.4.2 Effect of side chain polarity at the εL9' position

Figure 2.6B shows εL9' mutant $\log EC_{50}$ values plot against their corresponding $\Delta G_{C \rightarrow W}$ values. The plot shows that generally, as mutant side chain polarity increases, so does channel function. Among aliphatic hydrophobic mutants εL9'I, εL9'V, εL9'M, εL9'A, and εL9'G, as side chain hydrophobicity decreases, so do $\log EC_{50}$ values, resulting in increasing potentiation of channel function. Among polar residues, the correlation is not as clear, with the neutral hydrogen-bonding mutants εL9'N, εL9'Q, and εL9'H appearing to show increasing channel function as the side chains become less polar and the εL9'T and εL9'C neutral hydrogen-bonding mutants resulting in the same EC_{50} despite the increased polarity of the εL9'T side chain. As was also observed among the same mutants in the βL9' and δL9' screens, among negatively-charged εL9' mutants, the smaller and more polar εL9'D mutant potentiated channel function much more than the εL9'E mutant. While the εL9'K mutant did not result in receptors that could produce a detectable current, the strongly polar positively-charged εL9'R mutant resulted in a 39-fold gain-of-function, which is comparable to the increase in channel function caused by some of the neutral hydrogen-bonding εL9' mutants and similar to the 31-fold increase in channel function observed from the βL9'K mutant, which also introduces a positively-charged side chain into the pore. If an increase in side-chain polarity were strongly correlated with an increase in channel function, the εL9'R mutation would be expected to lead to a much higher gain-of-function than observed, since

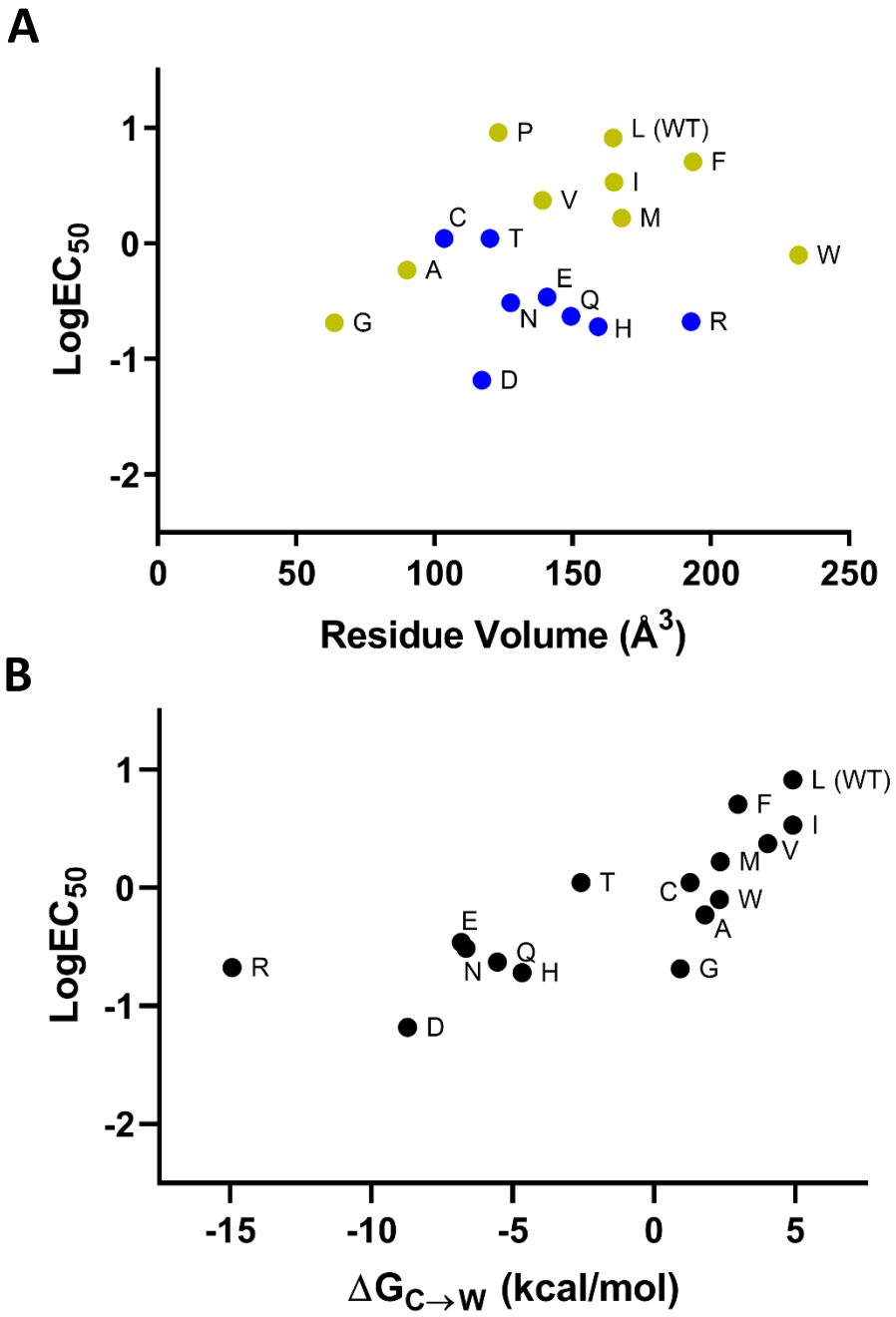

Figure 2.6: The effect of side-chain hydrophobicity and occupying volume at the εL9' position on channel function. (A) A plot of the side chain volumes against the $LogEC_{50}$ of all expressing εL9' mutants. Polar side-chains are colored in blue and hydrophobic side chains are colored in yellow. The x-axis represents the volume (measured in $Å^3$) that each residue occupies in space. **(B)** A plot of the residue side chain free energy of transfer from cyclohexane to water ($\Delta G_{C\rightarrow W}$) against the $LogEC_{50}$ of all expressing εL9' mutants. Each dot represents a represents an εL9' mutant with the substituting residue denoted by the corresponding single letter code. A more positive $\Delta G_{C\rightarrow W}$ value corresponds to increasing solubility in cyclohexane relative to water and thus increasing hydrophobicity. The converse is true for side chains with more negative values.

arginine is considered to have the most polar side chain among all residues according to the hydrophobic scale being used. This suggests that while the polarity of arginine's side chain may contribute to the observed increase in channel function, there may be other features of the side-chain in the context of its surrounding environment which contribute to the overall resulting effect on channel function, some of which may not necessarily promote an increase in channel function. While the destabilizing effect of such a mutation on the resting state can be easily considered, it is also possible that other features of the same side chain may prevent it from having a further destabilizing effect on the resting state, which may explain the lower-than-expected increase in channel function compared to wild-type. Overall, among all εL9' mutants, most polar substituted residues potentiate channel function to a greater degree than hydrophobic substituted residues, a trend εL9' mutants share in common with mutants of the L9' positions of all other subunits.

2.2.5 δL9' screen

Lastly, I generated L9' mutations in the δ subunit. Out of 19 δL9' mutants, 18 mutants expressed in oocytes to a level where ACh-induced currents could be detected. Representative whole-cell current responses to varying concentrations of ACh for various δL9' mutants are presented in Fig. 2.7 (see also Fig. S4), along with representative concentration-response curves. The EC_{50} values for each δL9' mutant obtained from the measured concentration-response curves are summarized in Table 2.4. All aliphatic hydrophobic substitutions at the δL9' position resulted in receptors with detectable currents, except for δL9'G. The δL9'I mutation did not appear to have any significant effect on channel function compared to wild-type while δL9'V, δL9'P, and δL9'M mutations led to small gains-of-function (ranging from 1.3- to 3-fold) and δL9'A led to a moderate 10-fold gain-of-function. Among aromatic substitutions, the δL9'F mutation led to a 2-fold loss-of-function which is the only significant loss-of-function compared to wild-type observed among all L9' mutations tested (across all subunits), while the comparatively more polar δL9'W and δL9'Y mutations led to similarly moderate 10- and 11-fold gains-of-function respectively. Among neutral hydrogen-bonding substitutions, a large range of effects on channel function were observed. While the mildly-polar δL9'C and δL9'T neutral hydrogen-bonding substitutions led to small 4- and 6-fold increases in channel function respectively, and the more polar δL9'S and δL9'N mutations resulted in large 37- and 48-fold gains-of-function respectively, the δL9'H mutant appeared to have no significant effect on channel function, while the δL9'Q mutant resulted in a

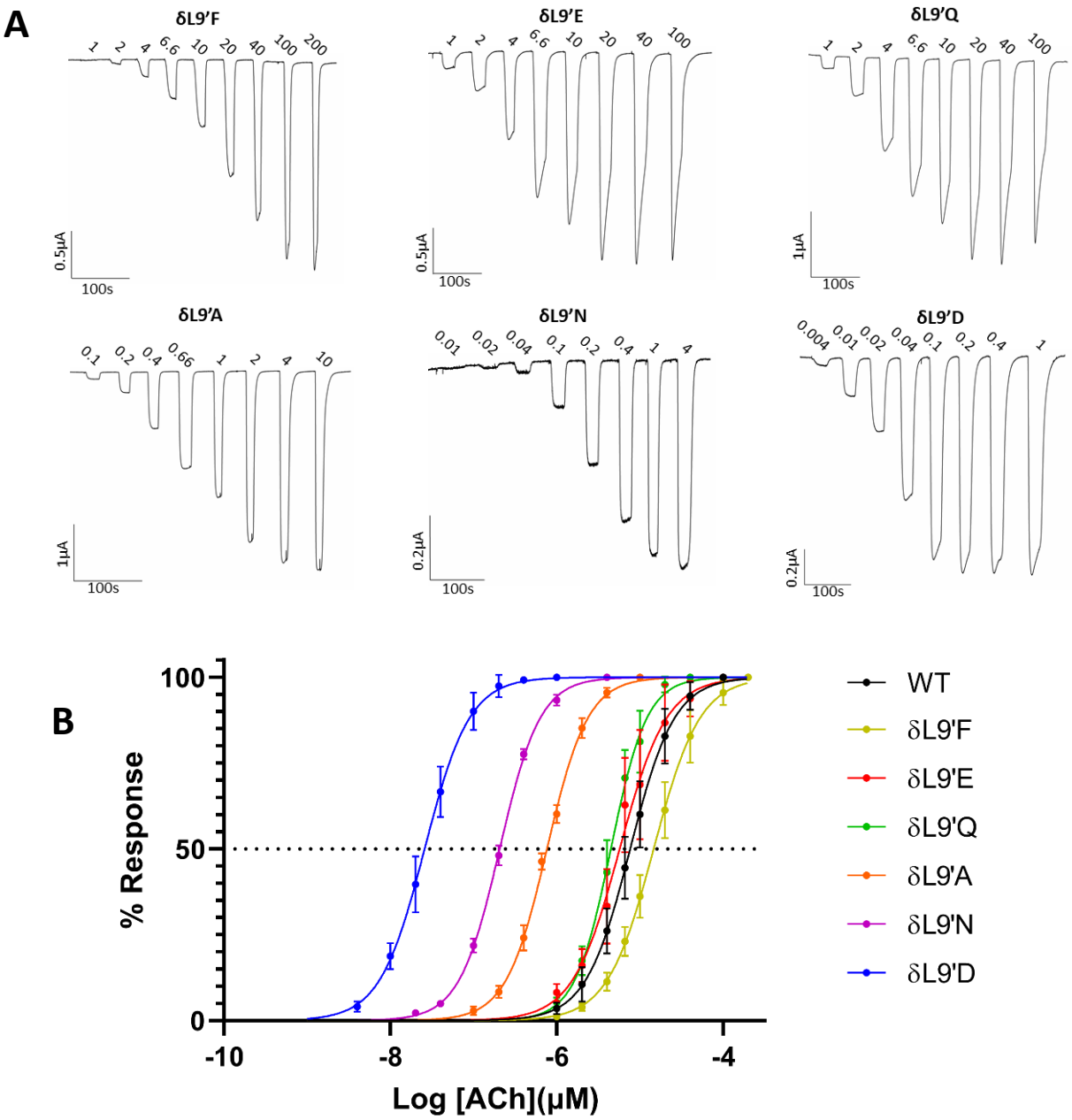

Figure 2.7: (A) Functional Characterization of δL9' mutants. (A) Whole-cell currents were recorded using TEVC electrophysiology. Currents were recorded from *Xenopus laevis* oocytes expressing WT and mutant nAChRs in response to increasing concentrations of ACh. A variety of hydrophobic, polar and charged δL9' mutants are shown here. Each trace represents currents generated by a single WT or δL9' mutant, with the mutant identity displayed above the trace. Each peak corresponds to the current elicited by a single concentration, with the specific concentration displayed above the peak, measured in μM. A scale is present on the lower left corner of each trace to indicate the change in current flowing through the cell measured in μA on the y-axis and the time elapsed since the start of recording measured in seconds on the x-axis. **(B) Dose-Response Relationships** of the corresponding mutants in (A). The WT mutant is represented by the black curve. Curve shifts to the left of WT indicate gains-of-function.

less than two-fold gain-of-function. The latter two mutations produce effects on channel function that are in stark contrast with the observed effects of the same mutations at the L9' positions of other subunits, which consistently result in large gain-of-function phenotypes. While both negatively-charged mutations expressed robustly, their effects on channel function were also starkly different in a manner similar to that observed among the neutral hydrogen-bonding substitutions. The δL9'D mutation resulted in a 308-fold gain-of-function, the largest gain-of-function recorded among all mutants in the δL9' screen, and the δL9'E mutation appeared to have little effect on channel function, while the equivalent mutation when expressed at other L9' positions results in a large gain-of-function. Both positively-charged substitutions produced robust detectable currents, resulting in 62- and 17-fold gains-of-function for δL9'K and δL9'R respectively, however, the dose-responses of these two mutants did not appear to follow the typical sigmoidal curve shape exhibited by all other mutants tested, reflected in each mutants' depressed Hill Slope value, and were not able to be approximated using a sigmoidal curve, suggesting an important but poorly understood impact on channel function that these mutations have only at the δL9' position.

2.2.5.1 Effect of side chain volume at the δL9' position

Figure 2.8A shows the plot of δL9' mutant logEC_{50} values against their corresponding residue volumes. In contrast to the other L9' screens, there does not seem to be any strong correlation between residue size and changes in channel function, either among hydrophobic or polar substitutions. Some hydrophobic aliphatic residues smaller than the wild-type leucine resulted in an increase in channel function such as δL9'V, δL9'P and δL9'A, but the absence of functional expression for the δL9'G mutation makes the comparison among this group of substitutions incomplete. Some hydrophobic aliphatic mutants similar in size to the wild-type nAChR such as δL9'M produce little increase in channel function (4-fold), while the δL9'I mutant appears to have no significant effect on channel function, which is consistent with the effects of the same mutations across the other subunits. Among aromatic mutations, δL9'F leads to a loss-of-function while δL9'W and δL9'Y, which are slightly larger but more polar, lead to gain-of-function phenotypes, suggesting that the polarity of the latter two residues may mainly be responsible for the potentiation of channel function they produce compared to δL9'F. The loss-of-function caused by the δL9'F mutation is only observed in the δL9' screen, while the equivalent

Table 2.4 – Role of side-chain volume and chemistry at δL9' in nAChR function

	Dose Response[a]					
Mutant	**EC_{50} (μM)**	**Hill Slope**	***n***	**Residue Volume ($Å^3$)**	**$\Delta G_{C\rightarrow W}$[e]**	**Fold-Change[f]**
WT	8.22 ± 1.87	1.61 ± 0.18	126	164.6	4.92	N/A
δL9'I	7.36 ± 1.18	1.69 ± 0.11	9	164.9	4.92	1.12
δL9'V	6.34 ± 1.18[b]	1.67 ± 0.06	8	139.1	4.04	1.30
δL9'M	2.70 ± 0.64[b]	1.67 ± 0.13	8	167.7	2.35	3.05
δL9'A	0.79 ± 0.06[b]	1.75 ± 0.10	8	90.1	1.81	10.4
δL9'G	**No current[d]**	-	-	-	-	-
δL9'P	6.38 ± 0.50[b]	1.72 ± 0.10	9	123.1	N/A	1.29
δL9'F	15.7 ± 3.09[b]	1.53 ± 0.17	10	193.5	2.98	0.52
δL9'W	0.80 ± 0.22[b]	1.74 ± 0.09	8	231.7	2.33	10.3
δL9'Y	0.72 ± 0.19[b]	1.31 ± 0.17	8	197.1	-0.14	11.4
δL9'C	2.08 ± 0.43[b]	1.78 ± 0.12	8	103.5	1.28	3.95
δL9'S	0.22 ± 0.03[b]	1.62 ± 0.45	37	94.2	-3.40	36.6
δL9'T	1.40 ± 0.35[b]	1.75 ± 0.17	9	120	-2.57	5.89
δL9'N	0.17 ± 0.05[b]	1.73 ± 0.14	8	127.5	-6.64	48.1
δL9'Q	4.90 ± 1.08[b]	1.91 ± 0.17	8	149.4	-5.54	1.68
δL9'H	7.12 ± 1.03	1.81 ± 0.17	8	159.3	-4.66	1.16
δL9'E	7.01 ± 2.84[c]	1.62 ± 0.36	11	140.8	-6.81	1.17
δL9'D	0.027 ± 0.005[b]	1.61 ± 0.17	12	117.1	-8.72	308
δL9'K	0.13 ± 0.04[b]	1.12 ± 0.28	8	170	-5.55	62.2
δL9'R	0.49 ± 0.57[b]	1.06 ± 0.45	11	192.8	-14.92	16.7

[a] Measurements were performed 2-7 days after injection of cRNA. Error values represent standard deviations.
[b] $p<0.0001$ relative to wild-type control via one-way ANOVA followed by Dunnett's post-hoc test.
[c] $p<0.05$ relative to wild-type control via one-way ANOVA followed by Dunnett's post-hoc test.
[d] Oocytes were tested 2-7 days after injection of 5-20ng of mutant cRNA and showed no dose response.
[e] Side-chain free energy of transfer from cyclohexane to water (kcal/mol).
[f] Calculated by dividing EC_{50} of mutant by EC_{50} of wild-type.

mutations in the β and ε subunits lead to small gains-of-function and a large gain-of-function in the α subunit. While some mildly polar neutral hydrogen-bonding mutants such as δL9'C and δL9'T lead to small gain-of-function phenotypes, and more polar neutral hydrogen-bonding mutants such as δL9'S and δL9'N lead to large gains-of-function, both of which are trends observed in all other subunits, the polar δL9'Q and δL9'H mutants, whose equivalent mutations in other subunits lead to large gain-of-function phenotypes, had little effect on channel function.

An interesting size-based comparison can be made between the effect δL9'Q and δL9'N mutants on channel function. The δL9'N and δL9'Q mutant side chains are both tipped with a carboxamide functional group, but the δL9'Q mutant side chain is larger by a single methylene group. The smaller δL9'N mutant leads to a 48-fold gain-of-function, while the larger δL9'Q mutant results in only a 1.7-fold gain-of-function, a nearly negligible increase in function. The same comparison can be made in the case of negatively-charged δL9'D and δL9'E mutants, both of which are tipped with a charged carboxylic acid group at the end of their side-chains, but the latter of which is larger by exactly one methylene group. The smaller δL9'D mutant leads to a 308-fold increase in channel function (the largest gain-of-function exhibited among all δL9' mutants) while the slightly larger δL9'E mutant appears to have little to no effect on channel function. The potential reason for these qualitative differences in channel function among mutants with such small differences in their side chains is currently unknown nor is it known why other mutants like δL9'H fail to elicit a large change in channel function as observed in other subunits. The phenomenon is further evaluated in the discussion.

These results show that, overall, at the δL9' position, a small change in the side chain volume of polar residues with identical functional groups can have a large influence on channel function. The same does not appear to be true regarding hydrophobic δL9' mutants. For positively-charged substitutes, only in the δ subunit are both L9'R and L9'K mutations able to result in detectable currents, allowing a comparison of the effect of their sizes on channel function, which according to Fig 2.8A shows that the δL9'K mutant which possesses the smaller side-chain potentiates channel function more than the δL9'R mutant which has a larger side-chain. However, the dose-responses of both these mutants are not able to be fitted by a sigmoidal curve, suggesting that while side chain size may have some effect on channel function, such effects are likely overshadowed by other effects stemming from the combination of the positive charge exhibited by both of these mutants and the δL9' position, which is the only subunit in which these effects on dose-response

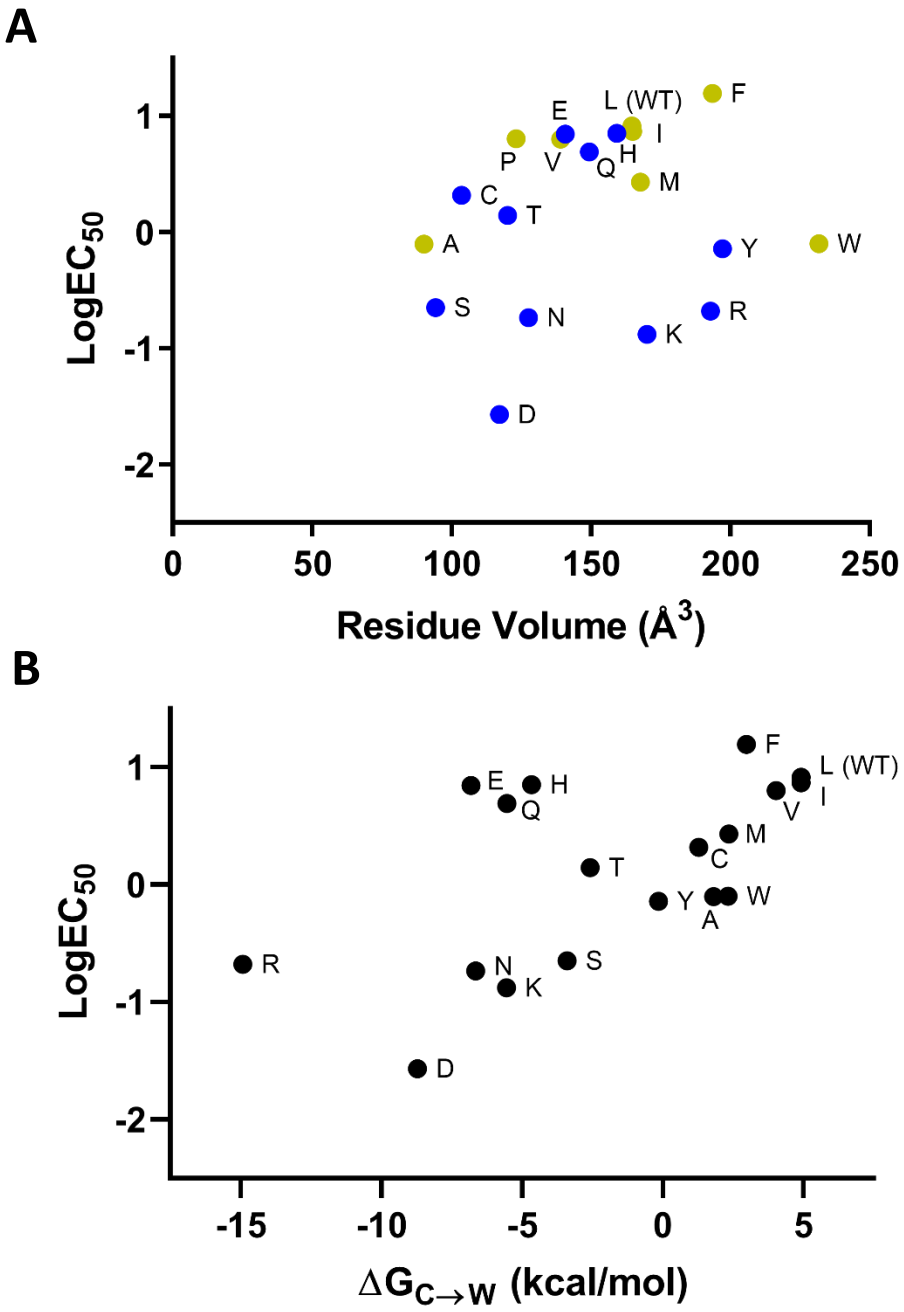

Figure 2.8: The effect of side-chain hydrophobicity and occupying volume at the δL9' position on channel function. (A) A plot of the side chain volumes against the $LogEC_{50}$ of all expressing δL9' mutants. Polar side-chains are colored in blue and hydrophobic side chains are colored in yellow. The x-axis represents the volume (measured in $Å^3$) that each residue occupies in space. **(B)** A plot of the residue side chain free energy of transfer from cyclohexane to water ($\Delta G_{C\rightarrow W}$) against the $LogEC_{50}$ of all expressing δL9' mutants. Each dot represents a represents an δL9' mutant with the substituting residue denoted by the corresponding single letter code. A more positive $\Delta G_{C\rightarrow W}$ value corresponds to increasing solubility in cyclohexane relative to water and thus increasing hydrophobicity. The converse is true for side chains with more negative values.

are observed for these mutants. Representative TEVC traces and resulting dose-response curves of the respective δL9'K and δL9'R mutants compared to wild-type are shown in Fig. 2.9.

2.2.5.2 Effect of side chain polarity at the δL9' position

Figure 2.8B shows δL9' mutant logEC_{50} values plot against their corresponding $\Delta G_{C \rightarrow W}$ values. The role of side-chain polarity is not as clear at the δL9' position compared to what other screens have revealed about the other L9' positions. There appears to be no clear correlation between side-chain polarity and channel function, as some polar mutations resulted in large gains-of-function (δL9'N, δL9'D, δL9'S) while other polar mutations resulted in little to no changes in channel function (δL9'Q, δL9'H, δL9'E), in contrast to the effect of equivalent mutations in other subunits. However, the latter mutations likely reveal important information about the unique properties of the δL9' position. As mentioned in the previous section, a small change in the size of polar residues with identical functional groups can cause a large difference in the effect of a given mutation on channel function. The smaller of these side chains appears to potentiate channel function strongly while the larger side chains appears to have little effect on channel function. Additionally, the δL9'H mutation which has no smaller counterpart has the same effect on channel function as the δL9'Q and δL9'E mutants. A series of possible explanations for these observations are addressed in the discussion. Finally, there does not seem to be a large difference between the effects of δL9'K and δL9'R on channel function despite the fact that the arginine side chain is classified as being much more polar than that of lysine, and yet δL9'K results in a greater degree of channel potentiation. As previously mentioned, there is likely a feature of the δL9' position among that mere differences in size or polarity cannot account for, and potential explanations for which are presented in the discussion.

2.2.6 Comparison of the functional effects of identical mutations among different subunits

The L9' screen has revealed many important similarities and differences in the functional consequences of mutations among L9' residues forming the channel gate. These similarities and differences may be shaped by the unique physico-chemical environments surrounding each L9' residue. This is supported by the observation that the effect on EC_{50} of introducing identical mutations at different L9' positions is different depending on the subunit containing the mutation.

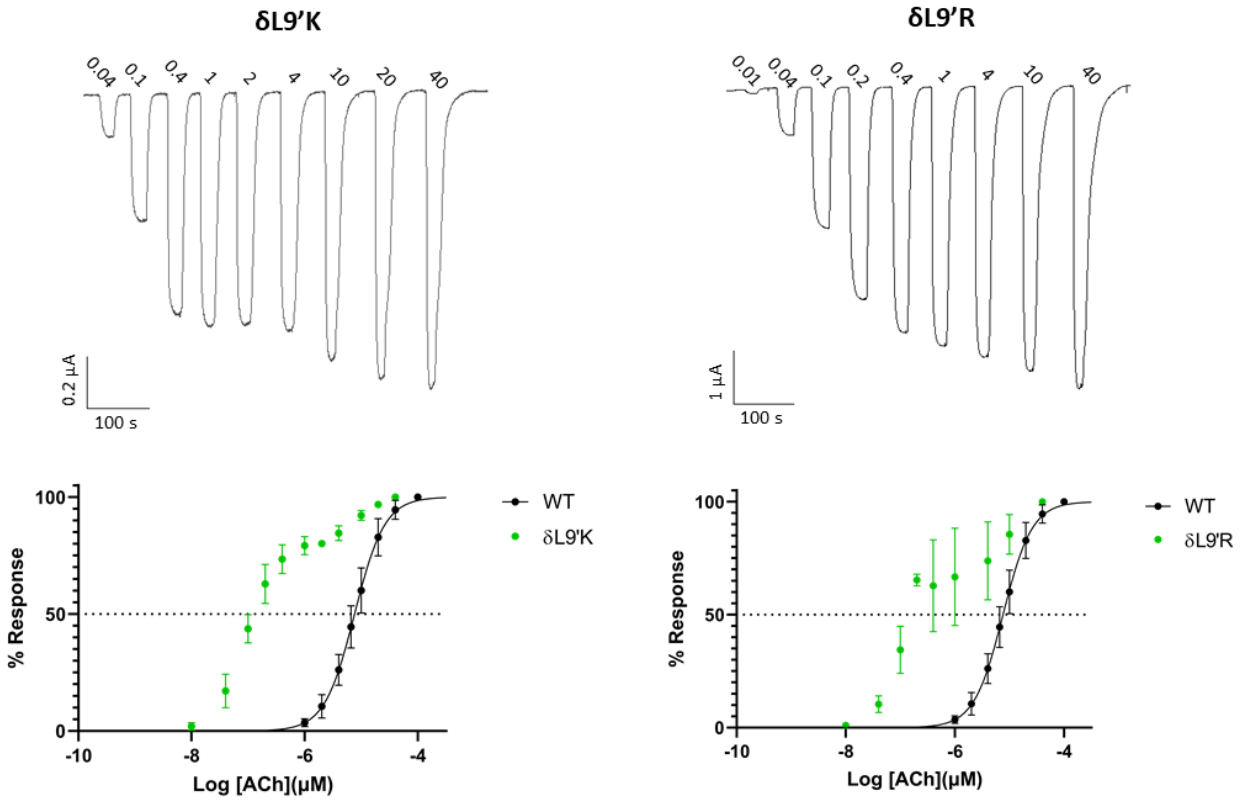

Figure 2.9: Effects of positively-charged δL9' mutants on channel function. At the top of the figure the TEVC traces for the δL9'K and δL9'R mutants are shown. Each peak corresponds to the current elicited by a single concentration of ACh, with the specific concentration displayed above the peak, measured in µM. A scale is present on the lower left corner of each trace to indicate the change in current flowing through the cell measured in µA on the y-axis and the time elapsed since the start of recording measured in seconds on the x-axis. Below the TEVC traces are the dose-response relationships for both δL9'K and δL9'R mutants, generated from several TEVC traces. The WT curve is shown in black. The dose-response relationships for the δL9'K and δL9'R mutants were not able to be fitted with a typical sigmoidal curve like the one displayed by WT. The concentration-dependence of the ACh-induced response appears to be altered or impaired in these mutants, the potential reasons for which are addressed in the discussion. The dose-response relationships of the other L9' mutants which introduce a positive charge into the pore (εL9'R and βL9'K) both display a typical sigmoidal curve and can be seen in Fig 2.13.

To assess the effects of certain L9' mutations on channel function, it is useful to compare the effects of introducing identical mutations at L9' positions in each subunit. Consistently, across all subunits, the L9'I and L9'V mutations caused the lowest gains-of-function compared to WT (Figure 2.10). Isoleucine and valine are considered similarly hydrophobic to leucine, and valine's side chain occupies only a slightly smaller volume than that of leucine, therefore it is not unexpected that small changes in side chain structure would lead to small changes in channel function. The hydrophobic L9'M mutations also resulted in mild potentiation of channel function compared to WT but did so slightly more than the L9'I or L9'V mutations across all subunits. While the methionine side chain occupies a total volume similar to that of isoleucine, the shape of its side chain is different, with a single methyl group on its end in contrast to the branched side chain of isoleucine presenting two dispersed methyl groups, which may be more effective at supporting a hydrophobic environment. The L9'A mutations introduce a smaller side chain into the pore compared to the previously mentioned hydrophobic substitutions. The L9'A mutations were found to consistently potentiate channel function. The increased function was larger than that observed with the L9'I, L9'V, or L9'M mutations across the β, δ, and ε subunits. Additionally, the effects of L9'A mutations on channel function were similar across L9' positions, ranging from 10- to 20-fold potentiation (Figure 2.10). The smallest possible substitution, the L9'G mutations led to higher gains-of-function compared to the L9'A mutations, potentiating channel function 54-fold at the βL9' position and 40-fold at the εL9' position. The αL9'G mutation led to a huge 498-fold gain-of-function, but it is not known whether both αL9' positions contributed to the gain equally or whether a glycine mutation at one particular αL9' position among the two played a dominant role. Since the αL9'A mutant did not express, I am not able to compare the effects of another small hydrophobic substitution at the αL9' position. The data suggest that for the aliphatic hydrophobic L9' substitutions, the more similar the residue side chain is in terms of size compared to the native leucine, the milder the functional consequences appear to be for channel function. Additionally, a decrease in side chain size among hydrophobic substitutes is weakly correlated with an increase in channel function. Introducing hydrophobic residues larger than the native leucine also generally leads to gains in channel function, especially when these residues are located in the α subunit. The L9'F mutations resulted in functional expression in all subunits, but the qualitative and quantitative effects of L9'F mutations on channel function varied depending on the subunit containing the mutation (Figure 2.11). The βL9'F and εL9'F mutants both caused slight gains-of-function, with

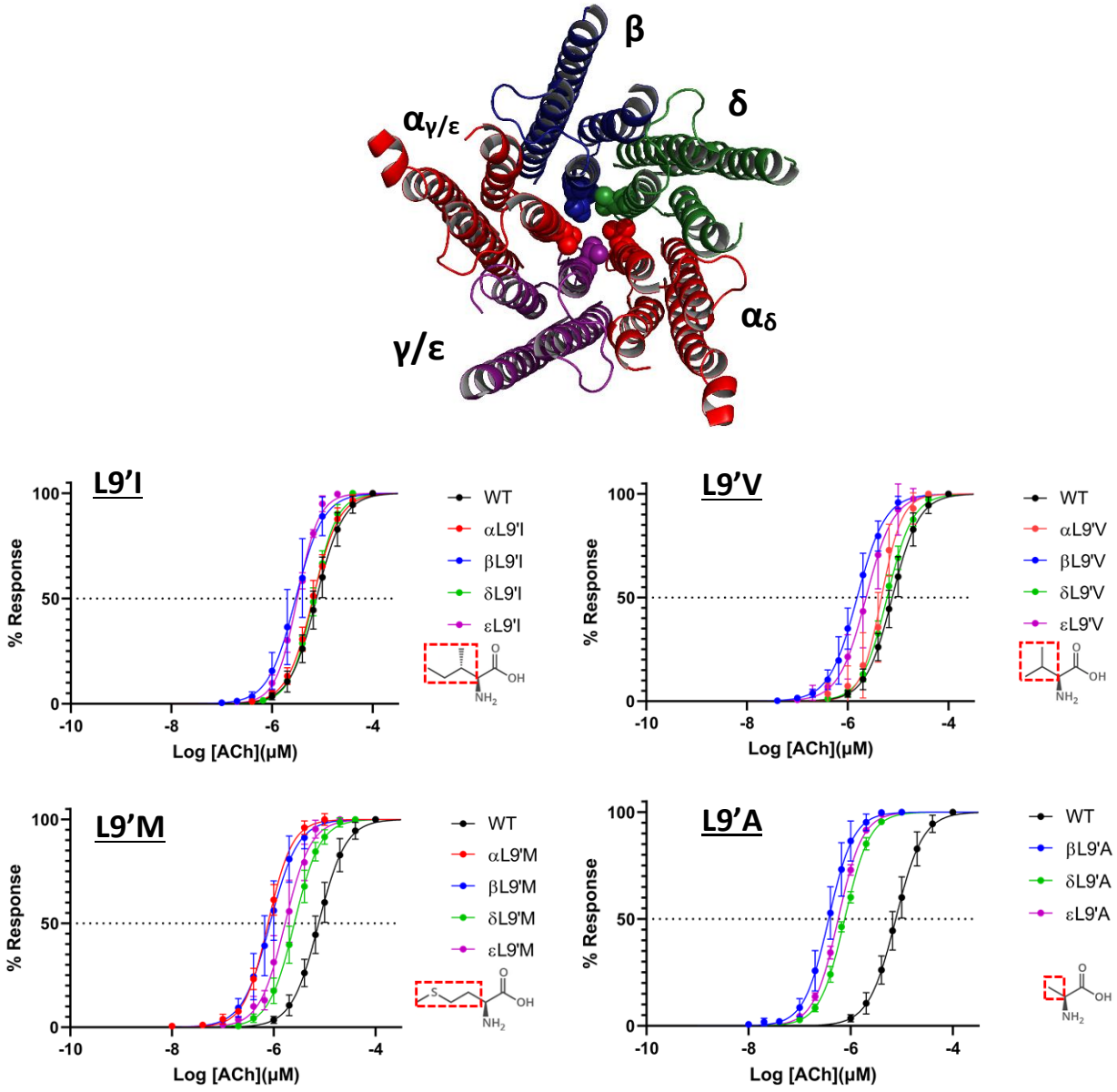

Figure 2.10: Hydrophobic aliphatic L9' substitutions. The cross-section of the TMD with subunits labeled and colored according to their identity is shown above the graphs as a reference. The dose response curve of each mutant is shown for all subunit L9' positions that led to detectable currents. In all dose-response graphs, the black curve represents the WT, and the color of all other curves refers to its subunit location according to the same coloring scheme shown in the TMD cross-section, with αL9' mutants in red, βL9' mutants in blue, δL9' mutants in green, and εL9' mutants in violet. The identity of each L9' mutation is displayed in the top left corner of each graph, and an image of the structure of each substituting amino acid is shown, with a dotted red box highlighting the residue side-chain. A left-shifted curve relative to WT indicates a gain-of-function, with increasing potentiation of channel function as the curve becomes more left-shifted.

4.4- and 1.6-fold increases in channel function respectively. This is similar to the effect observed with hydrophobic aliphatic substitutions similar in size to the native leucine. However, the αL9'F mutation, which introduces two phenylalanine side chains into the pore, potentiated channel function 88-fold, much higher than expected compared to the previous two L9'F mutations. In contrast, the δL9'F mutation actually impaired channel function about 2-fold. The similarities in the effects on channel function among L9'F mutations expressed in non-α subunits, in contrast with the massive gain-of-function observed in the αL9'F mutant may reflect that there is enough malleability at the channel gate to accommodate a single phenylalanine without causing large changes in channel function. However, simultaneous expression of two phenylalanines may strongly destabilize the resting state of the channel through steric clashes.

The more polar aromatic substitutions L9'W and L9'Y led to gains-of-function in the non-α subunits (αL9'W and αL9'Y did not result in functional expression), showing similar degrees of potentiation among the different L9' positions, ranging from 8- to 11-fold increases in channel function for L9'W mutations and 11- to 30-fold for L9'Y mutations (Fig 2.11). The presence of tyrosine's hydroxyl group or possibly tryptophan's indole group would render the hydrophobic channel gate more polar compared to both wild-type and L9'F substitutions. This could also plausibly lead to an enhancement of favorable interactions with water molecules (Beckstein and Sansom 2006), suggesting that enhancement of favorable interactions with water molecules in the open state may contribute to its stabilization.

The L9'C mutation is considered to be only weakly polar, as the sulfur in its thiol group has a low electronegativity compared to the oxygen of hydroxyl groups. The effect of L9'C mutations on channel function are similar across the subunits, ranging from a 4-fold gain-of-function in the δ subunit to a 21-fold gain-of-function in the β subunit (Figure 2.12). Cysteine's thiol group has fairly weak hydrogen bonding capabilities and is not expected to affect the polarity of the channel gate as much as a side chain containing a more strongly polar functional group. In all subunits except the β subunit, the effect of the L9'C substitution on EC_{50} is comparable to the effect of L9'M mutations, which is more hydrophobic and closer in size to L9'. Thus, it may be the case that the reduction in side chain size has a larger effect on the change in EC_{50} observed in L9'C mutants instead of enhanced polarity of the gate, although both are likely contributing factors. As a comparison, the serine side chain differs from the cysteine side chain by only a single atom, replacing the sulfur in the thiol group with an oxygen atom to form a hydroxyl group, making the

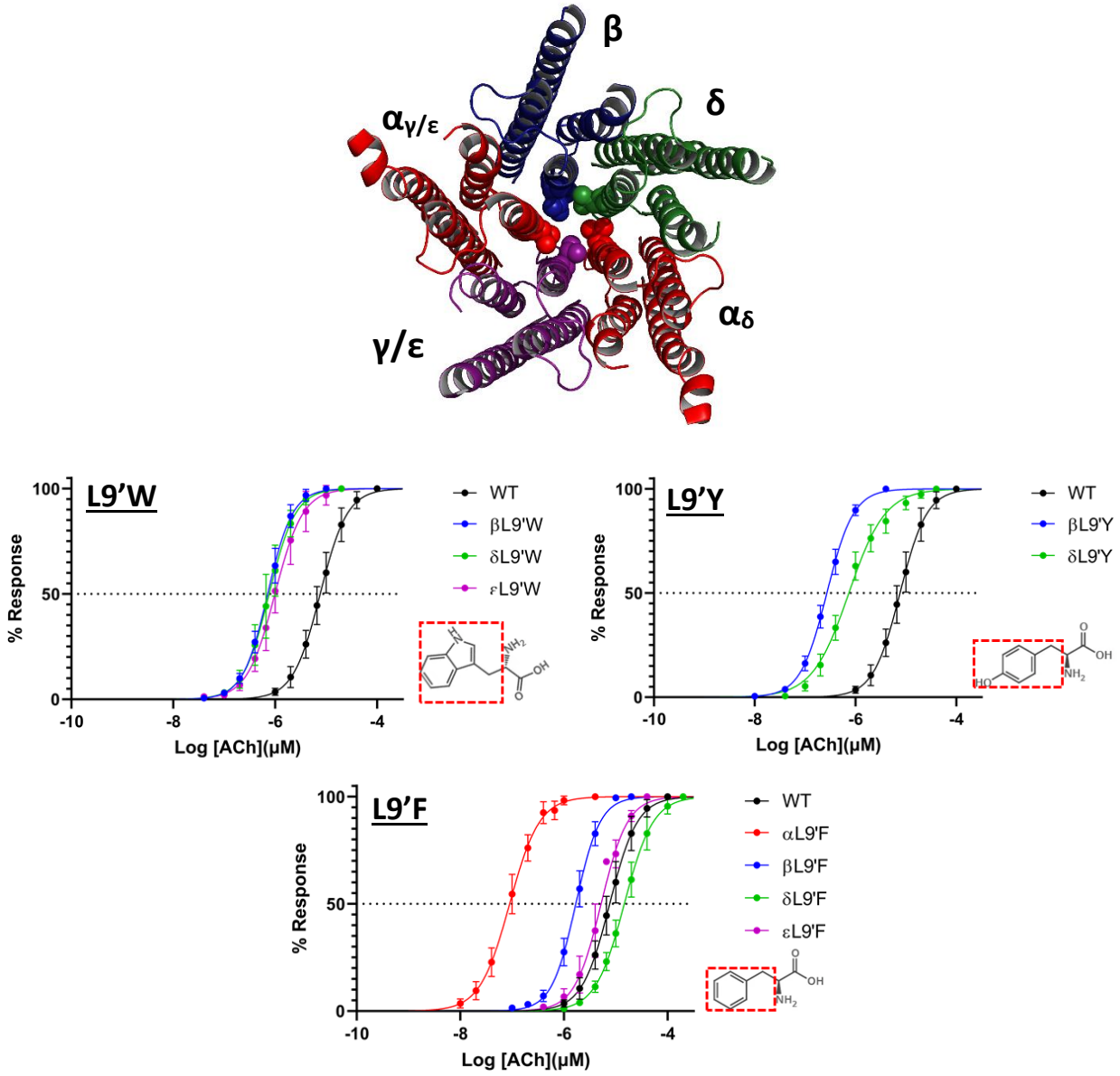

Figure 2.11: Aromatic L9' substitutions. The cross-section of the TMD with subunits labeled and colored according to their identity is shown above the graphs as a reference. The dose response curve of each mutant is shown for all subunit L9' positions that led to detectable currents. In all dose-response graphs, the black curve represents the WT, and the color of all other curves refers to its subunit location according to the same coloring scheme shown in the TMD cross-section, with αL9' mutants in red, βL9' mutants in blue, δL9' mutants in green, and εL9' mutants in violet. The identity of each L9' mutation is displayed in the top left corner of each graph, and an image of the structure of each substituting amino acid is shown, with a dotted red box highlighting the residue side-chain. A left-shifted curve relative to WT indicates a gain-of-function, with increasing potentiation of channel function as the curve becomes more left-shifted. A right-shifted curved in contrast denotes a loss-of-function, with increasing impairment the more right-shifted it becomes.

serine side-chain far more polar than that of cysteine. The L9'S mutations caused a much larger gain-of-function in both β (116-fold) and δ (37-fold) subunits compared to L9'C mutations at equivalent positions. The difference in effects on channel function between L9'C and L9'S is most likely explained by the higher polarity of the serine side chain relative to the cysteine side chain. The higher polarity of the serine side chain may strongly perturb the hydrophobic character of the channel gate, disrupting possible interactions between L9' residues to a greater extent. Its smaller size relative to the wild-type leucine also likely has a disruptive effect on these interactions. The threonine side chain contains both a hydroxyl group and a methyl group in a branched configuration. The L9'T mutations appear to potentiate channel function more than L9'V mutations and less than L9'S mutations across all subunits, with α and β subunit L9'T mutations leading to larger gains-of-function than δ and ε subunit L9'T mutations. The presence of the hydroxyl group on threonine's side chain renders threonine more polar than valine. Also, the presence of the additional methyl group renders threonine's side chain larger and less polar than serine. The methyl group of the threonine side chain may lessen the impact of the hydroxyl group on channel gate hydrophobicity, and interact more favorably with other hydrophobic methyl groups.

Among more polar neutral hydrogen-bonding mutants, L9'N mutations led to consistently large potentiation of channel function across the subunits, but L9'Q and L9'H mutants only led to large potentiation of channel function in the α, β, and ε subunits, and little to no change in channel function in the δ subunit (Fig 2.12). The lack of an effect on channel function by the δL9'H, and δL9'Q mutants is unusual given that other similarly polar δL9' substitutions (δL9'N and δL9'D) result in much higher gains-of-function compared to WT. The δL9'N mutation results in a 48-fold gain-of-function, comparable to the effects of the L9'N mutations across the subunits. However, the L9'Q mutant, whose slightly longer side chain only includes an additional methylene group compared to L9'N, results in a high gain-of-function in α, β, and ε subunits, but results in little change in function in the δ subunit. A similar phenomenon was observed with regards to the differences in effects between the δL9'D and δL9'E mutations. Across all non-α subunits, the L9'D mutation caused the highest gain-of-function in each L9' screen (no current detected for αL9'D) ranging from 125-fold for εL9'D to 308-fold for δL9'D (Fig. 2.13). In contrast, the L9'E substitution, whose side chain differs from that of L9'D by the presence of an additional methylene group caused moderate to large gains-of-function in α, β, and ε subunits but gave rise to a near

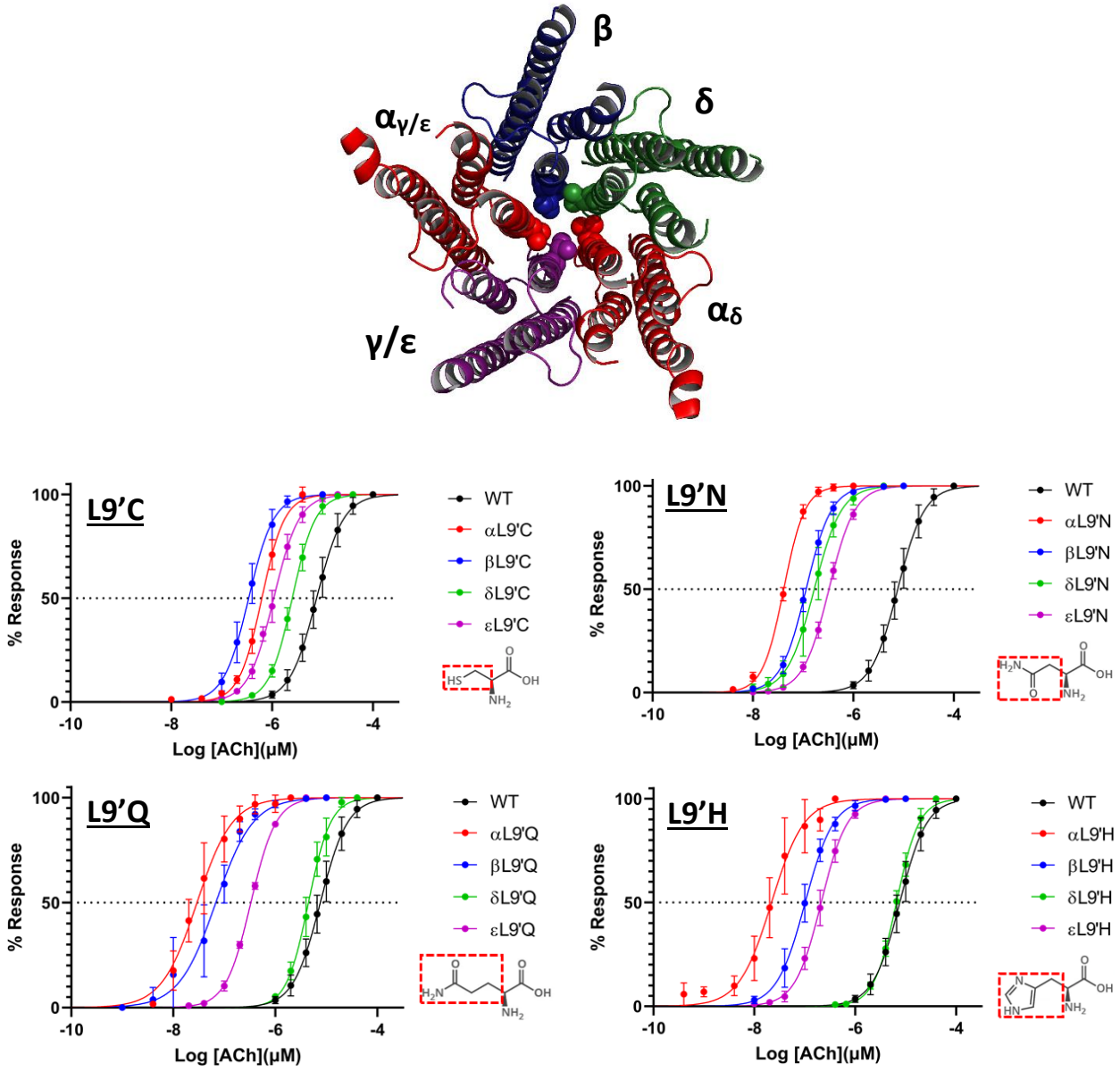

Figure 2.12: Neutral Hydrogen-bonding Polar L9' Substitutions. The cross-section of the TMD with subunits labeled and colored according to their identity is shown above the graphs as a reference. The dose response curve of each mutant is shown for all subunit L9' positions that led to detectable currents. In all dose-response graphs, the black curve represents the WT, and the color of all other curves refers to its subunit location according to the same coloring scheme shown in the TMD cross-section, with αL9' mutants in red, βL9' mutants in blue, δL9' mutants in green, and εL9' mutants in violet. The identity of each L9' mutation is displayed in the top left corner of each graph, and an image of the structure of each substituting amino acid is shown, with a dotted red box highlighting the residue side-chain. A left-shifted curve relative to WT indicates a gain-of-function, with increasing potentiation of channel function as the curve becomes more left-shifted.

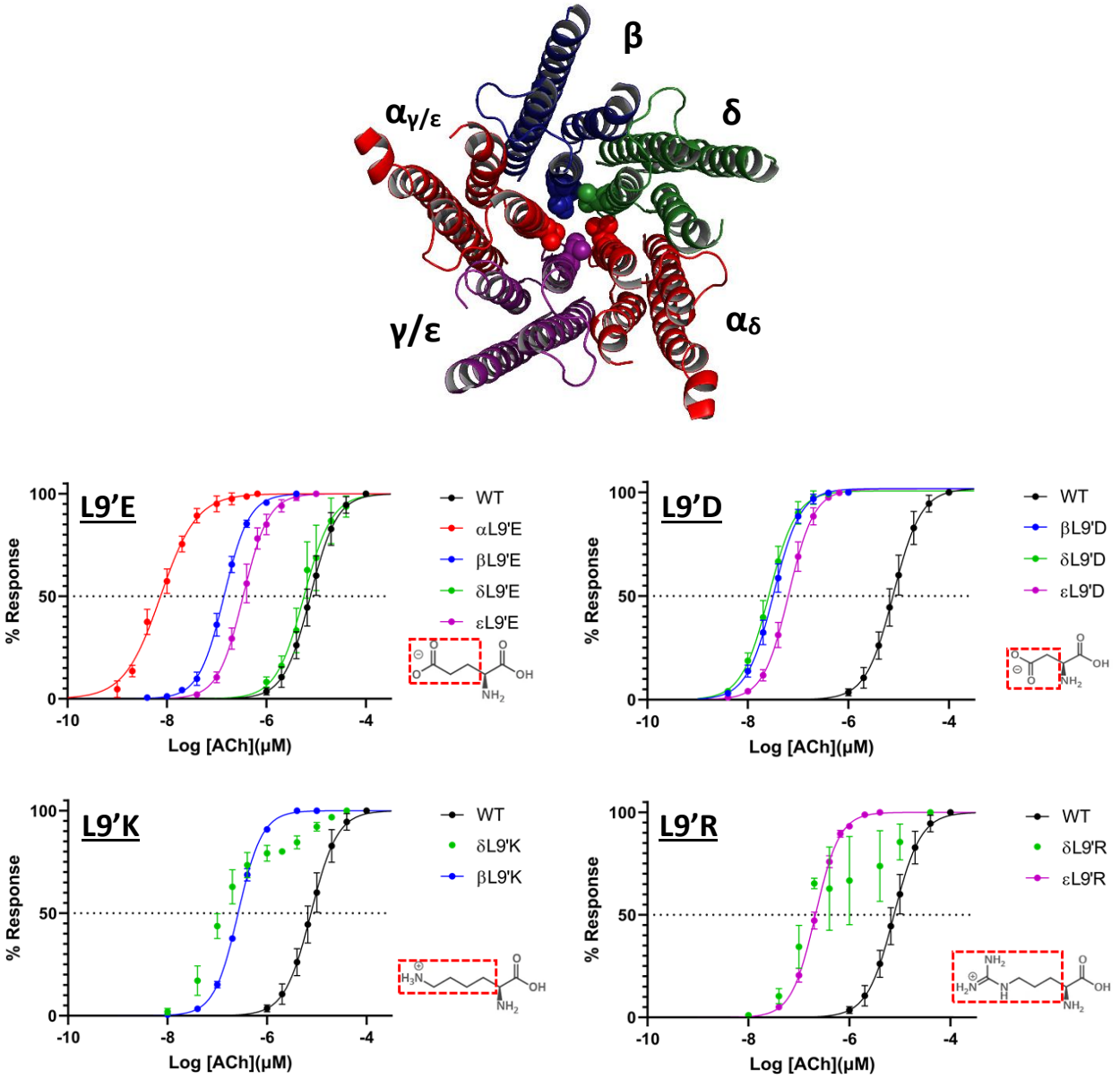

Figure 2.13 Ionizable L9' substitutions. The cross-section of the TMD with subunits labeled and colored according to their identity is shown above the graphs as a reference. The dose response curve of each mutant is shown for all subunit L9' positions that led to detectable currents. In all dose-response graphs, the black curve represents the WT, and the color of all other curves refers to its subunit location according to the same coloring scheme shown in the TMD cross-section, with αL9' mutants in red, βL9' mutants in blue, δL9' mutants in green, and εL9' mutants in violet. The identity of each L9' mutation is displayed in the top left corner of each graph, and an image of the structure of each substituting amino acid is shown, with a dotted red box highlighting the residue side-chain. A left-shifted curve relative to WT indicates a gain-of-function, with increasing potentiation of channel function as the curve becomes more left-shifted.

WT-nAChR phenotype when introduced at the δ subunit. The mutations introducing positively-charged side chains at the δL9' position also appear to produce different effects on channel function compared to the same mutations in other subunits. The βL9'K and εL9'R mutations result in gain-of-function phenotypes that produce a smooth sigmoidal dose-response curve. However, the δL9'K and δL9'R mutants, which also resulted in gains-of-function, display a rougher, less smooth sigmoidal curve (Fig 2.13), and have Hill slope value near 1, which indicates that the open state of these mutant receptors is more likely to be associated with the mono-liganded rather than the di-liganded form, suggesting that these mutations may produce long-range effects throughout the receptor that may extend to the agonist-binding site. These are the only two mutants in the entire L9' screen that exhibit this kind of response and it suggests that a particular feature of the δ9' position may be responsible for the differences observed in the effects of equivalent mutations between the different 9' positions. Potential reasons for the differences in channel function exhibited by these mutants in the δ subunit are explored further in the discussion.

2.3 Discussion

The various L9' mutational screens presented here yield a wealth of data concerning the effects of pore-lining mutations on nAChR function. Consistently, my data show that the introduction of polar side chains at the 9' position potentiates channel function, and typically does so more than the introduction of hydrophobic side chains. My data also show that in the α subunit the residue size has an impact on nAChR function, with increasing side chain size leading to increased channel function. In contrast, the β, ε and δ subunits are only weakly or not dependent at all on the size of the side chain of the 9' residues. Finally, while many of the changes in nAChR function induced by equivalent mutations in different subunits are qualitatively similar, the magnitude of these effects on EC_{50} differ substantially from one subunit to another, suggesting asymmetry in the roles of the different L9' residues in channel function. Overall, the data show that the L9' gate region is highly sensitive to mutation and that the identity of each 9' residue and host subunit plays a role tailoring the ACh-induced response. The combined results of the various L9' screens also shed light on the local interactions involving the L9' residues that influence the relative stabilities of the open and closed states to define the function of the human adult muscle nAChR, as discussed below.

Before further discussing the specific findings, it is first essential to note that the effects of the mutations on channel function noted above were assessed using the EC_{50} values derived from ACh concentration response curves. The use of EC_{50} values to assess channel function have both advantages and limitations. The primary advantage is that EC_{50} values can be measured in a relatively high-throughput fashion using TEVC electrophysiology, allowing the characterization of a large number of mutants in a short timeframe. As previously described, however, EC_{50} values are weighted averages of all rate constants concerning both agonist-binding and channel gating. As the distance separating the channel gate from the agonist binding site is large, changes in EC_{50} *likely* represent primarily changes in the coupling of agonist binding to channel gating. Such changes in channel function ultimately reflect changes in the *relative* stabilities of the resting versus the open state, which could be due to effects of the mutations on either the resting or the open state, or both.

Furthermore, the data is best interpreted in terms of our current understanding of the mechanism of channel gating. Evidence primarily from cryo-EM structures (Rahman *et al* 2020) and MD simulations (Beckstein & Sansom 2001, 2004, 2006) suggest that the nAChR controls the permeation of hydrated cations across the post-synaptic membrane via a hydrophobic gating mechanism. As discussed in Chapter 1, the close proximity and hydrophobicity of the L9' residues contribute to a hydrophobic constriction where the presence of liquid water or hydrated cations is rendered unfavorable in the resting state. Agonist-binding triggers the displacement of L9' residues from their resting state positions through translational, tangential, and/or rotational movements of the M2 helices, disrupting the favorable interactions between L9' residues that stabilize the resting state, resulting in the dilation of the constriction. The displacement of L9' residues may also cause exposure of polar residues to the pore which were previously shielded, decreasing the hydrophobicity of the constriction. The combination of increased diameter and decreased hydrophobicity sufficiently lowers the energetic barrier to hydrated cations, allowing them to permeate down their electrochemical gradients. In this context, the stability of the resting state therefore can be thought of as partially depending on the strength of favorable interactions between adjacent L9' residues driven by water exclusion from the region. A change in these interactions, induced either by a change in the hydrophobicity of a 9' residue or a change in the distance between L9' side chains could feasibly alter the stability of the resting state.

Effects of L9' residues polarity and size on channel function

In most cases studied here, increasing polarity of L9' substitutions correlate with increasing gains-of-function, suggesting that increasing polarity increases the relative stability of the open versus the resting state. In fact, since leucine is one of, if not the most hydrophobic side chain, nearly all the substitutions generated in this chapter lead to a more polar residue at the 9' position, which correlates with nearly all mutations leading to gains in function. L9' substitutions may potentiate channel function by destabilizing the resting state – i.e. the introduction of more polar side chains at the 9' position may weaken the hydrophobic driving force that underpins the favorable interactions between L9' residues in the closed, resting conformation. More polar substitutions may also enhance the penetration of liquid water into the gate region. The latter was demonstrated in an MD simulation performed by Beckstein and Sansom (2004) where they controlled the radius of a nanopore constriction by tuning the polarity of its walls, changing it gradually from a highly hydrophobic surface to a strongly hydrophilic surface. As the nanopore constriction surface was rendered more polar, water was able to maintain its liquid form at smaller constriction radii than was possible at the highly hydrophobic constriction. This suggests that the introduction of polar groups at a constriction lowers the energetic cost of water penetrating into the hydrophobic gate region. Applied to the muscle nAChR, the introduced polar group would be expected to enhance interactions with water molecules, which could lead to slower purging of water molecules from the gate during the O→R transition, allowing a longer period of hydrated cation permeation, biasing the receptor towards the open state. Note that alternatively or in addition, the introduction of a more polar side chain could potentiate channel function by increasing the stability of the open state by forming more favorable interactions with nearby residues, as discussed in Chapter 4.

The effect of changing side chain size at the 9' position on channel function is less clear than the effect of changing side chain polarity. In fact, the only clear correlation between changing residue size and changing channel function was observed with the αL9' mutants, where increasing side chain size amongst both the hydrophobic and the polar substitutions leads to an enhancement of channel function. In contrast, there is only weak or no side chain size dependence of residues at the 9' position in the β, ε, and δ subunits. One possible interpretation is that the relatively strong side chain dependence in the α subunit is because two α subunits are found in each pentamer and thus each mutation leads to two substitutions in the hydrophobic gate. The addition of two larger

bulky side chains could lead to destabilizing steric conflicts with adjacent L9' residues, whereas subtle adjustments in neighboring L9' residues may accommodate the introduction of only one mutation per pentamer. This interpretation is consistent with the potentiating effect of the αL9'F mutation (88-fold gain-of-function) which is much larger than the effects of other L9'F mutations which vary from a 2-fold loss-of-function for δL9' to a 5-fold gain-of-function for the βL9'F mutation. Another possibility is that side chain size can influence channel function through different mechanisms, depending on whether the side chain is larger or smaller than an optimal size. As noted, beyond a critical size, increasing bulk at the 9' position may lead to steric hindrance with adjacent L9' residues that de-stabilizes the closed resting state to potentiate channel function. On the other hand, smaller 9' residues may be too distant from the L9' residues on adjacent subunits to form van der Waals interactions, thus contributing to a loss of stability of the resting state. It is also possible that the increased distance between the relatively small 9' residues and adjacent L9' residues allows the penetration of water molecules into the previously occupied space to further destabilize the resting state or stabilize the open state to potentiate channel function. Consistent with these interpretations, a 2016 single channel electrophysiology study by Shen *et al* revealed that Ala mutation of the valine residues (βV266A and εV265A) in the adjacent 13' hydrophobic ring increased the rate of channel opening and channel closing, suggesting that the Ala mutations exert their effects on channel function through a simultaneous destabilization of the resting state and stabilization of the open state. In this context, it should be noted that glycine substitutions at the 9' positions of the α, β, and ε subunits each lead to some of the largest potentiations of channel function observed in this study, while δL9'G did not express. It is currently unclear whether the glycine substitutions influence function via one or both of the above noted mechanisms, or whether the increased flexibility of the polypeptide backbone in this region plays a role in the potentiating effects.

It is also possible that correlations between residue size and channel function are complicated by a functional sensitivity to side chain shape (Kearney *et al* 1996). For example, through both natural and non-natural amino acid substitutions, it was shown that the incorporation of two different stereoisomers of leucine, isoleucine and *allo*-isoleucine, at non-α subunit 9' positions of the mouse fetal muscle nAChR each led to unique changes in EC_{50} value. In fact, at the δL9' position, substituting the wild-type leucine (EC_{50} = 50μM) with isoleucine led to a slight gain-of-function (EC_{50} = 15μM) while substitution with *allo*-isoleucine led to a slight loss-of-function

(EC_{50} = 79μM) despite both stereoisomer side chains occupying the same volume. One possibility is that changing the shape of the side chain may change the inter-atomic distances between atoms belonging to the mutant 9' residue and adjacent L9' side chains, contributing to a change in the strength of van der Waals interactions between residues at the 9' position, leading to a change in the stability of the resting state.

Subunit-specific effects of L9' mutations on channel function

Predominantly, equivalent mutations exert qualitatively similar effects on channel function across the subunits, while exhibiting slight to moderate quantitative differences in EC_{50} values. As noted previously, the large gains-of-function observed following polar αL9' mutations compared to the effects of equivalent mutations in non-α subunits suggests that they are due to the presence of two mutations per pentamer. However, there also appear to be general subunit-specific trends among the non-α subunits with regards to changes in channel function. Among equivalent mutations introduced in non-α subunits, βL9' mutations, both hydrophobic and polar, generally potentiate channel function more than those at the εL9' and δL9' positions. One possible explanation for this observed trend, as outlined in a 2013 review by Nigel Unwin, is that movement of the β subunit, more specifically the βM2 helix, is the primary means by which agonist-binding is coupled to channel gating (Unwin 2013). In *Torpedo* nAChR, upon agonist-binding, the C-loop of the α_γ subunit in the ECD is drawn in toward the binding pocket, resulting in a tilting of the outer β-sheet, in turn, pushing the inner β-sheet towards the β subunit, which responds by engaging in a rocking motion away from the central pore axis. The outward rocking motion is thought to pull the βL9' residue away from the other L9' residues, marking the initial disruption of favorable interactions between L9' residues, resulting on channel opening. If the initial movement of the βL9' residue precedes the breaking of interactions between L9' residues required to open the channel gate, the introduction of a mutation at the β9' position could preemptively weaken those same interactions in the resting state, lowering the energetic cost of this step in the gating isomerization, biasing the receptor toward the open state to a greater extent than εL9' or δL9' mutations. It is currently unclear, however, whether the human adult muscle nAChR elicits channel opening via the above mechanism.

Some mutations, however, have qualitatively different effects on channel function in one subunit compared to equivalent mutations introduced at other 9' positions. Specifically, the L9'Q,

L9'H, and L9'E mutations introduced at the α, β and εL9' positions resulted in moderate to large gains-of-function, while the equivalent mutations introduced at the δL9' position produced EC_{50} values close to wild-type. One possibility is that the near WT-like EC_{50} values of the δL9'Q, δL9'H, and δL9'E mutations may simply reflect that the stability of either the resting state or open state is only minimally affected by those specific mutations. However, given the near ubiquity with which these and other polar mutations strongly potentiate channel function in other subunits, it does not seem likely that these mutations would have little to no effect on the stabilities of either state. Rather, a more plausible explanation is that these polar mutations destabilize the resting state by decreasing the hydrophobicity of the gate region, but also cause a simultaneous destabilization of the open state through steric conflicts or repulsive interactions with other surrounding residues. It is also possible that in the open state, these polar mutant side chains are shifted towards a more hydrophobic environment compared to those of equivalent mutations in the α, β, and ε subunits, an environment in which the continued presence of these polar side chains is energetically unfavorable to the open state. Consistent with these interpretations, the δL9'N and δL9'D mutations, which are tipped with the same polar functional groups as the δL9'Q and δL9'E side chains respectively, but are each shorter in length by a single methylene group, potentiate channel function 48- and 308-fold respectively. This suggests that while all four polar mutants may destabilize the resting state by decreasing the hydrophobicity of the region, the larger δL9'Q and δL9'E mutant side chains (as well as the δL9'H mutant side chain) encounter steric conflict or repulsive interactions with other residues in the open state, leading to its destabilization, while the δL9'N and δL9'D mutant side chains, by virtue of their smaller size, do not.

Notable effects of charged substitutions on channel function

Certain mutations produced unexpected effects on the dose responses of mutant nAChRs. Specifically, the δL9'K and δL9'R mutants, which introduce a positively-charged side chain into the pore and both of which lead to a gain-of-function, displayed distorted dose-response curves compared to other mutations in the various screens, while the βL9'K and εL9'R mutations, which also introduce positively-charged side chains into the pore, displayed normal sigmoidal curves. Furthermore, the Hill slope values of the δL9'K and δL9'R mutants are 1.12±0.28 and 1.06±0.45 respectively, which could indicate that the open state of these mutants are more likely to be associated with the mono-liganded versus the di-liganded form of the nAChR. The distortion is

observed in individual runs and does not only emerge upon averaging the data. The introduction of a positively-charged residue at the hydrophobic channel gate is expected to destabilize the resting state at any 9' position by decreasing the hydrophobic driving force that stabilizes the resting state. However, the effect of δL9'K and δL9'R mutants on the dose-response suggests that a specific difference of the δ9' position compared to other subunits contributes to this distorted dose-response. Following from the previous section, which suggested that a group of polar δL9' mutations may have effects on both the resting and open states, one possibility is that in addition to destabilizing the resting state, the δL9'K and δL9' mutant side-chains are sterically clashing with other surrounding residues, or being forced into a more hydrophobic environment compared to other subunits in the open state, leading to its destabilization. Further studies are obviously required to elucidate how these residues ultimately influence channel function. On the other hand, the negatively-charged δL9'E mutant had essentially no effect on the dose-response, possibly because the proximity of the pKa values of the anionic side chains (pKa ~ 4.0) are closer to neutral pH than pKa values of both cationic side chains (pKa ~ 10.5, 12.5) and because of the nature of the charge. The pKa value of a side chain is a measure of the strength of its acidity (or basicity) by using the inverse log of the acid dissociation constant Ka. In the low-dielectric constant hydrophobic pore region, the pKa values of the anionic side chains may increase to stabilize their neutral forms. While it might be expected for the pKa of both the positively-charged δL9'K and δL9'R side chains and negatively-charged δL9'E to shift towards neutrality upon changing, there is evidence that different factors govern the pKa values of basic vs. acidic side chains at the same internal position (Harms *et al* 2009). In a 2009 study, Harms *et al.* tested the pKa values of engineered ionizable residue side chains at various locations in a hyperstable form of Staphylococcal nuclease (SNase), and while they noticed that a glutamic acid residue engineered at position 38 (Glu38) experienced an increase in its pKa from 4.25 to 7.2, the researchers observed that a lysine engineered at the same internal position (Lys38) displayed an unchanged or possibly slightly elevated pKa value compared to the pKa value in bulk water. The researchers attributed the pKa shift of the side chain of Glu38 to enhanced participation in an internal hydrogen bonding network to compensate for loss of interactions with water, and attributed the unchanged pKa of Lys38 to water penetration at the internal position leading to stabilization of lysine's positive charge. This study suggests that the particular microenvironment surrounding a specific position in a protein can lead to an increase in the pKa values of acidic side chains, pushing them towards

the neutral form, and the same microenvironment can leave the charged form of the basic ionizable residues unchanged. Applied to the human adult muscle nAChR, the microenvironment surrounding the δL9' position in the open state may favor the protonated, charged state of basic side chains like δL9'K and δL9'R and the protonated, uncharged state of acidic side chains like δL9'E. In fact, the cation selectivity of the nAChR channel pore may favor the protonated Lys and Arg side chains.

Interestingly, a 2005 study by Cymes *et al* previously characterized the δL9'K and δL9'H mutants using single-channel measurements, primarily to establish the protonation states of these basic ionizable side chains engineered along the δM2 helix of adult mouse muscle nAChR. The study determined the protonation state of the individual side chains by detecting oscillations between two discrete levels of conductance, with the lower conductance level denoting the protonated and thus positively-charged form of the side chain, and the higher conductance level denoting the neutral, uncharged form of the side chain. The study established that the δL9'K mutant side chain was most likely in the charged, protonated state at pH 7.4, because only a single reduced conductance level could be observed, and the δL9'H mutant showed oscillations between two conductance levels, but the deprotonation rate was found to be twice the protonation rate, and therefore, the side chain mostly existed in the deprotonated, neutral form. This may provide an explanation as to why δL9'K and δL9'R mutations result in gain-of-function phenotypes with distorted dose-responses, while δL9'H results in no appreciable change to EC_{50} compared to wild-type while presenting a normal-looking dose-response curve.

So, if certain δL9' residues sterically clash with other residues or are forced into a more hydrophobic environment compared to other residues, how might this be accomplished through movements of L9' residues? While we do not have high-resolution structures of muscle nAChRs in the open state, we do have high quality MD simulations as well as solved structures of other pLGICs in various conformational states to suggest the possible movements of L9' residues upon channel opening. A recent MD simulation of the R→O gating transition of the GlyR focusing on the movement of L9' residues was performed to explore energetically stable open state conformations of L9' residues (Dämgen & Biggin 2019). Previous MD simulations had shown that without certain restraints on the peptide backbone, the L9' residues undergo a 'hydrophobic collapse' in the open state, leading to a non-conducting channel. To avoid this, the researchers used an equilibration protocol that prevented the pore from collapsing while giving the protein

maximum freedom to explore alternative open conformations. Their MD simulations suggested that upon channel opening, the L9' residues swing in a clockwise direction from the lumen into hydrophobic pockets comprising residues from the principal M2 helix (the one containing the L9' residue in question), and the complementary M2 and M1 helices of the adjacent subunit. The movements of L9' residues into these hydrophobic pockets appeared to stabilize the open state upon agonist-binding. The result is a widening of the pore and a stable configuration of L9' residues in hydrophobic pockets comprising identical residues. While the case is different for muscle-type nAChR due to its nature as a heteropentamer instead of a homopentamer, the mechanism observed in the MD simulation may be applicable to the broader family of pLGICs. To further support these observations, three stuctures of the GlyR representing the closed, open and desensitized states were recently solved in a lipid nanodisc environment, showing that the M2 helices undergo a undergo a slight clockwise shift upon channel opening, rotating the L9 residue from the lumen toward the hydrophobic protein interior (Kumar *et al* 2020). If the human adult muscle-type nAChR channel opening occurs similarly to that observed in the GlyR, the residue composition of the hydrophobic pockets, and perhaps the large-scale motions of the different M2 helices upon channel opening may explain differences in the effects of L9' mutations on channel function among the different subunits. The hydrophobic pockets in the human adult muscle nAChR would be lined by a different combination of residues in different orientations, possibly resulting in pockets of different shapes or polarities, ensuring that each L9' residue faces a slightly different microenvironment. An especially small, or hydrophobic pocket encapsulating the δL9' residue in the open state, or a comparatively more pronounced rotation of the δM2 helix may be destabilizing for the larger δL9'Q, δL9'H and δL9'E mutant side chains, but relatively inconsequential for the smaller δL9'N and δL9'D mutant side chains which may not reach deeply enough into the protein interior to experience repulsive or steric effects. Much more information on opening and closing rate constants of the specific mutant nAChRs of interest needs to be acquired to enhance confidence in the interpretation of the EC_{50} data and importantly, more information related to the positions of L9' residues in the open state needs to be obtained through a high-resolution structure of adult muscle nAChR in the open state.

Chapter 3

Probing local interactions surrounding βL9’ and δL9’ that govern channel function

3.0 Introduction

In Chapter 2, I showed that most mutations to L9' result in a left-shift in the concentration-response to ACh (i.e. lower EC_{50} values), suggestive of gain-of-function phenotypes, with polar mutations generally potentiating channel function to a greater extent than hydrophobic mutations. While there are likely complex mechanisms underlying the observed changes in function, I hypothesized that interactions between L9' residues and surrounding residues stabilize the resting state, with the disruption of these interactions leading to a decrease in the stability of the resting state to promote channel gating. I also hypothesized that polar mutations, may form favorable interactions with surrounding residues in the open state, thus leading to its stabilization relative to the resting state. While the observed decreases in EC_{50} do not give direct insight on how these mutations alter local interactions to influence the relative energies of the resting versus the open states, double mutant cycle analysis can be used to detect whether interactions between two residues contribute energetically channel function. In a double mutant cycle analysis, the putatively interacting residues are mutated to alanine, first individually and then simultaneously. The EC_{50} values of both the individual and double mutants are then compared to the wild-type to assess whether the effects of the mutations are additive, and thus independent, or non-additive, and thus dependent. If the effect of the double mutant on channel function is significantly different than the additive effects of both single mutations, this suggests that an interaction between two residues contributes energetically to channel function.

In this chapter, I used the *Torpedo* 2BG9 nAChR structure to identify residues that could interact with L9' to stabilize either the resting or open states. I designed two separate double mutant cycles to probe for interactions between βL9'/δL9' and the 6' and 10' residues on the adjacent αM2/βM2 helices. I also designed an additional double mutant cycle to probe for newly formed interactions between βL9'S and the 6' and 10' αM2 residues in the open state upon mutation to a polar residue. Although I was unable to find key interactions involving the noted L9' residues that play a role stabilizing the resting or open state, a higher-resolution 2.7Å cryo-EM structure of the *Torpedo* nAChR was published during the writing of this thesis (Rahman *et al* 2020). This newer structure suggested that the L9' residues adopt different orientations than suggested by the 2BG9 structure thus offering multiple possible explanations for the observed findings. In particular, my data are consistent with the new 2.7Å resolution nAChR structure in that the new structure places

the L9' residues on adjacent M2 helices closer to each other than to adjacent residues. Overall, my data provide additional support to the new 2.7Å resolution model.

3.1 Materials and Methods

The methods used for the generation of mutants, oocyte preparation and electrophysiological characterization of mutants are described in section 2.1 of Chapter 2.

3.1.1 Mutant Cycle Analysis

Mutant cycle analysis allows one to determine the extent to which two or more protein residues are energetically coupled (Horovitz and Fersht, 1990; Lee and Sine, 2005). My mutant cycles were performed using the averaged EC_{50} values for ACh as follows:

$$\Omega = \frac{\left(EC_{50}\left(mut_{1,2}\right)\right) * \left(EC_{50}(WT)\right)}{\left(EC_{50}(mut_1)\right) * \left(EC_{50}(mut_2)\right)}$$

Where Ω is the coupling constant, *WT* is the control, *mut1* is the first mutant of interest, *mut2* is the second mutant of interest, and *mut1,2* is the double mutant. Note that *WT* usually refers to the wild-type nAChR, but in some cases refers to the background upon which the double mutants are generated. Typically, many studies use the coupling constant to calculate how much energy the interaction between two residues contributes to channel gating using the following equation:

$$\Delta\Delta G = -RTln\Omega$$

Where ΔΔG is the free energy of coupling, R is the gas constant (8.314 J/mol*K) and T is the temperature (K). However, because I am using EC_{50} values for the mutant cycle, and EC_{50} values are composites of agonist-binding and channel gating, ΔΔG energy values may not solely reflect the energy contributed to gating, and thus some studies have avoided using this practice out of caution (Daeffler *et al* 2012). Because I wish to also remain cautious in my analysis, I only establish the degree of coupling in this thesis, and do not assign an energetic value to interactions. However, I do establish a threshold for the significance of energetic couplings between residues by using as references the energies of van der Waals interactions, which are the weakest kinds of interactions. While the strengths of van der Waals interactions can vary depending on the

environment, their strength are typically in the range of 1-4 kJ/mol. To establish a threshold for significance, I generally considered two residues to be energetically coupled when Ω differs from 1 by a factor of at least 2 (i.e., $\Omega \geq 2$ or $\Omega \leq 1/2$), which corresponds to an $\Delta\Delta G$ of ±1.72 kJ/mol, which is close to the average strength of a single interatomic van der Waals interaction.

My mutant cycles were performed such that I calculated the coupling constant Ω resulting from the removal of an interaction between two residues. The presence of interactions between two or more residues is detected by assessing channel function following their removal, which is achieved by substituting the residues with non-interacting residues such as alanine. For example, to test an interaction between an L9' residue and a neighbouring polar residue: βL262 and αS248, my *WT* would be the wild-type nAChR, where both βL262 and αS248 are present. Each single mutant represents the removal of one or several functional groups by replacement with alanine, which removes several -CH_3 groups from βL262 and an -OH group from αS248 (i.e., *mut1* = βL262A and *mut2* = αS248A). The double mutant represents the removal of both functional groups and replacement with alanine (i.e., *mut1,2* = βL262A+αS248A). In a second scenario where I calculated an interaction between the βL9'S mutant and adjacent polar group (e.g. αS252), the βL9'S mutant is treated as the wild-type component, rendering the equation as follows: *WT* = βL9'S+αS252, where βL9'S and the polar αS252 residues are both present, *mut1* = βL9'S+αS252A, where one polar -OH group has been removed, *mut2* = βL9'A+aS252, where the other -OH has been removed, and *mut1,2* = βL9'A+αS252A where both polar groups have been removed. In both examples, $\Omega>2$ signifies that the interaction in question is beneficial, while $\Omega<0.5$ signifies that the interaction in question is detrimental (Daeffler *et al* 2012).

3.2 Results

To identify candidate residues that could be energetically coupled to an L9' residue, I used the cryo-EM 4Å resolution *Torpedo* nAChR structure (PDB: 2BG9) to analyze the spatial orientation among pore-lining residues near the channel gate, as this was the only structure available at the commencement of this project (Unwin 2005). While the structure shows the L9' residues close to the central axis of the pore, the side chains project towards the M2 helices of adjacent subunits (Figure 3.1). Residues closest to the L9' residues were prime candidates for potential direct interactions, and the structure suggests that the L9' residues are close to the

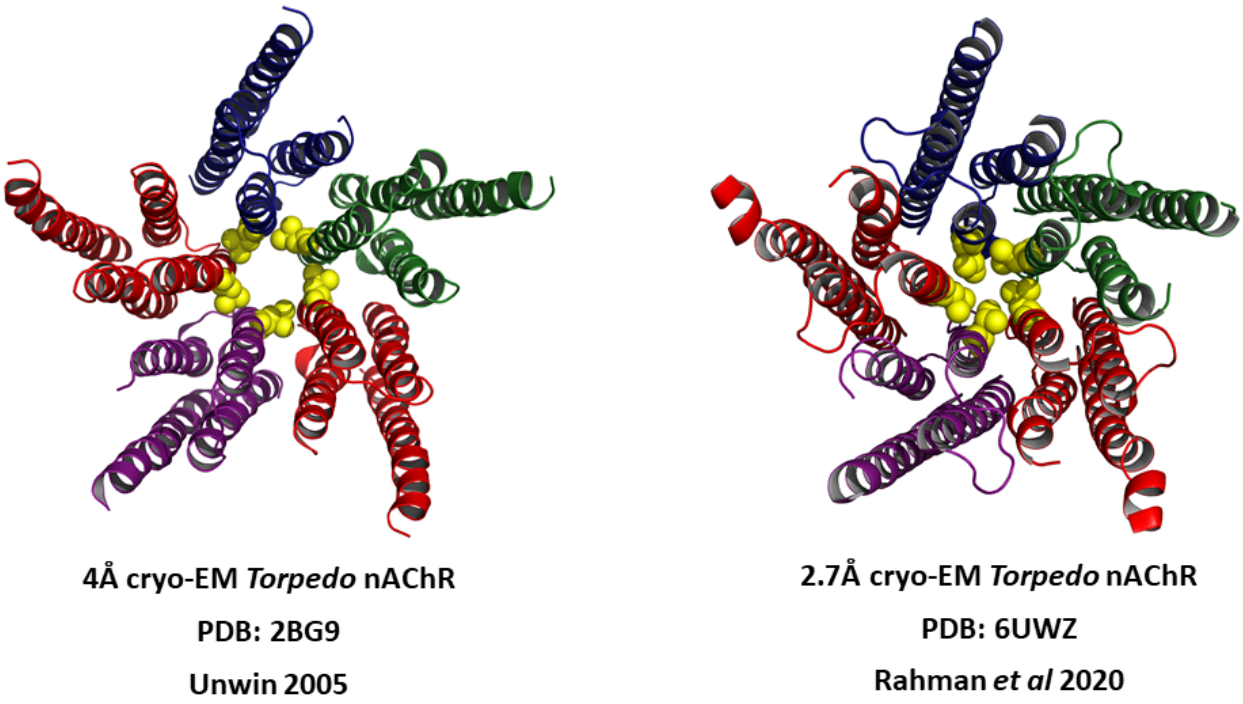

Figure 3.1: Transmembrane domain of the 4Å and 2.7Å resolution structures of muscle nAChR. The image on the left shows a top-down view of the TMD of the 4Å resolution *Torpedo* nAChR (PDB: 2BG9) (Unwin 2005), while the image on the right shows the TMD of the 2.7Å *Torpedo* nAChR (PDB: 6UWZ) (Rahman *et al* 2020). The 4Å resolution structure shows the L9' residue side chains mostly pointing away from the central pore axis and towards the M2 helices of adjacent subunits. The newer 2.7Å resolution structure shows the L9' residue associate more tightly around the central pore axis with most L9' residues oriented towards the L9' residue of an adjacent subunit.

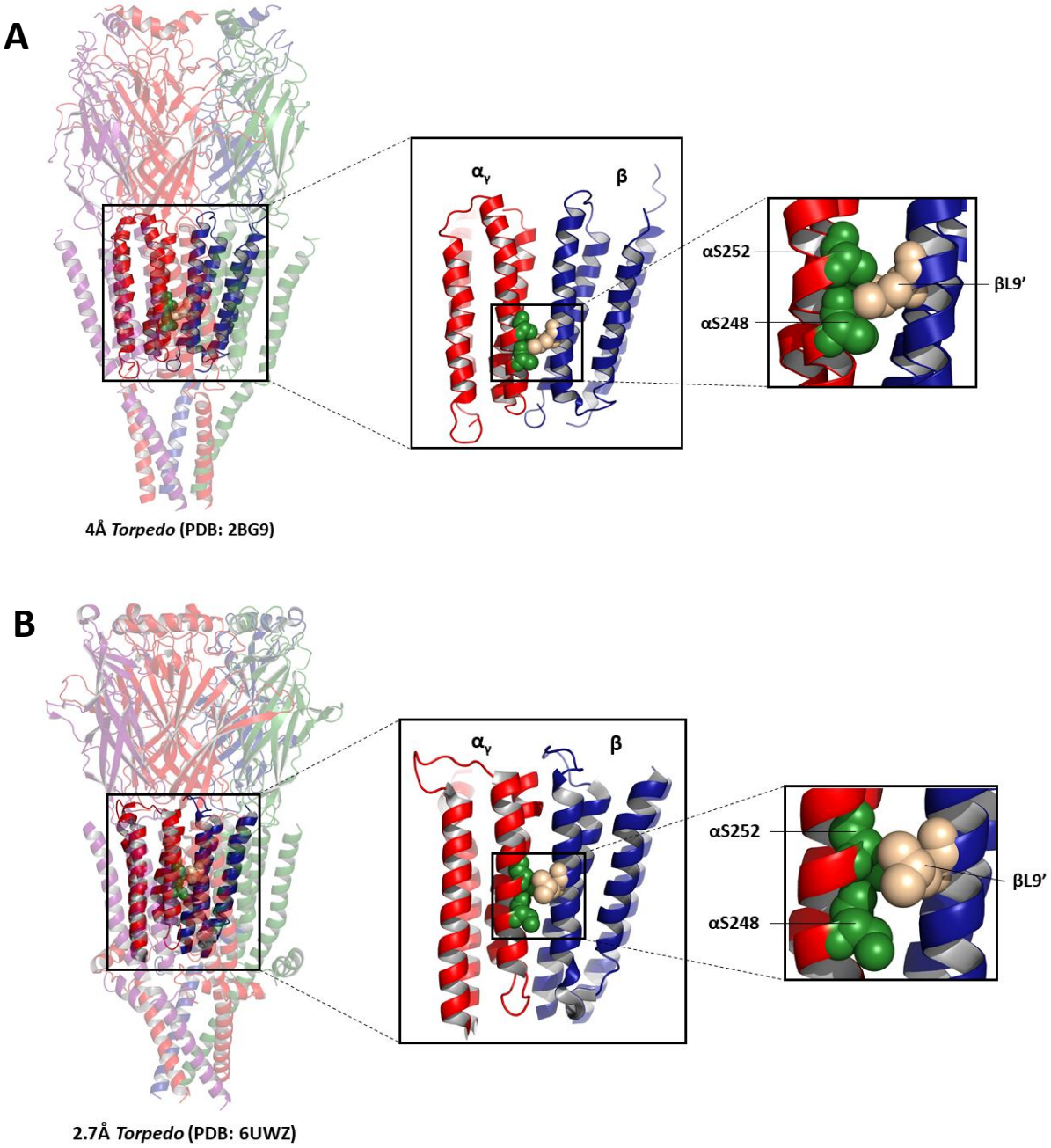

Figure 3.2: Side-chain orientations of βL9', αS248 and αS252 in lower and higher resolution cryo-EM *Torpedo* structures in the resting state. (A) The relative orientations of βL9' (tan spheres), αS248 and αS252 (green spheres) in the lower resolution 4Å *Torpedo* structure. The structure shows βL9' neatly nestled between αS248 and αS252, suggesting direct interactions in the resting state. **(B)** The relative orientations of βL9' (tan spheres), αS248 and αS252 (green spheres) in the higher resolution 2.7Å *Torpedo* structure. This newer structure shows a shorter M2 segment, and a βL9' residue that is more oriented towards the central pore axis. The newer structure also shows βL9' in closer contact with αS252 compared to αS248, while in the lower resolution structure, βL9' appears equidistant from both αS248 and αS252.

residues of the 6' and 10' positions on adjacent subunits. I first used two separate double mutant cycles, to probe interactions between βL9' and the 6' and 10' positions on the αM2 helix, αS248 and αS252 respectively, and another to test for interactions between δL9' and the 6' and 10' residues of the adjacent βM2 helix, βF259 and βT263 respectively. I also employed the use of a third double mutant cycle to test for the presence of newly-formed interactions between βL9'S and αS248/αS252. The effects of each mutation on channel function were characterized using TEVC electrophysiology, yielding EC_{50} values which were subsequently used in the equation shown in section 3.1.1 to establish the degree of energetic coupling between residues.

3.2.1 Do interactions between βL9' and αS248/αS252 stabilize the resting state?

To test for the presence of interactions between βL9' and nearby αS248 and αS252 residues, the residues were mutated first individually, and then simultaneously to alanine to remove potential interactions, producing a series of single, double, and triple mutants (when treating αS248+αS252 as a single unit). Table 3.1 shows the results of TEVC characterization of these mutants. The βL9'A mutation resulted in a 20-fold gain-of-function while the individual αS248A and αS252A mutations both potentiated channel function mildly, leading to 1.9- and 3.7-fold gains-of-function respectively. Interestingly, when the two serine residues are treated as a single unit by mutating them both to alanine simultaneously, the resulting αS248A+αS252A mutant is an 8.3-fold loss-of-function compared to wild-type. The interaction between αS248 and αS252 was determined to have a $\Omega = 56$ (Table 3.2), indicating strong coupling between αS248 and αS252 residues beneficial to gating. This result suggests that these two serine residues collectively serve an important role in channel function.

The double mutant βL9'A+αS248A resulted in a 17-fold increase in channel function compared to wild-type nAChR, a value approximately half of what would be expected if the effect of the two individual mutations were purely additive (1.9*19.4 = 36.9-fold). The measurement for interactions between βL9' and αS248 yielded a coupling constant value of $\Omega = 2.10$, indicating only weak coupling between these residues. The double mutant βL9'A+αS252A yielded a 43-fold increase in channel function compared to wild-type, which is also lower than expected if the effects of the two individual mutations were purely additive (3.7*19.4 = 71.8-fold), but the coupling constant in this case is $\Omega = 1.64$, suggesting weak if any interactions that influence channel function. To measure the combined interactions of the αS248+αS252 serine pair with the βL9'

Table 3.1: Role of αS248/αS252-βL9' interactions in channel function

	Dose Response[a]				
	WT-nAChR[c]		βA9'-nAChR[d]		Potentiation[e]
Mutation(s)	EC_{50} (μM)	n	EC_{50} (μM)	n	
None	8.22 ± 1.87	126	0.424 ± 0.118[b]	28	19.4
αS248A	4.44 ± 1.41[b]	7	0.480 ± 0.149[b]	8	9.3
αS252A	2.24 ± 0.747[b]	12	0.190 ± 0.030[b]	7	11.8
αS248A+αS252A	68.2 ± 10.6[b]	5	10.7 ± 1.38	4	6.4

[a] Measurements were performed 2-7 days after injection of cRNA. Error values represent standard deviations.
[b] $p<0.0001$ relative to wild-type control via one-way ANOVA followed by Dunnett's post-hoc test.
[c] WT-nAChR contains only the mutation(s) listed under the "mutation(s)" column.
[d] βA9'-nAChR contains βL9'A in addition to the mutation(s) listed under the mutation(s) column.
[e] EC_{50} of mutant on WT-nAChR background divided by EC_{50} of mutant on βA9'-nAChR background.

Table 3.2: Ω-values probing for energetic coupling between βL9' and αS248/αS252

	βL9'→A	αS248→A
Mutants	**Ω**	**Ω**
αS248A	2.10	N/A
αS252A	1.64	56
αS248A+αS252A	3.04	N/A

residue, a βL9'A+αS248A+αS252A triple mutant was generated which treats the αS248+αS252 serine pair as a single unit. The single βL9'A mutant resulted in a 19.6-fold gain-of-function while the αS248A+αS252A double mutant resulted in an 8.3-fold loss-of-function. If the αS248A+αS252A and βL9'A mutations exerted their effects on channel function independently, a net 2.4-fold gain-of-function would be expected (0.12-fold * 19.6-fold = 2.36-fold). Instead, the βL9'A+αS248A+αS252A triple mutant results in a very slight 1.3-fold loss-of-function phenotype. Overall, these data suggest that interactions between βL9'A and either αS248A or αS252A play little to no role in stabilizing the resting and/or open states.

3.2.2 Do interactions between δL9' and βF259/βT263 stabilize the resting state?

Based on the results from the previous analysis indicating only weak or no interactions between βL9' and αS248/αS252, I wanted to explore whether the same held true for potential interactions between a different L9' residue and surrounding residues. I reasoned that since α subunit mutants introduce two mutations per pentamer, the coupling constants obtained from the analysis may not accurately reflect a change in interactions only at the α/β interface. This is because an α subunit mutation introduces a change at two distinct locations in the TMD. To address this potential ambiguity, I repeated the same experiment as described in section 3.2.1, but in this instance, I tested for the presence of interactions between δL9' and βF259/βT263, the equivalent 6' and 10' residues on the β subunit, in which only one mutation per pentamer is present for single mutants and two for double mutants. The δL9'A mutation led to a 10.4-fold gain-of-function, while the βF259A mutation resulted in an EC_{50} that was considered not significantly different from wild-type following a one-way ANOVA test. Should these mutations exert their effects on channel function independently, the double mutant would be expected to result in nearly the same gain-of-function as the δL9'A single mutant (10.4-fold) since the βF259A mutation does not significantly alter channel function. The resulting double mutant leads to an EC_{50} = 0.973μM, an 8.5-fold gain-of-function, which is not largely different from the 10.4-fold gain-of-function of the single δL9'A mutation. These results indeed suggest that the effects of each mutation on channel function are independent of one another, and there are no significant interactions between δL9' and βF259 acting to stabilize either the resting or open states. I also explored the possibility that interactions between δL9' and βT263 stabilize the resting state. Through the functional characterization of the corresponding single and double mutants, it was observed that the δA9'+βT263A double mutant's

Table 3.3: Role of βF259/βT263-δL9' interactions in channel function

	Dose Response[a]				
	WT-nAChR[c]		δA9'-nAChR[d]		Potentiation[e]
Mutation(s)	EC_{50} (μM)	n	EC_{50} (μM)	n	
None	8.22 ± 1.87	126	0.792 ± 0.062[b]	28	10.4
βF259A	6.94 ± 1.20	10	0.973 ± 0.146[b]	3	7.13
βT263A	4.64 ± 1.05[b]	7	0.650 ± 0.111[b]	5	7.14
βF259A+βT263A	4.44 ± 0.862[b]	3	0.574 ± 0.202[b]	4	7.74

[a] Measurements were performed 2-7 days after injection of cRNA. Error values represent standard deviations.
[b] $p<0.0001$ relative to wild-type control via one-way ANOVA followed by Dunnett's post-hoc test.
[c] WT-nAChR contains only the mutation(s) listed under the "mutation(s)" column.
[d] δA9'-nAChR contains δL9'A in addition to the mutation(s) listed under the mutation(s) column.
[e] EC_{50} of mutant on WT-nAChR background divided by EC_{50} of mutant on δA9'-nAChR background.

Table 3.4: Ω-values probing for energetic coupling between δL9' and βF259/βT263

	δL9'→A
Mutants	Ω
βF259A	1.46
βT263A	1.45
βF259A+βT263A	1.34

12.6-fold gain-of-function is close to the expected 18.4-fold gain-of-function if the two single mutants were to exert their effects on channel function independently and additively. This suggests that there are no significant interactions between δL9' and βT263 that contribute towards stabilization of either the resting or open states. The effect of expressing a δA9' mutation simultaneously with either the βF259A or the βT263A mutation results in nearly the same level of channel function potentiation at 7.13- and 7.14-fold compared to each respective mutant. The effect of expressing a δA9' mutation simultaneously with both βF259A and βT263A mutations yields little change in potentiation (7.74-fold) compared to adding a δA9' mutation to either individual mutants (Table 3.3). This further suggests that the change in channel function elicited by a δA9' mutation is not influenced by a change in interactions with either βF259 or the βT263 residues.

3.2.3 Do interactions between βS9' and αS248/αS252 stabilize the open state?

Next, I wanted to test for the presence of interactions between βL9'S (referred to as βS9'), a polar mutant, and the same two serine residues to see if the introduction of such a residue at the βL9' position leads to the formation of new interactions which act to stabilize the open state. In this case, the "wild-type" mutant is βS9', and the alanine mutations serve to remove any potential interactions between βS9' and the two serine residues being investigated. To first test for the presence of interactions between βS9' and αS248, the residues were mutated to alanine individually, and then simultaneously. The βA9' mutation resulted in a 6-fold loss-of-function compared to βS9', while the βS9'+αS248A mutation resulted in a slight 1.3-fold gain-of-function (Table 3.5). If the individual mutations exerted their effects on channel function independently, the double mutant would be expected to display the additive effects of the two single mutations, producing a receptor with a 4.6-fold loss-of-function phenotype. The βA9'+αS248A double mutant resulted in a less functional phenotype than expected, impairing channel function 6.8-fold. While the observed double mutant is less functional, the similar level of channel function impairment to what was expected from the combined effects of the two single mutants suggests that interactions between βS9' and αS248 are not significantly beneficial to gating, reflected in a coupling constant $\Omega<2$ (Table 3.6).

I also tested whether interactions between βS9' and αS252 stabilize the open state. The two single mutants βA9' and βS9'+αS252A lead to a 6-fold loss-of-function and a 2-fold gain-of-

Table 3.5: Role of αS248/αS252-βS9' interactions in channel function

	Dose Response[a]				
	βS9'-nAChR[d]		βA9'-nAChR[e]		Potentiation[f]
Mutation(s)	EC_{50} (μM)	n	EC_{50} (μM)	n	
None	0.071 ± 0.014	51	0.424 ± 0.118	26	0.17
αS248A	0.053 ± 0.003[b]	4	0.480 ± 0.149	8	0.11
αS252A	0.034 ± 0.003[c]	11	0.190 ± 0.030	7	0.18
αS248A+αS252A	2.30 ± 0.224[b]	4	10.7 ± 1.38[b]	4	0.21

[a] Measurements were performed 2-7 days after injection of cRNA. Error values represent standard deviations.
[b] $p<0.0001$ relative to wild-type control via one-way ANOVA followed by Dunnett's post-hoc test.
[c] $p<0.005$ relative to wild-type control via one-way ANOVA followed by Dunnett's post-hoc test.
[d] βS9'-nAChR contains βL9'S in addition to the mutation(s) listed under the mutation(s) column.
[e] βA9'-nAChR contains βL9'A in addition to the mutation(s) listed under the "mutation(s)" column.
[f] EC_{50} of mutant on βS9'-nAChR background divided by EC_{50} of mutant on βA9'-nAChR background.

Table 3.6: Ω-values probing for energetic coupling between βS9' and αS248/αS252

	βS9'→A
Mutants	**Ω**
αS248A	1.52
αS252A	0.94
αS248A+αS252A	0.78

function compared to the 'wild-type' βS9' respectively. The functional state of the double mutant βA9'+αS252A (2.7-fold loss-of-function) is close to the phenotype expected if the two single mutants exerted their effects on channel function independently (2.9-fold loss-of-function). This is confirmed by a coupling constant value of $\Omega = 0.94$, which is close to a value of 1, suggesting that each mutant exerts its effects on channel function independently, and that there are no interactions between βS9' and αS252 that contribute toward stabilization of the resting state or the open state.

3.3 Discussion

The mutant cycle analyses showed that there are only weak if any interactions between βL9' and either αS248 or αS252 that influence channel function. Likewise, the equivalent analysis performed on δL9' and βF259/βT263 failed to show any significant interactions between δL9' and either βF259 or βT263. Furthermore, it was shown that there are no new interactions formed between βS9' and either αS248 or αS252 that stabilize the open state, implying that the gains-of-function elicited by the βA9', δA9', and βS9' mutants are due to changes among a different set of interactions than those investigated in this chapter.

When I initially targeted the αS248 and αS252 residues for potential interactions with βL9', the best available cryo-EM structure of a muscle-type nAChR at the time was Unwin's 4Å *Torpedo* structure (Unwin, 2005), which showed βL9' nestled tightly between αS248 and αS252, leading to the hypothesis that βL9' directly interacts with both residues to stabilize the resting state. A very recent publication shows a higher-resolution 2.7Å *Torpedo* structure in which the βL9' and αS248/αS252 residues have a different orientation (Rahman *et al* 2020). βL9' projects its side chain more towards the central pore axis, and the αS248 and αS252 residues are shielded from the channel lumen by βL9' (Fig 3.2). The 4Å structure suggests that αS248 and αS252 are approximately equidistant from βL9' while in the 2.7Å structure, αS252 is closer to βL9' than αS248. While past and current cryo-EM structures of muscle-type nAChR can assign secondary structure to amino acid sequence, many cryo-EM structures are not yet high-resolution enough to be able to assign side-chain rotamers with confidence. Additionally, since we do not have any high-resolution structures of muscle-type nAChR in the open state, we are not able to predict the extent of structural change that occurs upon channel opening. This suggests that selecting potential interacting residues based mostly on their physical proximity to other residues in lower-resolution

cryo-EM structures may not be a suitable strategy to successfully find strong inter-residue interactions that contribute to a change in channel function.

In the context of a hydrophobic gating mechanism, the relative orientations of the residues under focus in Rahman *et al*'s 2.7Å *Torpedo* nAChR structure offer multiple possible explanations for the gains-of-function observed in the hydrophobic βL9'A/δL9'A mutations and the polar βL9'S mutation. As previously discussed, MD simulations suggest hydrophobic driving forces lead to favorable interactions between L9' residues which stabilize the resting state, and that a change in these interactions could potentially lead to a change in the stability of the resting state. The new structure which shows the L9' residues mainly oriented towards one another instead of adjacent M2 helices, supports this interpretation. The mutation of an L9' residue to Ala results in a decrease in residue size, which could weaken or eliminate favorable van der Waals interactions that help stabilize the resting state, and also results in a decrease in hydrophobicity, reducing the strength of the hydrophobic driving forces keeping L9' residues together in the resting state. Another possibility is that the void formed by the decrease in residue size allows penetration of water molecules deeper into the gate region, potentially destabilizing the resting state through a decrease in gate hydrophobicity. The reduction in L9' side chain size could also potentially expose polar residues previously shielded from the pore, stabilizing the open state through favorable interactions with water and hydrated cations. Alternatively, in the wild-type nAChR there may be steric hindrance experienced by L9' in the open state that is alleviated through mutation to a residue with a smaller side chain, easing the transition from the resting to the open state. The βS9' mutant, which introduces a smaller and more polar side chain than the native leucine into the pore, potentiates channel function to a greater degree than the βA9' mutant or δA9', but likely exerts its effects on channel function in similar ways. The degree to which both the βA9' and βS9' mutants reduce side chain size compared to wild-type is nearly identical, suggesting that the effects of size reduction on channel function is likely similar between both mutants. However, the βS9' mutant side chain is much more polar than the βA9' mutant, suggesting that the βS9' mutant side chain destabilizes the resting state to greater extent than βA9', contributing to the greater gain-of-function. In addition, the hydroxyl group of the βS9' mutant side chain, unlike the methyl group of the βA9' mutant side chain, is capable of forming hydrogen bonds, and as such, may stabilize the open state through formation of favorable interactions with water molecules in the open state.

The strongest interaction contributing to channel function that was detected by the mutant cycle analysis was not between L9' and surrounding residues but rather between the αS248 and αS252 residues. The replacement of each residue with alanine individually only led to a modest gain-of-function. The double mutant resulted in an 8.3-fold loss-of-function, suggesting a strong coupling between the residues ($\Omega = 56$), that contributes to the stabilization of the open state relative to the resting state. On the other hand, the interaction between βF259 and βT263, the equivalent 6' and 10' residues of the β subunit, produced a coupling constant with value $\Omega = 1.13$, indicating no significant interactions between those residues that contribute towards gating. This suggests that the strong interaction observed between αS248 and αS252 may serve a particular function in the context of a gating. Studies performed by Unwin's research group suggest that channel opening requires only a subtle structural change to the M2 helices to widen the pore sufficiently to allow permeation of hydrated cations (Miyazawa *et al* 2003). One of their studies showed a link between a switch in the conformation of the α subunits and channel opening, likely triggered by a rotation of the pore-lining αM2 helices by about 15º (Unwin *et al* 2002). Rahman *et al*'s 2.7Å resolution structure suggests that while a small rotational movement of αM2 could slightly dilate the pore by moving αL9' away from the central pore axis, such a rotation of αM2 could also expose the αS248 and αS252 residues to the channel lumen. This would allow the αS248 and αS252 residues to participate in favorable interactions with hydrated cations, resulting in a simultaneous dilation of the pore and reduction in channel gate hydrophobicity, promoting passage of hydrated cation through the channel in the open state. If the interaction between these two serine residues helps to stabilize the open state, however, it is curious that we observed a modest gain-of-function for each individual Ser to Ala mutation instead of a loss-of-function. Further structural studies are required to shed light on the role of these two residues in channel function.

Although I was not able to detect local interactions involving the L9' residues that contribute to channel function, my data suggest that Rahman *et al*'s 2.7Å structure, which shows L9' residues in close contact with each other forming a tight constriction, is accurate. Therefore, future studies that seek to understand the underlying causes of changes in channel function upon mutation of L9' residues should aim to measure the energetic contributions between the various L9' residues towards the stabilization of the resting or open states. Furthermore, while this Chapter highlights the lack of observed changes in inter-residue interactions between L9' and nearby residues upon mutation, it also stresses the need for further research into the role of water molecules on the

stability of the channel gate, since the hydrophobic gating mechanism implies that interactions between L9' residues and water molecules also likely change upon mutation. Future studies could make use of high-quality MD simulations to test how the behavior of water molecules near the channel gate changes when L9' residues are mutated to a series of different mutations. It is expected that in the coming years, improvements in computing power will allow for longer and more accurate MD simulations that can shed light on what is happening at the channel gate level. Pharmaceutical treatments aimed at restoring wild-type function in mutant nAChRs should be designed with the goal of re-establishing the relative stabilities of the resting versus open states. This could be achieved either through direct interactions of the therapeutic agent with the gate region or alternatively through allosteric modulation of the receptor, causing changes in interactions among specific residues along the 'conformation wave' that affect the coupling of binding to gating.

Chapter 4

General Discussion and Future Directions

The research in this thesis has been aimed towards probing the effects of different L9' mutations on channel function and trying to understand the factors which contribute to the observed changes in channel function. Not only is it important to understand how these factors can lead to change in channel function, but it is also important to understanding how specific changes induced by a particular mutation can contribute to development of a CMS.

The results in Chapter 2, which primarily focuses on characterizing the functional effects of substituting L9' residues with every naturally-occurring amino acid in the human adult muscle nAChR, suggest that substituted L9' residue size and polarity both have an effect on channel function, but that polar mutations generally exerts a more potentiating effect than nonpolar mutations. The effect of a particular L9' mutation on channel function also appears to depend on the subunit carrying the mutation, and while the results show that equivalent mutations introduced at different L9' positions mostly led to similar changes in channel function, some polar and charged δL9' mutations resulted in qualitatively different effects on channel function. The stabilities of the resting and open states of each of these particular mutations on channel function remain to be elucidated. Future studies using single-channel electrophysiology will provide additional information regarding the opening and closing rate constants which could be used to determine the stabilities of each state of the channel. While my study concerns the human adult muscle nAChR, its findings may be useful in the study of other human nAChR subtypes such as the α7 or α4β2 receptors. It may also provide broader insight into the channel function of other pLGICs and ion channels, some of which are suggested to also operate via a hydrophobic gating mechanism (as reviewed by Aryal *et al* 2015). As such, while the L9' residues comprise the narrowest constriction of the channel, the V13' residues above them are likely to also contribute to the hydrophobic environment that constitutes the channel gate. A future study would be to perform a mutant screen of the V13' residues similar to the one done on the L9' residues, followed by single channel electrophysiology studies of specific V13' mutants.

In Chapter 3, I evaluated the hypothesis that changes in channel function elicited by L9' mutations are partially due to changes in local interactions between L9' residues and nearby residues such as the 6' and 10' residues of adjacent subunits. The L9' residues appeared to be oriented towards the 6' and 10' residues of the adjacent subunit in the 4Å *Torpedo* structure, and appeared to be in closer contact with these residues than with other L9' residues. The results show

that there are little to no interactions between βL9' and δL9' residues and neighboring 6' and 10' residues on the adjacent subunit which contribute to channel function. This is supported by the newer 2.7Å resolution structure, which shows the L9' residue more oriented towards each other than towards the 6' and 10' residues. While interactions between residues that strongly couple binding to gating remain to be discovered, the lack of detected interactions highlights the need for high-resolution nAChR structures of the open state which are able to assign side chain rotamers with confidence. A high-resolution structure of the open state of the *Torpedo* or human adult nAChR could help direct the search for interactions between residues that contribute energy towards channel gating. In addition, advancements in lipid nanodisc technology will permit the structural determination of the human adult muscle nAChR. While mutant cycle analysis is a useful tool, understanding the behavior of water molecules near the channel gate is also important in the context of the hydrophobic gating mechanism and requires a different method. Future studies could make use of high-quality MD simulations to understand how interactions between L9' residues and water molecules change upon mutation to influence their behavior near the channel gate.

In conclusion, my research has highlighted the role played by various factors that contribute to the effects of a particular mutation on channel function of human adult muscle nAChR. It is hoped that the findings of this study can help in the design of therapeutic agents that allosterically modulate mutant nAChRs with an aim to restore wild-type gating characteristics for those suffering from CMS.

References

References

Akabas, M., Kaufmann, C., Archdeacon, P. and Karlin, A. (1994) Identification of Acetylcholine Receptor Channel-Lining Residues in the Entire M2 Segment of the α Subunit. *Neuron* 13: 919-927.

Albuquerque, E., Pereira, E., Alkondon, M, and Rogers, S. (2009) Mammalian nicotinic acetylcholine receptors: from structure to function. *Physiological Reviews* 89(1): 73-120.

Aryal, P., Sansom, M., and Tucker, S. (2015) Hydrophobic Gating in Ion Channels. *The Journal of Molecular Biology* 427: 121-130.

Beckstein, O., Biggin, P., and Sansom, M. (2001) A Hydrophobic Gating Mechanism for Nanopores. *The Journal of Physical Chemistry* 105: 12902-12905.

Beckstein, O., and Sansom, M. (2004) The influence of geometry, surface character, and flexibility on the permeation of ions and water through biological pores. *Physical Biology* 1: 42-52.

Beckstein, O., and Sansom, M. (2006) A Hydrophobic Gate in an Ion Channel: The Closed State of the Nicotinic Acetylcholine Receptor. *Physical Biology* 3(2): 147-159.

Bertrand, D., & Terry Jr., A.V (2018) The wonderland of neuronal nicotinic acetylcholine receptors. *Biochemical Pharmacology* 151: 214-225.

Blanton, M., Dangott, L., Raja, S., Lala, A., and Cohen, J. (1998) Probing the Structure of the Nicotinic Acetylcholine Receptor Ion Channel with the Uncharged Photoactivable Compound [3H]Diazofluorene. *The Journal of Biological Chemistry* 273(15): 8659-8668.

Bouzat, C., Gumilar, F., Spitzmaul, G., Wang, H., Rayes, D., Hansen, S., Taylor, P., and Sine, S. (2004) Coupling of agonist binding to channel gating in Ach-binding protein linked to an ion channel. 430(7002): 896-900.

Brejc, K., van Dijk, W., Klassen, R., Schuurmans, M., van der Oost, J., Smit, A., and Sixma, T. (2001) Crystal Structure of an ACh-binding protein reveals the ligand-binding domain of nicotinic receptors. *Nature* 411: 269-276.

Chevessier, F., Faraut, B., Ravel-Chapuis, A., Richard, P., Gaudon, K., Bauché, S., Prioleau, C., Herbst, R., Goillot, E., Ioos, C., Azulay, J., Attarian, S., Leroy, J., Fournier, E., Legay, C., Schaeffer, L., Koenig, J., Fardeau, M., Eymard, B., Pouget, J., and Hantaï, D. (2004) MUSK, a

new target for mutations causing congenital myasthenic syndrome. *Human Molecular Genetics* 13(24): 3229-3240.

Celie, P., van Rossum-Fikkert, S., van Dijk, W., Brejc, K., Smit, A., and Sixma, T. (2004) Nicotine and carbamylcholine binding to nicotinic acetylcholine receptors as studied in AChBP crystal structures. *Neuron* 41(6): 907-914.

Cetin, H., Epstein, M., Liu, W., Maxwell, S., Rodriguez Cruz, P., Cossins, J., Vincent, A., Webster, R., Biggin, P., and Beeson, D. (2019) Muscle acetylcholine receptor conversion into chloride conductance at positive potentials by a single mutation. *Proceedings of the National Academy of Sciences* 116(42): 21228-21235.

Cymes, G., Ni, Y., and Grosman, C. (2005) Probing ion-channel pores one proton at a time. *Nature* 438: 975-980.

Daeffler, K., Lester, H., and Dougherty, D. (2012). Functionally important aromatic-aromatic and sulfur-π interactions in the D2 dopamine receptor. *Journal of the American Chemical Society* 134: 14890-14896.

Dämgen, M., and Biggin, P. (2019) A Refined Open State of the Glycine Receptor Obtained via Molecular Dynamics Simulations. *Structure* 28: 130-139.

Domville, J. and Baenziger, J. (2018) An allosteric link connecting the lipid-protein interface to the gating of the nicotinic acetylcholine receptor. *Scientific Reports* 8: 3898.

Engel, A. (2007) The Therapy of Congenital Myasthenic Syndromes. *Neurotherapeutics* 4(2): 252-257.

Engel, A., Ohno, K., and Sine, S. (2003) Sleuthing molecular targets for neurological diseases at the neuromuscular junction. *Nature Reviews Neuroscience*: 4(5): 339-352.

Engel, A., Ohno, K., Bouzat, C., Sine, S. and Griggs, R. (1996) End-Plate Acetylcholine Receptor Deficiency Due to Nonsense Mutations in the ε Subunit. *Annals of Neurology* 40(5): 810-817.

Engel, A., Shen, X., Selcen, D., and Sine, S. (2015) Congenital myasthenic syndromes: pathogenesis, diagnosis, and treatment. *The Lancet* 14: 420-434.

Filatov, G., and White, M. (1995) The Role of Conserved Leucines in the M2 Domain of the Acetylcholine Receptor in Channel Gating. *Molecular Pharmacology* 48: 379-384.

Fukudome, T., Ohno, K., Brengman, J., and Engel A. (1998) AChR Channel Blockade by Quinidine Sulfate Reduces Channel Open Duration in the Slow-Channel Congenital Myasthenic Syndrome. *Annals of the New York Academy of Sciences* 841: 199-202.

Gomez, C., Maselli, R., Gammack, J., Lasalde, J., Tamamizu, S., Cornblath, D., Lehar, M., McNamee, M., and Kuncl, R. (1996) A β-Subunit Mutation in the Acetylcholine Receptor Channel Gate Causes Severe Slow-Channel Syndrome. *Annals of Neurology* 39: 712-723.

Grosman, C., Zhou, M., and Auerbach, A. (2000) Mapping the conformational wave of acetylcholine receptor channel gating. *Nature* 403(6771): 773-776.

Harms, M., Casteñeda, C., Schlessman, J., Sue, G., Isom, D., Cannon, B., and García-Moreno, B. (2009) The pKa Values of Acidic and Basic Residues Buried at the Same Internal Location in a Protein are Governed by Different Factors. *Journal of Molecular Biology* 389: 34-47.

Harpaz, Y., Gerstein, M., and Chothia, C. (1994) Volume changes on protein folding. *Structure* 2: 641-649.

Harper, M., Fukodome, T., and Engel, A. (2003) Treatment of slow-channel congenital myasthenic syndrome with fluoxetine. *Neurology* 60(10): 1710-1713.

Herrmann, D., Horvath, R., Sowden, J., Gonzales, M., Sanzhez-Mejias, A., Guan, Z., Whitaker, R., Almodovar, J., Lane, M., Bansagi, B., Pyle, A., Boczonadi, V., Lochmüller, H., Griffin, H., Chinnery, P., Lloyd, T., Littelton, T., and Zuchner, S. (2014) Synaptotagmin 2 Mutations Cause an Autosomal-Dominant Form of Lambert-Eaton Myasthenic Syndrome and Nonprogressive Motor Neuropathy. *The American Journal of Human Genetics* 95(3): 332-339.

Hessa, T., Kim, H., Lundin, C., Boekel, J., Andersson, H., Nilsson, I., White, S. and von Heijne, G. (2005) Recognition of transmembrane helices by the endoplasmic reticulum translocon. *Nature* 433: 377-381.

Horovitz, A. and Fersht, A.R. (1990). Strategy for analysing the co-operativity of intramolecular interactions in peptides and proteins. *Journal of Molecular Biology* 214: 613-617.

Imoto, K., Busch, C., Sakmann, B., Mishina, M., Konno, T., Nakai, J., Bujo, H., Mori, Y., Fukuda, K., and Numa, S. (1988) Rings of negatively charged amino acids determine the acetylcholine receptor channel conductance. *Nature* 335: 645-648.

Janin, J. (1979) Surface and inside volumes in globular proteins. *Nature* 277: 491-492.

Kearney, P., Zhang, H., Zhong, W., Dougherty, D., and Lester, H. (1996) Determinants of Nicotinic Receptor Gating in Natural and Unnatural Side Chain Structures at the M2 9' Position. *Neuron* 17: 1221-1229.

Kumar, A., Basak, S., Rao, S., Gicheru, Y., Mayer, M., Sansom, M., and Chakrapani, S. (2020) Mechanisms of activation and desensitization of full-length glycine receptor in lipid nanodiscs. *Nature Communications* 11: 3752.

Kyte, J., and Doolittle, R. (1982) A simple method for displaying the hydropathic character of a protein. *Journal of Molecular Biology* 157: 105-132.

Labarca, C., Nowak, M., Haiyun, Z., Tang, L., Deshpande, P., and Lester, H. (1995) Channel gating governed symmetrically by conserved leucine residues in the M2 domain of nicotinic receptors. *Nature* 376(6540): 514-516.

Lee, W. and Sine, S. (2005) Principal pathway coupling agonist binding to channel gating in nicotinic receptors. *Nature* 438(7065): 243-247.

Leo, A., Hantsch, C., and Elkins, D. (1971) Partition coefficients and their uses. *Chemical Reviews* 71: 525-592.

Levin, E., McClernon, J., and Rezvani, A. (2006) Nicotinic effects on cognitive function: behavioral characterization, pharmacological specification, and anatomic localization. *Psychopharmacology* 184(4): 523-539.

Maselli, R., Arredondo, J., Cagney, O., Ng, J., Anderson, J., Williams, C., Gerke, B., Soliven, B., and Wollmann, R. (2010) Mutations in *MUSK* causing congenital myasthenic syndrome impair MuSK-Dok-7 interaction. *Human Molecular Genetics* 19(12): 2370-2379.

Maselli, R., Fernandez, J., Arredondo, J., Navarro, C., Ngo, M., Beeson, D., Williams, C., Wollmann, R., Yarov-Yarovoy, V., and Ferns, M. (2012). G2 Agrin Mutation Causing Severe Congenital Myasthenic Syndrome Mimics Functional Characteristics of Non-neural (z−) Agrin. *Human Genetics* 131(7): 1123-1135.

Miller, C. (1989) Genetic Manipulation of Ion Channels: A New Approach to Structure and Mechanism. *Neuron* 2: 1195-1205.

Mishina, M., Takai, T., Imoto, K., Noda, M., Takahashi, T., and Numa, S. (1986) Molecular distinction between fetal and adult forms of muscle acetylcholine receptor. *Nature* 321: 406-411.

Miyazawa, A., Fujiyoshi, Y., and Unwin, N. (2003) Structure and gating mechanism of the acetylcholine receptor pore. *Nature* 423: 949-955.

Nelson, M., Kuryatov, A., Choi, C., Zhou, Y., and Lindstrom, J. (2003) Alternate Stoichiometries of α4β2 Nicotinic Acetylcholine Receptors. *Molecular Pharmacology* 63(2): 332-341.

Ohkawara, B., Cabrera-Serrano, M, Nakata, T., Milone, M., Asai, N., Ito, K., Ito, M., Masuda, A., Ito, Y., Engel, A., and Ohno, K. (2014) LRP4 third β-propeller domain mutations cause novel congenital myasthenia by compromising agrin-mediated MuSK signaling in a position-specific manner. *Human Molecular Genetics* 23(7): 1856-1868.

Ohno, K., Brengman, J., Tsujino, A. and Engel, A. (1998) Human endplate acetylcholinesterase deficiency caused by mutations in the collagen-like tail subunit (ColQ) of the asymmetric enzyme. *Proceedings of the National Academy of Sciences* 95(16): 9654-9659.

Ohno, K., Quiram, P., Milone, M., Wang, H., Harper, M., Pruitt, N., Brengman, J., Pao, L., Fischbeck, K., Crawford, T., Sine, S., and Engel, A. (1997) Congenital myasthenic syndromes due to heteroallelic nonsense/missense mutations in the acetylcholine receptor ε subunit gene: identification and functional characterization of six new mutations. *Human Molecular Genetics* 6(5): 753-766

Ohno, K., Wang, H., Milone, M., Bren, N., Brengann, J., Nakano, S., Quiram, P., Pruitt, J., Sine, S., and Engel, A. (1996) Congenital Myasthenic Syndrome Caused by Decreased Agonist Binding Affinity Due to a Mutation in the Acetylcholine Receptor ε Subunit. *Neuron* 17: 157-170.

Radzicka, A., and Wolfenden, R. (1988) Comparing the Polarities of the Amino Acids: Side-Chain Distribution Coefficients between the Vapor Phase, Cyclohexane, 1-Octanol, and Neutral Aqueous Solution. *Biochemistry* 27: 1664-1670.

Rahman, M., Teng, J., Worrell, B., Noviello, C., Lee, M., Karlin, A., Stowell, M., and Hibbs, R. (2020) Structure of the Native Muscle-type Nicotinic Receptor and Inhibition by Snake Venom Toxins. *Neuron* 106: 1-11.

Revah, F., Bertrand, D., Galzi, J., Devillers-Thiéry, A., Mulle, C., Hussy, N., Bertrand, S., Ballivet, M., and Changeux, J. (1991) Mutations in the channel domain alter desensitization of a neuronal nicotinic receptor. *Nature* 353: 846-849.

Rose, G., Geselowitz, A., Lesser, G., Lee, H., and Zehfus, M. (1985). Hydrophobicity of amino acid residues in globular proteins. *Science 229*(4716): 834-838.

Schara, U., Christen, H.S., Durmus, H., Hietala, M., Krabetz, K., Rodolico, C., Schreiber, G., Topaloglu, H., Talim, B., Voss, W., Pikho, H., Abicht, A., Müller, J., and Lochmüller, H. (2010)

Long-term follow-up in patients with congenital myasthenic syndrome due to CHAT mutations. *European Journal of Paediatric Neurology* 14: 326-333.

Shafferman, A., Kronman, C., Flashner, Y., Leitner, M., Grosfeld, H., Ordentlich, A., Gozes, Y., Cohen, S., Ariel, N., Barak, D., Harel, M., Silman, I., Sussman, J., and Velan, B. (1992) Mutagenesis of Human Acetylcholinesterase. *The Journal of Biological Chemistry* 267(25): 17640-17648.

Shen, X., Brenman, J., Edvardson, S., Sine, S., and Engel, A. (2012) Highly fatal fast-channel syndrome caused by AChR ε subunit mutation at the agonist binding site. *Neurology* 79(5): 449-454.

Shen, X., Crawford, T., Brengman, J., Acsadi, G., Iannaconne, S., Karac, E., Khoury, C., Mah J., Edvardson, S., Bajzer, Z., Rodgers, D., and Engel, A. (2011) Functional Consequences and Structural Interpretation of Mutations of Human Choline Acetyltransferase. *Human Mutations* 32(11): 1259-1267.

Shen, X., Selcen, D., Brengman, J., and Engel, A. (2014) Mutant SNAP25B causes myasthenia, cortical hyperexcitability, ataxia, and intellectual disability. *Neurology* 83(24): 2247-2255.

Shen, X., Okuno, T., Milone, M., Otsuka, K., Takahashi, K., Komaki, H., Giles, E., Ohno, K., and Engel, A. (2016) Mutations Causing Slow-Channel Myasthenia Reveal That a Valine Ring in the Channel Pore of Muscle AChR is Optimized for Stabilizing Channel Gating. *Human Mutation* 37(10): 1051-1059.

Sine, S., Ohno, K., Bouzat, C., Auerbach A., Milone, M., Pruitt, J., and Engel, A. (1995) Mutation of the acetylcholine receptor α subunit causes a slow-channel myasthenic syndrome by enhancing agonist binding affinity. *Neuron* 15: 229-239.

Sine, S., Shen, X., Wang, H., Ohno, K., Lee, W., Tsujino, A., Brengmann, J., Bren, N., Vajsar, J., and Engel, A. (2002) Naturally Occurring Mutations at the Acetylcholine Receptor Binding Site Independently Alter ACh Binding and Channel Gating. *The Journal of General Physiology* 120(4): 483-496.

Sine, S. and Engel, A. (2006) Recent advances in Cys-loop receptor structure and function. *Nature* 440: 448-455.

Thompson, M., Domville, J., and Baenziger, J. (2020) The functional role of the αM4 transmembrane helix in the muscle nicotinic acetylcholine receptor probed through mutagenesis and coevolutionary analyses. *The Journal of Biological Chemistry* 295: 11056-11067.

Tsai, R., Fan, W., El Tayar, N., Carrupt, P., Testa, B., and Kier, L. (1993) Solute-water interactions in the organic phase of a biphasic system: Structural influence of organic solutes on the "water-dragging" effect. *Journal of the American Chemical Society* 115: 9632–9639.

Unwin, N. (1993) Nicotinic Acetylcholine Receptor at 9Å Resolution. *Journal of Molecular Biology* 229: 1101-1124.

Unwin, N., Miyazawa, A., Li, J., and Fujiyoshi, Y. (2002) Activation of the Nicotinic Acetylcholine Receptor Involves a Switch in Conformation of the α Subunits. *Journal of Molecular Biology* 319: 1165-1176.

Unwin, N. (2005) Refined structure of the nicotinic acetylcholine receptor at 4Å resolution. *Journal of Molecular Biology* 346(4): 967-989.

Unwin, N. and Fujiyoshi, Y. (2012) Gating Movement of Acetycholine Receptor Caught by Plunge-Freezing. *Journal of Molecular Biology* 422: 617-634.

Unwin, N. (2013) Nicotinic acetylcholine receptor and the structural basis of neuromuscular transmission: insights from Torpedo postsynaptic membranes. *Quarterly Reviews in Biophysics* 46(4): 283-322.

Wang, H., Auerbach, A., Bren, N., Ohno, K., Engel, A., and Sine, S. (1997) Mutation in the M1 Domain of the Acetylcholine Receptor α Subunit Decreases the Rate of Agonist Dissociation. *Journal of General Physiology* 109(6): 757-766.

Wang, H., Milone, M., Ohno, K., Shen., X., Tsujino, A., Batocchi, A., Tonali, P., Brengman, J., Engel, A., and Sine, S. (1999) Acetylcholine receptor M3 domain: stereochemical and volume contributions to gating. *Nature Neuroscience* 2(3): 226-233.

Weeks, J., Chandler, D., and Andersen, H. (1971) Role of Repulsive Forces in Determining the Equilibrium Structure of Simple Liquids. *The Journal of Chemical Physics* 54(12): 5237-5247.

Weeks, J., Vollmayr, K., and Katsov, K. (1997) Intermolecular forces and the structures of uniform and Non-uniform liquids. *Physica A – Statistical Mechanics and its Applications* 244: 461-475.

White, B. and Cohen, J. (1992) Agonist-induced Changes in the Structure of the Acetylcholine Receptor M2 Regions Revealed by Photoincorporation of an Uncharged Nicotinic Noncompetitive Antagonist. *The Journal of Biological Chemistry* 267(22): 15770-15783.

Widom, B. (1967) Intermolecular Forces and the Nature of the Liquid State. *Science* 157(3787): 375-382.

Wilson, G. and Karlin A. (1998) The Location of the Gate in the Acetylcholine Receptor Channel. *Neuron* 20: 1269-1281.

Wimley, W., and White, S. (1996) Experimentally determined hydrophobicity scale for proteins at membrane interfaces. *Nature Structural Biology* 3: 842-848.

Wolfenden, R. (2007) Experimental Measures of Amino Acid Hydrophobicity and the Topology of Transmembrane and Globular Proteins. *The Journal of General Physiology* 129(5): 357-362.

Wolfenden, R., Andersson, L., Cullis, P., and Southgate, C. (1981) Affinities of amino acid side chains for solvent water. *Biochemistry* 20: 849–855.

Xi, J., Yan, C., Liu, W., Qiao, K., Lin, J., Tian, X., Wu, H., Lu, J., Wong, L., Beeson, D. and Zhao, C. (2017) Novel SEA and LG2 Agrin mutations causing congenital Myasthenic syndrome. *Orphanet Journal of Rare Diseases* 12(1): 182.

Zhong, W., Gallivan, J., Zhang, Y., Lintong, L., Lester, H., and Dougherty, D. (1998) From *ab initio* quantum mechanics to molecular neurobiology: A cation-π binding site in the nicotinic receptor. *Proceedings of the National Academy of Sciences* 95: 12088-12093.

Zhu, C., Gao, Y., Li, H., Meng, S., Li, L., Fransisco, J., and Zeng, X. (2016) Characterizing hydrophobicity of amino acid side chains in a protein environment via measuring contact angle of a water nanodroplet on planar peptide network. *Proceedings of the National Academy of Sciences* 113(46): 12946-12951.

Zhu, H., Grajales-Reyes, G., Alicea-Vázquez, V., Grajales-Reyes, J., Robinson, K., Pytel, P., Báez-Pagán, C., Lasalde-Dominicci, J., and Gomez, C. (2015) Fluoxetine is neuroprotective in slow-channel myasthenic syndrome. *Experimental Neurology* 270: 88-94.

Zong, Y. and Jin, R. (2013) Structural mechanisms of the agrin–LRP4–MuSK signaling pathway in neuromuscular junction differentiation. *Cellular and Molecular Life Sciences* 70: 3077-3088.

Zwart, R., and Vijverberg, H. (1998) Four Pharmacologically Distinct Subtypes of α4β2 Nicotinic Acetylcholine Receptors Expressed in *Xenopus laevis* Oocytes. *Molecular Pharmacology* 54(6): 1124-1131.

Supplementary Information:

Whole Cell Electrophysiological Recordings

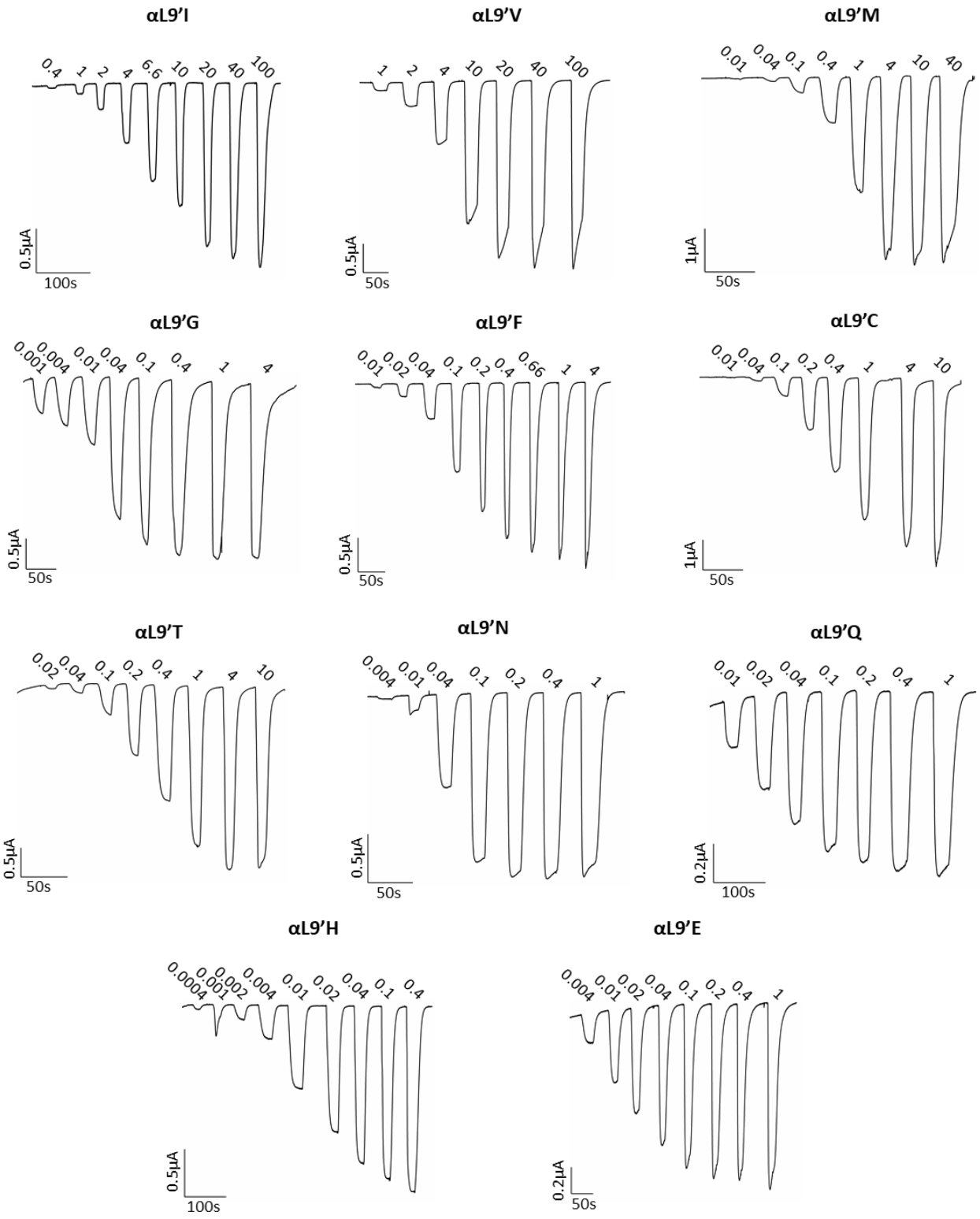

Figure S1: Whole Cell Electrophysiological Recordings from αL9' mutants

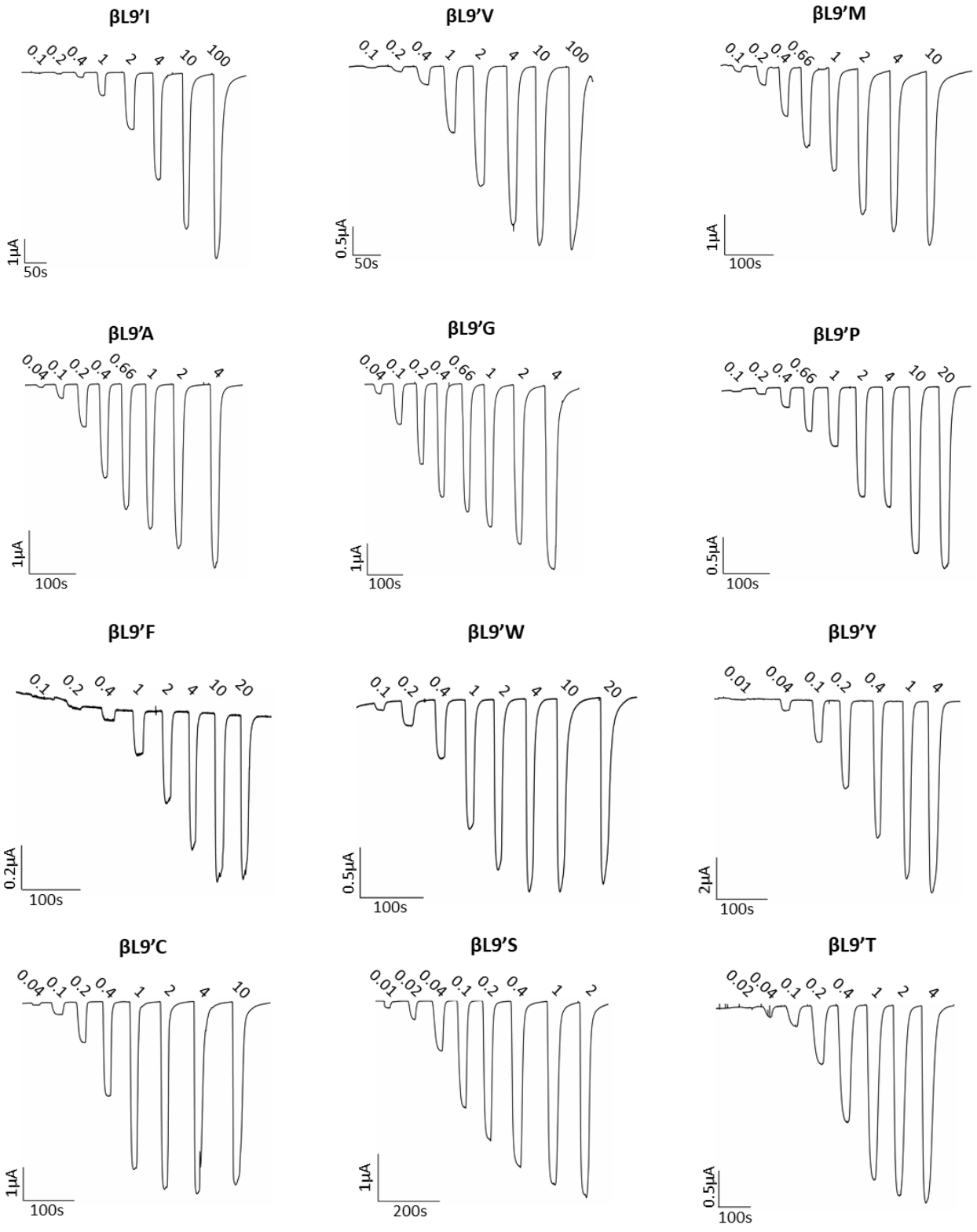
βL9'I
0.1 0.2 0.4 1 2 4 10 100
1μA
50s
βL9'V
0.1 0.2 0.4 1 2 4 10 100
0.5μA
50s
βL9'M
0.1 0.2 0.4 0.66 1 2 4 10
1μA
100s
βL9'A
0.04 0.1 0.2 0.4 0.66 1 2 4
1μA
100s
βL9'G
0.04 0.1 0.2 0.4 0.66 1 2 4
1μA
100s
βL9'P
0.1 0.2 0.4 0.66 1 2 4 10 20
0.5μA
100s
βL9'F
0.1 0.2 0.4 1 2 4 10 20
0.2μA
100s
βL9'W
0.1 0.2 0.4 1 2 4 10 20
0.5μA
100s
βL9'Y
0.01 0.04 0.1 0.2 0.4 1 4
2μA
100s
βL9'C
0.04 0.1 0.2 0.4 1 2 4 10
1μA
100s
βL9'S
0.01 0.02 0.04 0.1 0.2 0.4 1 2
1μA
200s
βL9'T
0.02 0.04 0.1 0.2 0.4 1 2 4
0.5μA
100s

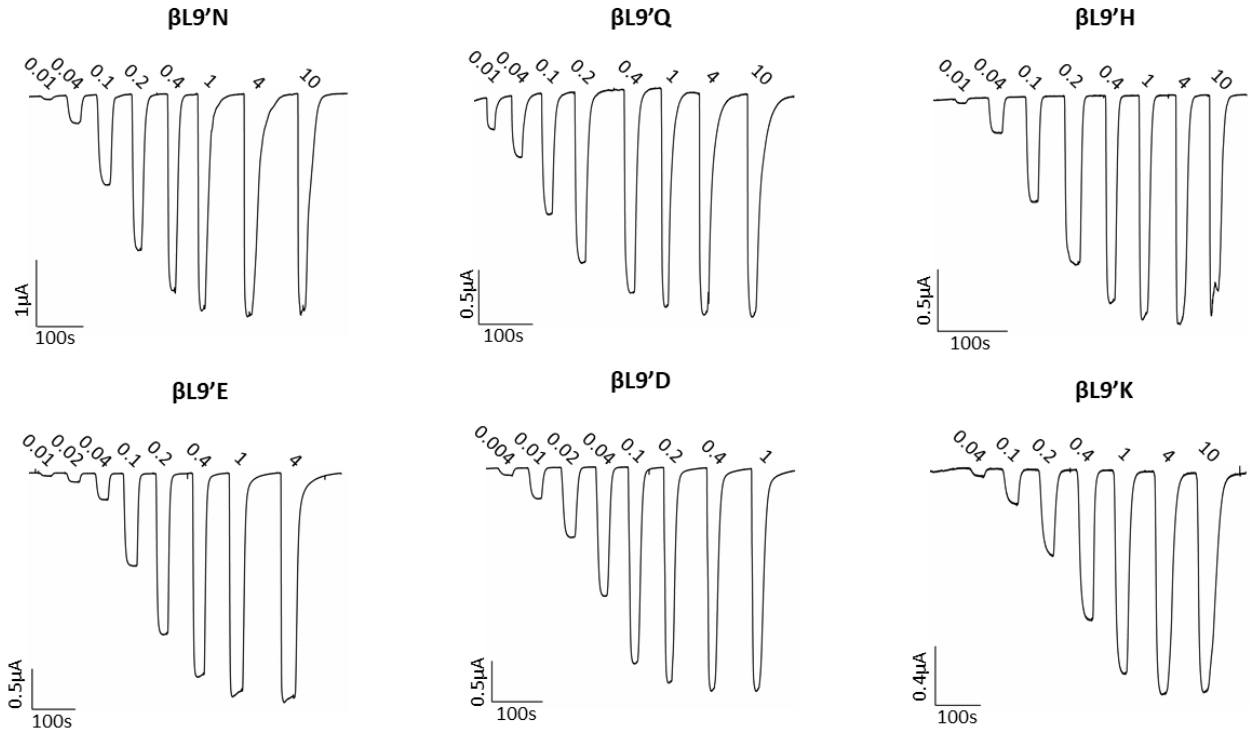

Figure S2: Whole Cell Electrophysiological Recordings from βL9' mutants

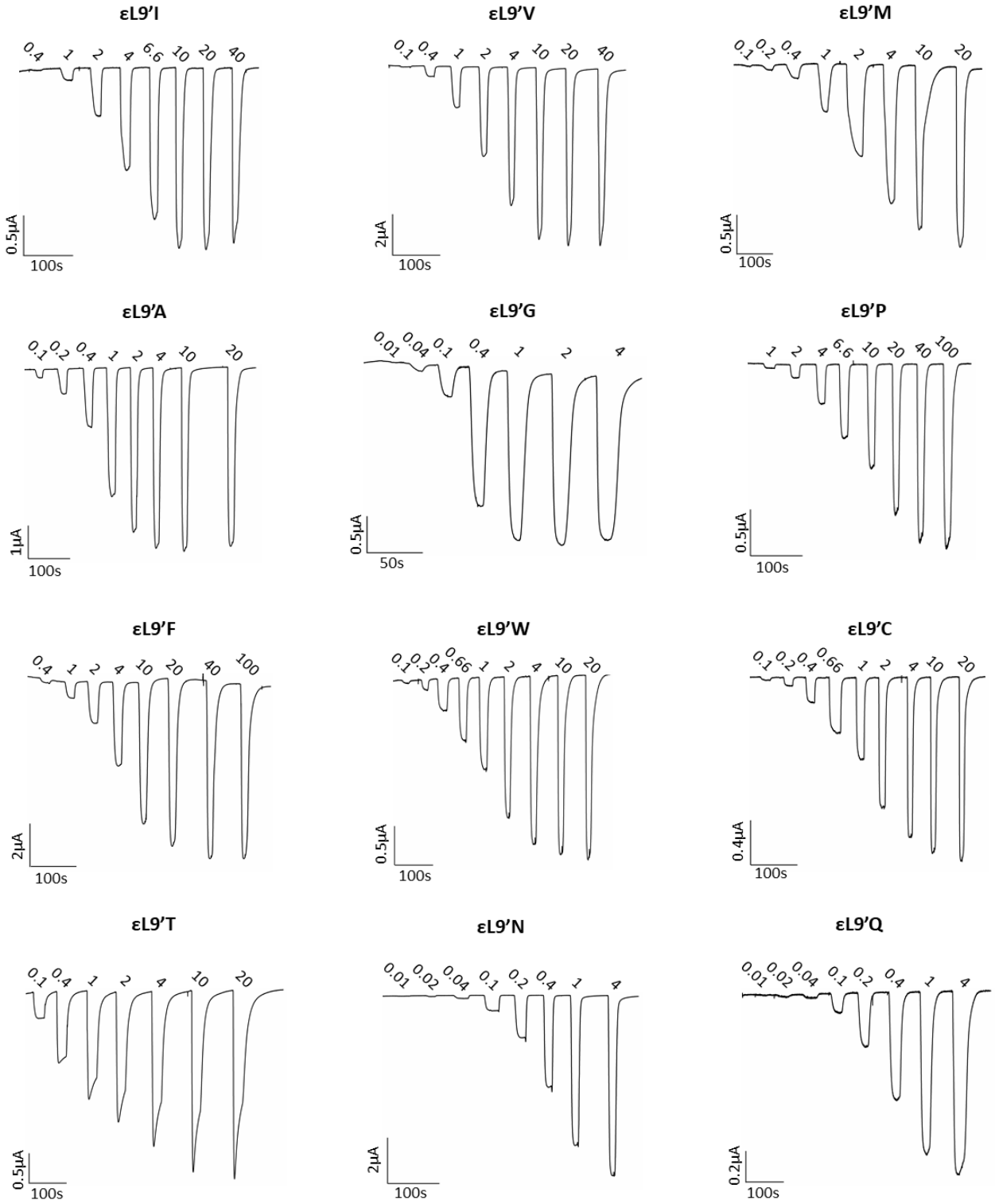
εL9'I
0.4 1 2 4 6.6 10 20 40
0.5μA
100s
εL9'V
0.1 0.4 1 2 4 10 20 40
2μA
100s
εL9'M
0.1 0.2 0.4 1 2 4 10 20
0.5μA
100s
εL9'A
0.1 0.2 0.4 1 2 4 10 20
1μA
100s
εL9'G
0.01 0.04 0.1 0.4 1 2 4
0.5μA
50s
εL9'P
1 2 4 6.6 10 20 40 100
0.5μA
100s
εL9'F
0.4 1 2 4 10 20 40 100
2μA
100s
εL9'W
0.1 0.2 0.4 0.66 1 2 4 10 20
0.5μA
100s
εL9'C
0.1 0.2 0.4 0.66 1 2 4 10 20
0.4μA
100s
εL9'T
0.1 0.4 1 2 4 10 20
0.5μA
100s
εL9'N
0.01 0.02 0.04 0.1 0.2 0.4 1 4
2μA
100s
εL9'Q
0.01 0.02 0.04 0.1 0.2 0.4 1 4
0.2μA
100s

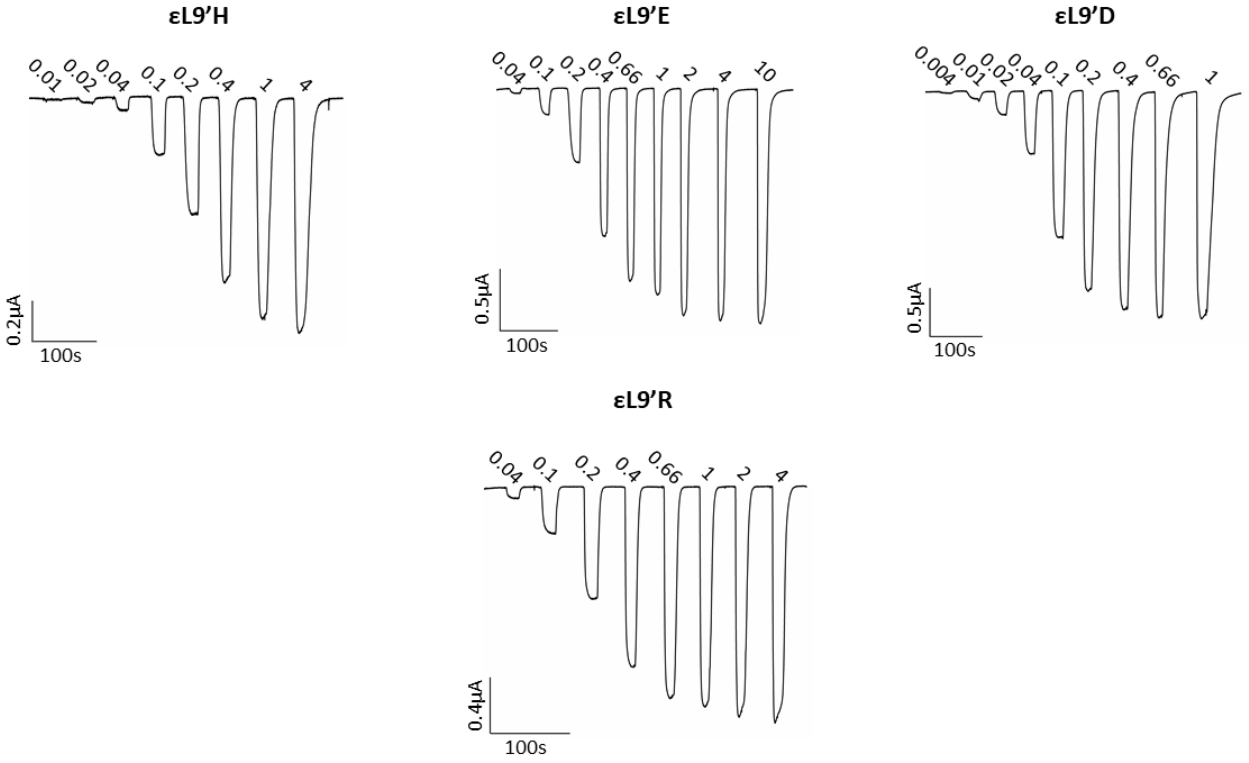

Figure S3: Whole Cell Electrophysiological Recordings from εL9' mutants

δL9'I

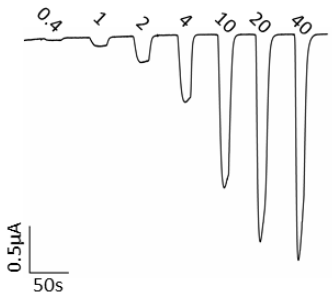

δL9'V

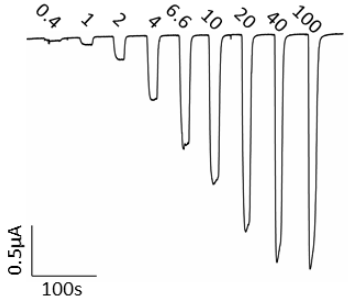

δL9'M

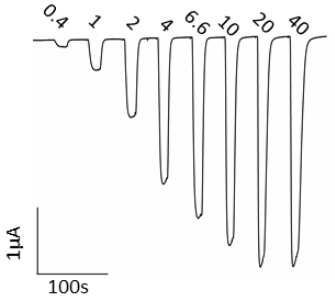

δL9'A

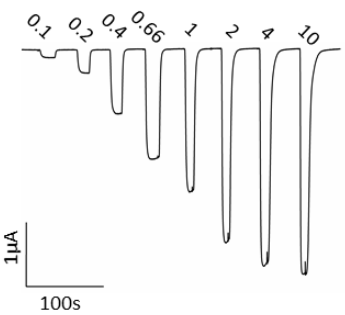

δL9'P

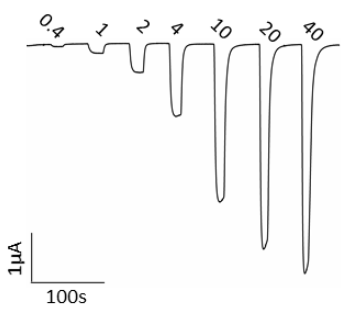

δL9'F

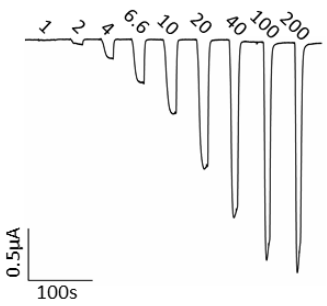

δL9'W

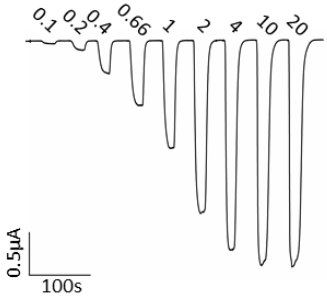

δL9'Y

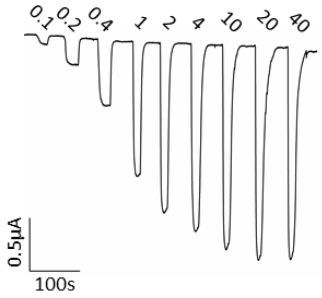

δL9'C

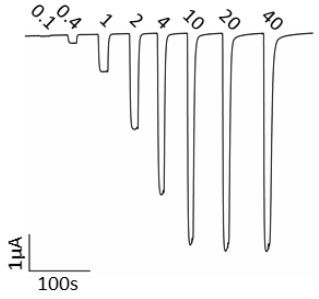

δL9'S

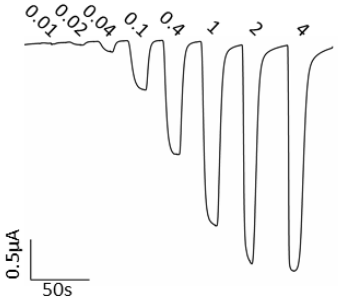

δL9'T

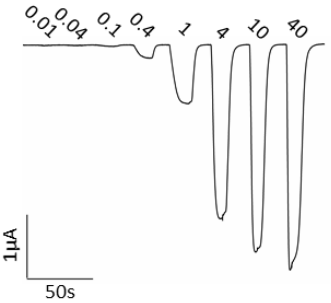

δL9'N

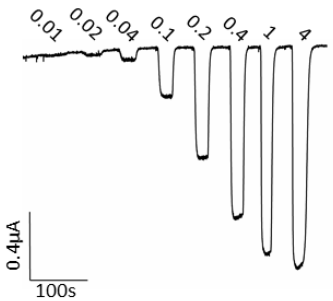

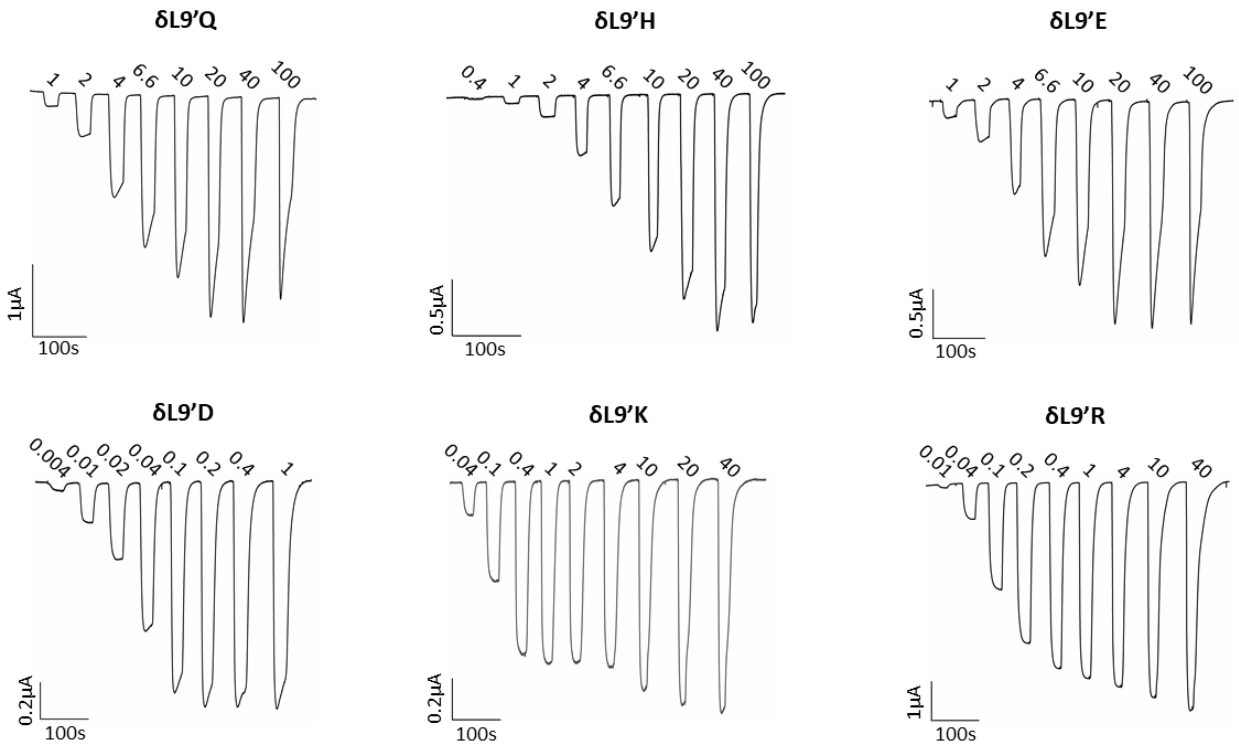

Figure S4: Whole Cell Electrophysiological Recordings from δL9' mutants

Permissions

Figure 2A+B

Source: Ohno, K., Quiram, P., Milone, M., Wang, H., Harper, M., Pruitt, N., Brengman, J., Pao, L., Fischbeck, K., Crawford, T., Sine, S., and Engel, A. (1997) Congenital myasthenic syndromes due to heteroallelic nonsense/missense mutations in the acetylcholine receptor ε subunit gene: identification and functional characterization of six new mutations. *Human Molecular Genetics* 6(5): 753-766

Permissions: Reproduced with permission from Oxford University Press and Dr. Andrew Engel

License Number: 4933781057069

Figure 2C+D

Source: Engel, A., Shen, X., Selcen, D., and Sine, S. (2015) Congenital myasthenic syndromes: pathogenesis, diagnosis, and treatment. *The Lancet* 14: 420-434.

Permissions: Reprinted from *The Lancet* with permission from Elsevier and Dr. Andrew Engel.

License Number: 4937970782464

Figure 2E

Source: Sine, S. and Engel, A. (2006) Recent advances in Cys-loop receptor structure and function. *Nature* 440: 448-455.

Permissions: Reprinted with permission from Dr. Steven Sine and Springer Nature Customer Service Center GmbH

License Number: 4937961351216